Report
R-19-20
June 2020

Modelling of the near-field hydrogeology

Report for the safety assessment SR-PSU (PSAR)

Elena Abarca
Diego Sampietro
Jordi Sanglas
Jorge Molinero

SVENSK KÄRNBRÄNSLEHANTERING AB

SWEDISH NUCLEAR FUEL
AND WASTE MANAGEMENT CO

Box 3091, SE-169 03 Solna
Phone +46 8 459 84 00
skb.se

SVENSK KÄRNBRÄNSLEHANTERING

ISSN 1402-3091
SKB R-19-20
ID 1865971

June 2020

Modelling of the near-field hydrogeology

Report for the safety assessment SR-PSU (PSAR)

Elena Abarca, Diego Sampietro, Jordi Sanglas, Jorge Molinero
Amphos 21 Consulting S.L.

Summary

The present work is an extension of the analysis of the hydrological behaviour of the near-field carried out as part of the long-term safety assessment for the SFR extension application (Abarca et al. 2013, 2014). It concerns the future hydrogeological conditions in the near-field of the SFR 1 (the existing facility) and the SFR 3 (the planned extension). The term near-field refers to the engineered barrier system (EBS) components that are designed to contain the waste, and the host rock in the vicinity of the repository.

After the Preliminary Safety Assessment Review, it was necessary to update the post-closure safety assessment taking into account new considerations. The layout of the SFR 3 has been adjusted to the currently planned dimensions of the vaults, access tunnels and ramps. Moreover, technical developments relating to the concrete structures have been incorporated in the analysis.

Four steady-state flow fields calculated from an updated regional hydrogeology model are integrated into the repository-scale models. They represent four different positions of the shoreline relative to the repository: a case with the repository submerged, a case with the shoreline passing over the repository and two cases where the repository footprint is well above the shoreline. In addition to the base case, a set of cases investigating different hydraulic properties of repository components have been simulated to assess the impact on groundwater flow in the repository. The computed groundwater flow rates in the repository under saturated and steady-state conditions serve as input to the radionuclide transport model that is used to show compliance with radiation safety regulations.

Sammanfattning

Föreliggande arbete är en utökning av en tidigare rapporterad analys av framtida hydrogeologiska förhållanden i närfältet för utbyggnad av SFR (Abarca et al. 2013, 2014). Rapporten behandlar framtida hydrogeologiska förhållanden i närfältet av SFR 1 (existerande anläggning) och SFR 3 (planerad utbyggnad). Med närfältet avses förvarssalarna med dess komponenter och barriärer samt berget i förvarets närhet.

Efter den preliminära säkerhetsanalysen (Preliminary Safety Assessment Review), var det nödvändigt att uppdatera analysen av säkerhet efter förslutning. Närfältmodellerna av SFR 3 är anpassad till de nu aktuella dimensionerna på förvarssalarna, åtkomsttunnlarna och ramperna. Vidare inkluderas den senaste tekniska utvecklingen av förvarets betongkonstruktioner i analysen.

Fyra stationära flödesfält har beräknats på förvarsskal utifrån den uppdaterade regionala hydrogeologimodellen. Flödesfälten svarar mot olika lägen som förvaret har i förhållande till Östersjöns strandlinje. I det första fallet ligger förvaret helt under havet. I det andra passerar strandlinjen genom förvaret. I de två sista fallen ligger förvaret väl över strandlinjen. Ytterligare beräkningsfall redovisas vilka undersöker förändring i flöden genom förvaret orsakat av degraderade barriärer, olika förslutningsalternativ och permafrost. De under mättade och stationära förhållanden beräknade grundvattenflödena i förvaret tjänar som indata till radionuklidtransportmodellering, utförd för att visa överensstämmelse med strålsäkerhetsföreskrifterna.

Contents

1 Introduction and objective 7
1.1 Objective 7
1.2 Outline of the report 8

2 Methodology 9
2.1 Chain of models 9
2.2 Definition of the simulation cases 10
2.3 Data transfer to Ecolego 10

3 Modifications in the repository scale models 11
3.1 Repository layout 11
3.2 Extent to the SFR 1 and SFR 3 models 12
3.3 Representation of rock vaults 13
3.4 Partitioning of vaults for radionuclide transport simulations 17
3.5 Representation of the tunnels 19
3.6 Initial state of the repository materials 20
3.7 Properties of the host rock 20
3.8 Governing equations 21
3.8.1 Groundwater flow 21
3.8.2 Boundary conditions 21

4 SFR 1 Calculation cases 23
4.1 Base case 23
4.1.1 Groundwater flow field at 2000 AD 23
4.1.2 Groundwater flow field at 2500 AD 24
4.1.3 Groundwater flow field at 3500 AD 25
4.1.4 Groundwater flow field at 5000 AD 26
4.1.5 Total flow through the vaults and waste 27
4.2 Barrier degradation 28
4.2.1 Concrete degradation 28
4.2.2 Plug degradation 32
4.2.3 No barriers 34
4.2.4 Ice lens 36
4.3 Estimation of uncertainty associated with the geosphere 37
4.4 Summary of the calculation cases 40

5 SFR 3 Calculation cases 43
5.1 Base case 43
5.1.1 Groundwater flow field at 2000 AD 43
5.1.2 Groundwater flow field at 2500 AD 44
5.1.3 Groundwater flow field at 3500 AD 45
5.1.4 Groundwater flow field at 5000 AD 46
5.1.5 Total flow through the vaults and waste 47
5.2 Barrier degradation 48
5.2.1 Concrete degradation 48
5.2.2 Plug degradation 51
5.2.3 No barriers 52
5.3 Estimation of uncertainty associated with the geosphere 54
5.4 Summary of the calculation cases 56

6 Alternative initial state for the 1BMA and 2BMA concrete 59

7 1BMA vault-scale model 61
7.1 Geometry of the 1BMA vault 61
7.2 Mesh 62
7.3 Boundary conditions and rock properties 63

7.4 Calculation cases 63
7.4.1 Observables 64
7.4.2 Groundwater flow through the 1BMA vault and waste 65
7.4.3 Axial distribution of the water flow in the waste 66
7.5 Summary of the calculation cases 68

References 69

Appendix A Properties of the repository materials 71

Appendix B Flow tables 73

Appendix C Alternative Initial state 83

Appendix D Flow in the 1BMA vault for the different degradation states 87

Appendix E Cross sectional plots of the 1BMA vault 89

1 Introduction and objective

The Swedish Nuclear Fuel and Waste Management Company (SKB) operates the repository for low- and intermediate-level nuclear waste (SFR) located in Forsmark. An extension of the SFR is planned to mainly accommodate wastes arising from the decommissioning of Swedish nuclear power plants. The hydrological behaviour of the near-field of the SFR and its extension was analysed as part of the long-term safety assessment for the SFR extension application, SR-PSU. Future hydrogeological conditions of SFR 1 (the existing facility) and SFR 3 (the planned extension) were explored in Abarca et al. (2013, 2014). The term near-field refers to the engineered barrier system (EBS) components that are designed to contain the wastes, and the host rock in the vicinity of the repository.

In Abarca et al. (2013, 2014), numerical models were set up and solved in COMSOL Multiphysics to increase the understanding of the near-field hydrology and to generate consistent input data for the radionuclide transport calculations. Two repository-scale models, one for SFR 1 and another for SFR 3 were developed.

Since the publication of Abarca et al. (2013, 2014), there have been some updates in the layout of the planned SFR 3 repository and also some new technical developments relating to the concrete structures. Therefore, it has been necessary to update the post-closure safety assessment taking into account these new considerations.

In this report, the work in Abarca et al. (2013) is extended to include those modifications and to analyse their impact on the groundwater flow field around the SFR 1 and SFR 3 repositories. This report is a continuation of that work and should be read as a supplement to it, not as a stand-alone report. Most of the modelling details are described in Abarca et al. (2013), whereas this report focusses on the modifications.

1.1 Objective

The objective of this work is to update the post-closure safety evaluation that contributed to the Preliminary Safety Assessment Review SR-PSU (F-PSAR) by modifying the existing models of the repositories SFR 1 (the existing facility) and SFR 3 (the planned extension).

The geometry of the models follows the 2.0 layout (SKB 2014b) except for these modifications:

- The ramp will connect to existing tunnels and a larger ramp radius than in the previous layout is considered.
- The direction of vaults is mirror reflected compared with the previous layout.

The resulting geometry follows the 2.6 layout and incorporates the following changes with respect to Abarca et al. (2013, 2014):

- The removal of the separate ramp for transporting the reactor pressure vessels.
- The connection of the existing access tunnels to SFR 1 and SFR 3 and the update of the size of the ramp radius.
- The direction of the vaults in SFR 3 is mirror reflected.
- A gas-venting system is incorporated in the geometry of 1BMA and 2BMA (Elfwing et al. 2017, von Schenck et al. 2018).
- The 1BMA concrete structures are updated and the hydraulic properties take account of new technical developments relating to concrete structures (Elfwing et al. 2016, von Schenck et al. 2015).

In addition, the near-field hydrogeology for SFR 1 and SFR 3 has been updated through the implementation of new boundary conditions from an updated regional hydrogeological model (Öhman and Odén 2018).

A set of barrier degradation cases have been computed using the repository-scale models of SFR 1 and SFR 3. The flows through predefined control volumes have been computed and tabulated as input to radionuclide transport calculations following the procedure in Abarca et al. (2013).

1.2 Outline of the report

Chapter 2 describes briefly the methodology used, defines the set of cases considered in the analysis and describes how the results are transferred to Ecolego for the radionuclide transport simulations.

Chapter 3 describes the modifications made to the models for SFR 1 and SFR 3 repositories with respect to the set-up presented in Abarca et al. (2013).

Chapter 4 analyses the results of the groundwater flow simulations carried out with the SFR 1 repository-scale model. First, a base case is considered with hydraulic properties for the engineered barriers at their initial states. In addition to the base case, a set of cases were used to investigate the effects of modifying the hydraulic properties of repository components on groundwater flow in the repository. Four simulations that correspond to different shoreline positions were considered.

Chapter 5 analyses the results of the groundwater flow simulations carried out with the SFR 3 repository-scale model. A base case and a set of additional cases were used to investigate the effects of modifying the hydraulic properties of repository components on groundwater flow in the repository vaults under four different shoreline positions.

Chapter 6 analyses the potential reduction in flow through the 1BMA and 2BMA wastes assuming a high-performance construction concrete for 2BMA and for the reinforcement of 1BMA.

Chapter 7 extends the analysis to include an assessment of a reinforcement/repair case for 1BMA that does not rely on a foundation with injected cement. Specific questions concerning the effects and extent of concrete degradation of the 1BMA structure were investigated using a vault-scale model.

2 Methodology

2.1 Chain of models

This work analyses the groundwater flow field around and within the SFR repository. It evaluates the impact of different boundary conditions and hydraulic properties on the groundwater flow in the different vault and waste compartments of SFR 1 and SFR 3. The methodology is that applied in Abarca et al. (2013). The two repositories are represented in separate models (Figure 2-1). The commercial finite element code COMSOL Multiphysics (COMSOL 2017) has been used for the analysis. In addition to the geometry of the repository itself, the models also include a volume of surrounding rock.

The pressure field at the boundaries is extracted from the regional hydrogeology model (Öhman and Odén 2018) implemented in DarcyTools (Svensson et al. 2010), as detailed in Abarca et al. (2013). The regional hydrogeology model by Öhman and Odén (2018) includes SFR 1 as well as the latest version of the planned extension SFR 3 (layout 2.6). Their representation of the tunnel system is divided into backfill and plug materials, comprising mechanical concrete plugs in bentonite-filled tunnels, as described by Luterkort et al. (2012). The backfill in general tunnel sections, ramps, and all disposal rooms except the Silo is assigned a hydraulic conductivity of 10^{-5} m/s to minimize complications of numerical instability (Öhman and Odén 2018). Four different pressure fields are considered to represent the time-evolution of the groundwater flow due to land rise. Land rise causes the shoreline position to move and consequently changes the conditions above the repository from being initially submerged to being an emerged terrestrial landscape. Land rise is the main contributor to changing groundwater flow over time.

The rock conductivity field corresponds with the Base_Case1_DFN_R85 in Öhman and Odén (2018). Two additional realizations of the rock permeability are used to assess the range of variability in the computed flows due to uncertainties in the geosphere hydraulic description. These realizations are considered as representatives of two cases, one that leads to a higher and one that lead to a lower average tunnel flow with respect to the Base case. They are referred in Öhman and Odén (2018) as nc_DEP_R07_DFN_R85 and nc_NoD_R01_DFN_R18, respectively.

Following the nested modelling approach described in Abarca et al. (2014) a vault model of the 1BMA vault was generated based on the repository scale model of SFR 1. The objective was to extend the simulation cases to include an assessment of a reinforcement/repair case for 1BMA that does not rely on a foundation with injected cement.

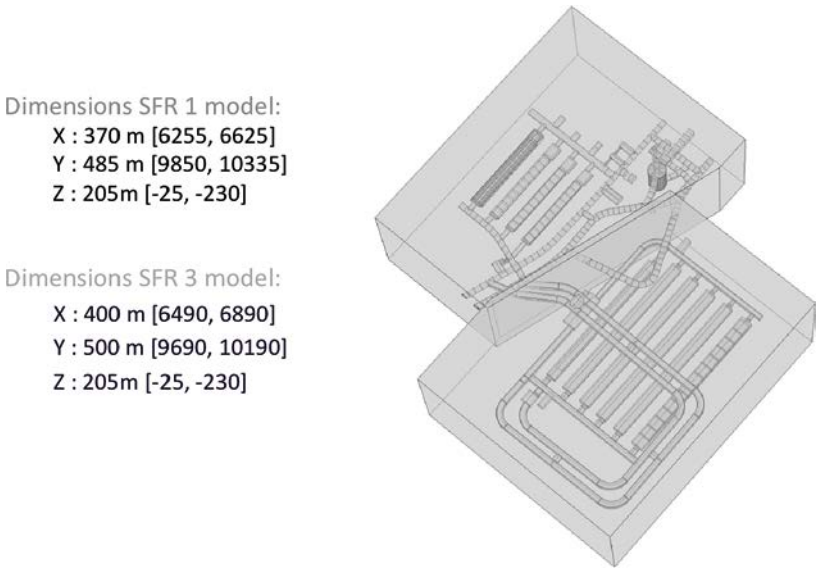

Figure 2-1. *3D model domains of the COMSOL model of the SFR 1 and SFR 3 repositories (Abarca et al. 2013).*

2.2 Definition of the simulation cases

A set of cases investigating different hydraulic properties of repository components was simulated to assess the impact on groundwater flow in the repository. These cases include most of the cases analysed in Abarca et al. (2013) such as the degradation of the concrete barriers, the degradation of the plugs, a no barriers case, an ice lens case for the Silo and two cases of variability in the rock properties. In addition to the cases in Abarca et al. (2013), a case of an alternative initial state was used to analyse the potential reduction of flow in the 1BMA and 2BMA vaults by using a high-performance construction concrete. The list of all the simulation cases is presented in Table 2-1. The values of the hydraulic conductivity of all the repository materials for each simulation case are presented in Table A-1 in Appendix A. The values for each of the materials were selected to cover the range of suggested data on hydraulic conductivities in concrete materials to be used in the SR-PSU for different time periods and for different parts of SFR (SKB 2014b). All the assumptions underlying the assigned values can be found in Abarca et al. (2013).

Table 2-1. Table of simulation cases.

ID	Simulation case		Shoreline position	SFR 1	SFR 3
1	**Base case**		1	x	x
2			2	x	x
3			3	x	x
4			4	x	x
5	**Alternative initial state**		1	x	x
6			2	x	x
7			3	x	x
8			4	x	x
9	**Concrete degradation**	**Moderate**	1	x	x
10			2	x	x
11			3	x	x
12			4	x	x
13		**Severe**	1	x	x
14			2	x	x
15			3	x	x
16			4	x	x
17		**Complete**	1	x	x
18			2	x	x
19			3	x	x
20			4	x	x
21	**Plug degradation**	**Moderate**	4	x	x
22		**Severe**	4	x	x
23		**Complete**	4	x	x
24	**No barriers**		4	x	x
25	**Ice lens**		4	x	
26	**High flow**		1	x	x
27			4	x	x
28	**Low flow**		1	x	x
29			4	x	x

2.3 Data transfer to Ecolego

The results of the groundwater flow simulations performed with the repository-scale models were tabulated to serve as input for radionuclide transport calculations with Ecolego. The data transfer from COMSOL to Ecolego (Facilia 2015) was based on and related to commonly defined control volumes. The partitioning of each vault into control volumes for Ecolego is described in detail in Section 3.4. This transfer of information follows the procedure described in Abarca et al. (2013).

3 Modifications in the repository scale models

This section describes the set-up of the repository scale models that have been used for the simulations. The full description of the repository scale models of the SFR 1 and SFR 3 is presented in detail in Abarca et al. (2013). The information reported here focusses on the modifications carried out after the SR-PSU (F-PSAR).

3.1 Repository layout

Little hydrogeological interaction between SFR 1 and SFR 3 is expected (Öhman et al. 2014). Therefore, two repository-scale models, one for the SFR 1 and another for the repository extension, SFR 3 were developed (Figure 2-1).

The SFR 1 repository is composed of four vaults: 1BMA, 1BLA, 1BTF, and 2BTF and a Silo (Figure 3-1). The SFR 3 will be composed of six additional vaults: 2BMA, 2BLA, 3BLA, 4BLA, 5BLA and BRT. A detailed summary of the characteristics of the different vaults and engineering elements that form SFR 1 and SFR 3 can be found in Abarca et al. (2013). The layout has been updated from the layout 1.5 used in Abarca et al. (2013) to the layout 2.6 (see details in Section 2.1 and SKB 2014b). The main changes are:

- Removal of the separate access ramp for reactor pressure vessels. In the updated design, the reactor pressure vessels will be segmented and the existing SFR 1 access ramps will be used. The SFR 3 ramp will have a larger radius and will connect to the existing tunnels according to Figure 3-2a in Öhman and Odén (2018).
- The direction of the SFR 3 vaults is mirror reversed.
- The dimensions of the SFR 3 vaults, especially BRT and 2BMA, have been modified. The new dimensions are given in Table 3-1.

Table 3-1. Geometric characteristics of the SFR 3 vaults in layout 2.6.

	BRT	2–5BLA	2BMA
Tunnel Length (m)	255*	275.0	275.0
Tunnel Width (m)	15.8*	17.9	20.4*
Tunnel Height (m)	14.0*	14.0*	16.4*
Tunnel Volume (m^3)	53 884*	67 187*	85 508*
Waste Length (m)	220.5*	243.4	214.5*†
Waste Width (m)	11.5*	14.0	17.9*
Waste Height (m)	5.5*	9.14	7.8*
Waste Volume (m^3)	13 947*	31 150.0	27 465*

* Value changed with respect to layout 1.5 used in Abarca et al. (2013).
† Value corresponds to 13 sections each of length 16.5 m.

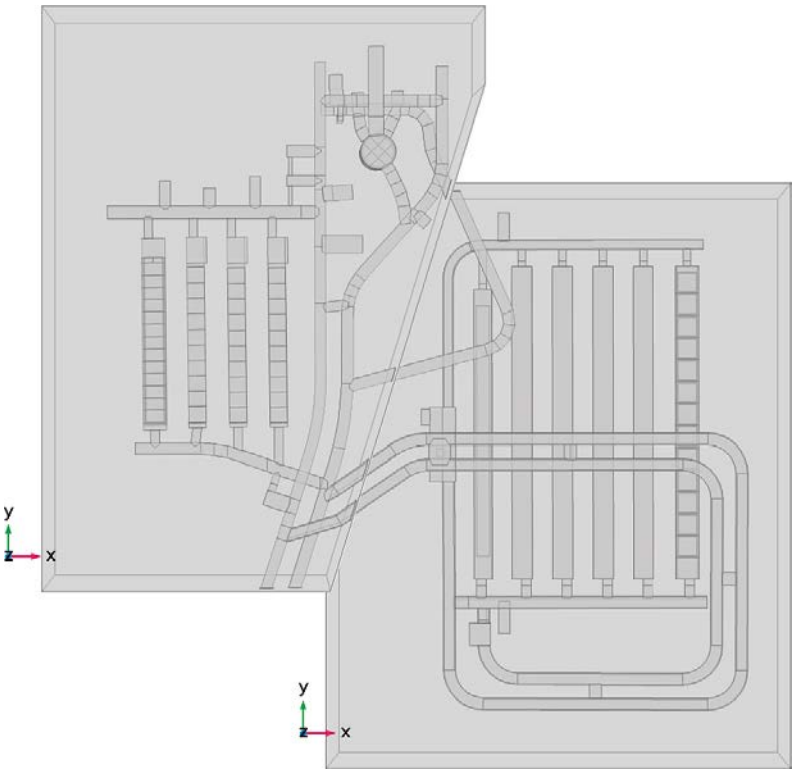

Figure 3-1. *Geometry of SFR 1 (on the left) and SFR 3 (on the right) from the CAD files as imported into COMSOL. The intersections between the access ramp to SFR 1 and the access tunnels to SFR 3 is also illustrated.*

3.2 Extent to the SFR 1 and SFR 3 models

The volume of rock surrounding the repositories is identical to that defined in Abarca et al. (2013). This extent of the rock domain was chosen such that any change in the hydraulic properties of the repository will not impact the pressure at the model boundaries. Section 4.1 in Abarca et al. (2013) describes how the size of the model domain was selected based on this prerequisite. The dimensions and geometries of the SFR 1 and SFR 3 models are presented in Figure 2-1 and in Table 3-2 and Table 3-3. The reference coordinate system (position and orientation) is consistent with the one used in the Site Descriptive model (SDM) report (SKB 2013).

Table 3-2. Local coordinates of the vertices defining the SFR 1 COMSOL model.

X (m)	Y (m)	Z_{max} (m)	Z_{min} (m)
6625.00	10335.00	−25	−230
6625.00	10271.00	−25	−230
6496.12	9850.00	−25	−230
6255.00	9850.00	−25	−230
6255.00	10335.00	−25	−230

Table 3-3. Local coordinates of the vertices defining the SFR 3 COMSOL model.

X (m)	Y (m)	Z_{max} (m)	Z_{min} (m)
6890.00	9690.00	−25	−230
6490.00	9690.00	−25	−230
6490.00	9865.96	−25	−230
6589.19	10190.00	−25	−230
6890.00	10190.00	−25	−230

3.3 Representation of rock vaults

An overview of the vault model geometries follows below focusing on the changes with respect to the geometry described in Abarca et al. (2013). For further details, the reader is referred to Abarca et al. (2013).

The components of the SFR 1 repository (Figure 3-2) are basically unchanged except for 1BMA. The two BTF vaults, the 1BLA vault and the Silo are treated identically as in the repository-scale model of Abarca et al. (2013).

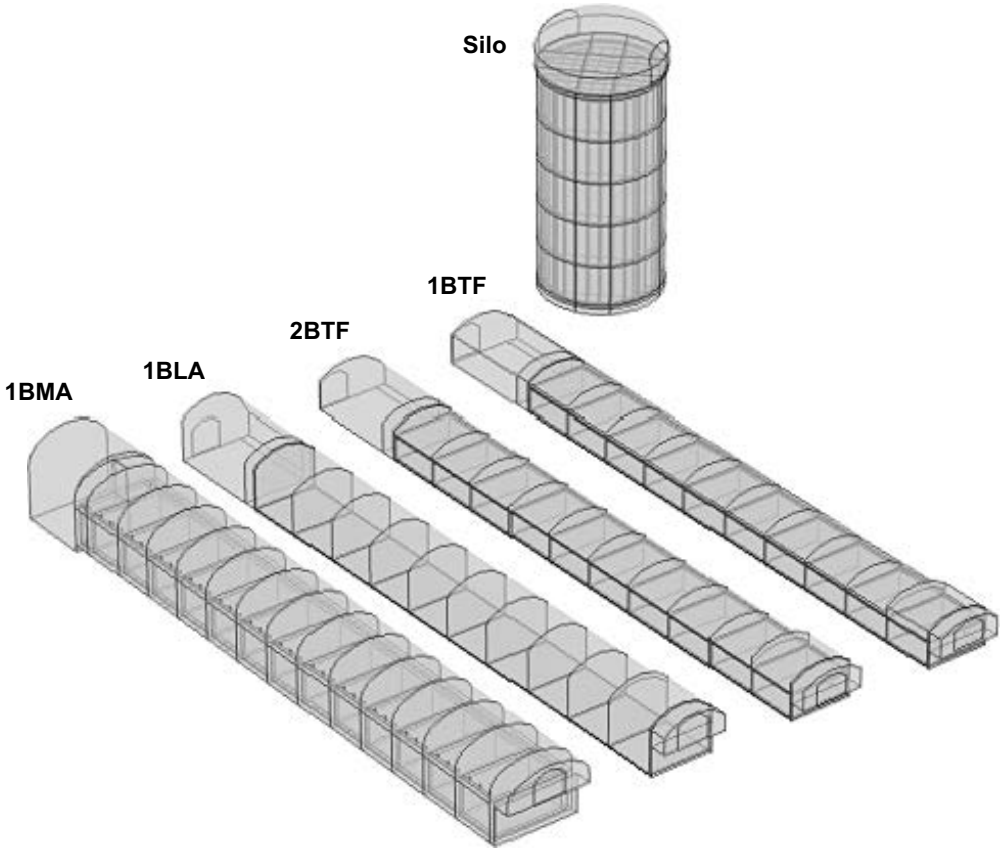

Figure 3-2. *Geometry of the vaults in the SFR 1 repository-scale model.*

1BMA vault: 1BMA is a rock vault for intermediate-level waste. Constructed from reinforced concrete, 1BMA is divided by inner walls into 13 large and two smaller storage compartments. This is a vault whose internal structure has been substantially modified compared with the structure assumed in Abarca et al. (2013). The existing structure (walls and lid) will be reinforced upon closure. Therefore, the reinforced concrete structures have been included in the model according to SKB (2014b), as shown in Figure 3-3. Only the reinforced concrete structures are explicitly incorporated in the model geometry. In the repository scale model, a domain of homogenized properties integrates both the waste and the existing concrete walls, i.e., the existing walls are not discretized in the model geometry. The concrete compartments rest on a foundation of macadam and crushed rock that will be injected with concrete. In the model, the grouted foundation is treated as a material with its own specific properties. In addition, channels filled with grout will provide relief of gas build-up in each compartment. The gas-relief system is formed by 3 gas evacuation channels (GEC) of 0.25 m × 0.20 m × lid thickness evenly distributed per waste compartment, except for the small compartments (14 and 15) that have one GEC per compartment. At closure, the rock cavern will be filled with permeable backfill material. In the model, the waste is treated as a homogeneous block and individual packages are not resolved in the geometry, as shown in Figure 3-4.

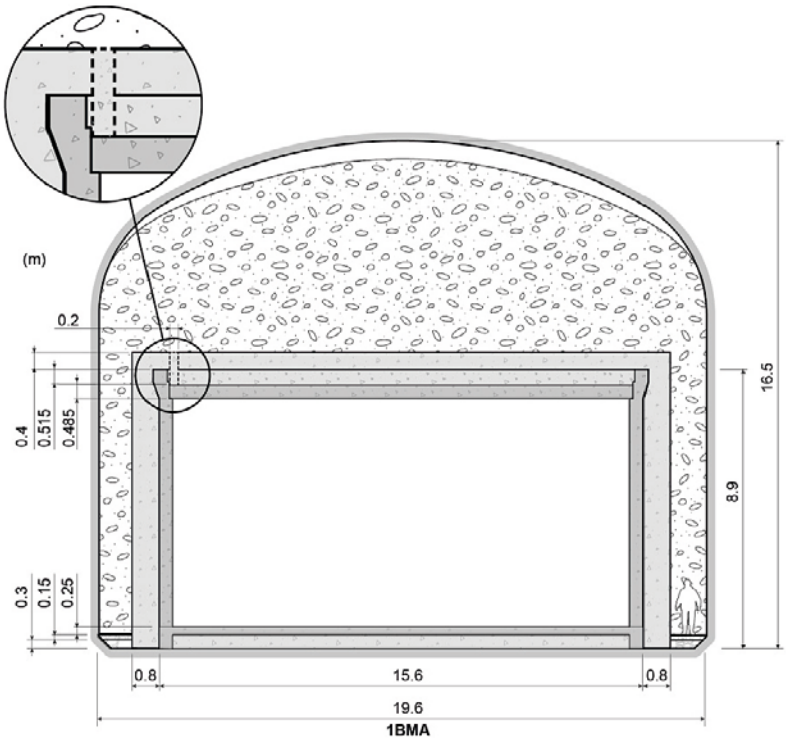

Figure 3-3. *Geometry of the 1BMA vault with gas-relief system modified from SKB (2014b) that has been used to define the dimensions of the reinforced concrete structures.*

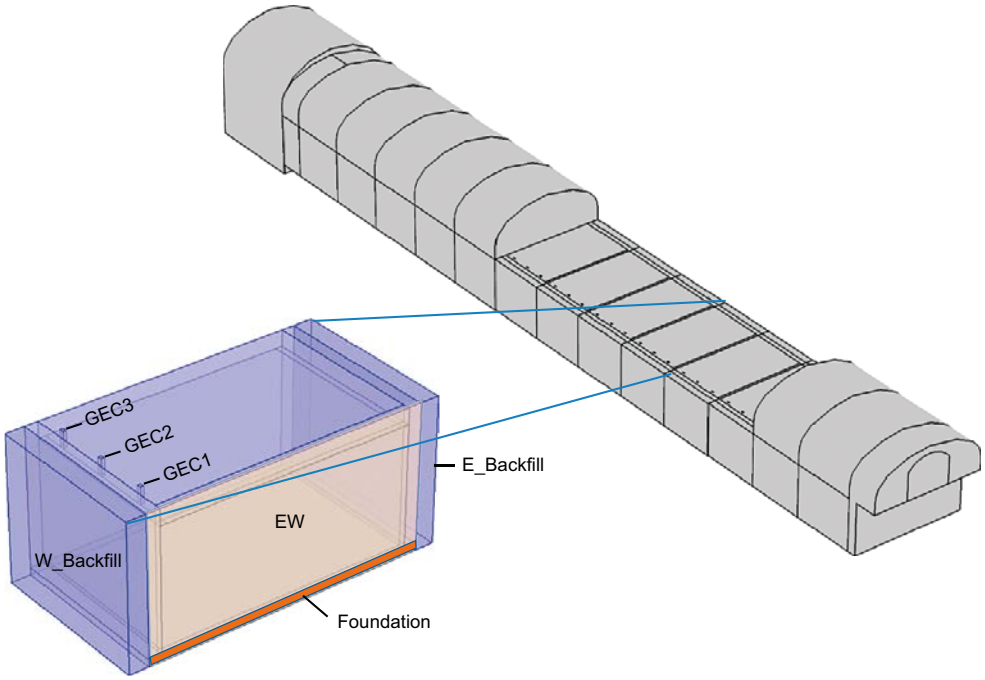

Figure 3-4. *Geometry of the 1BMA vault in the SFR 1 repository as implemented in the repository scale model. The orange volume corresponds to the encapsulated waste (EW) that includes the reinforced concrete walls. The waste compartments rest on a foundation formed by a gravel layer (macadam) injected with grout.*

The changes in SFR 3 rock vaults (Figure 3-5) are described next.

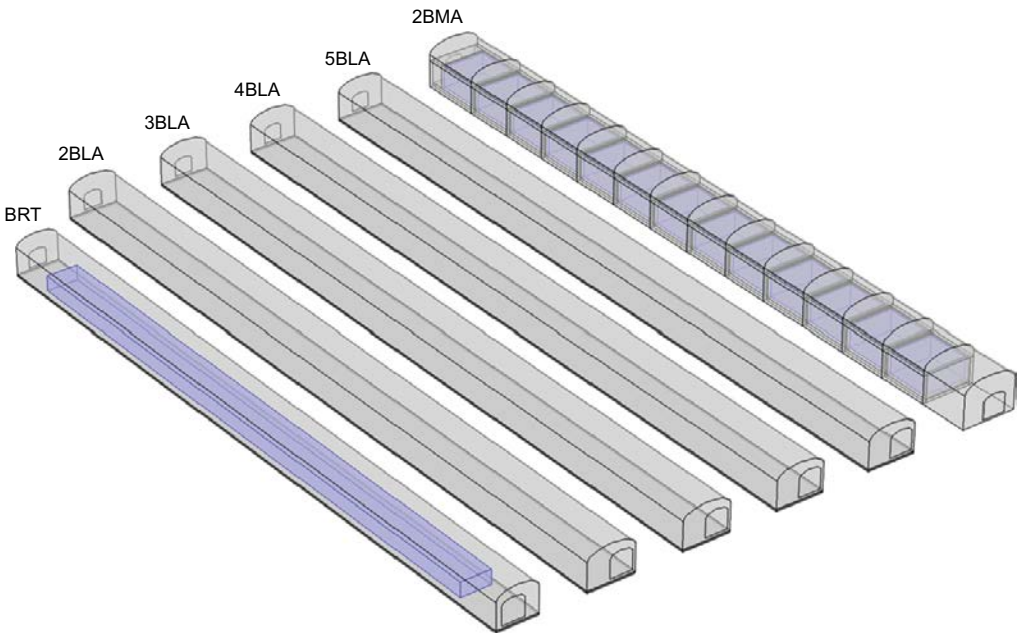

Figure 3-5. *Geometry of the vaults in the SFR 3 repository scale model. BRT and 2BMA have discretized waste domains (blue).*

BRT vault (Figure 3-5): The dimensions of this vault have been modified according to Table 10-1 in SKB (2014b). The vault will contain segmented parts of the reactor pressure vessels from the nuclear power plants embedded in concrete. The grouted waste of BRT sits on a concrete floor cast on a layer of crushed rock. As in Abarca et al. (2013), a homogeneous waste domain is considered, surrounded by backfill material on top and to the sides. The adjusted vault dimensions are W:11.5 m, H: 5.5 m, L: 220.5 m.

2–5BLA vaults (Figure 3-5): The 2–5BLA vaults will contain low level waste in standard steel containers, standing on a concrete floor cast on a layer of crushed rock. The waste is assumed to have the same hydraulic properties as the highly permeable backfill that fills the vault. These vaults have been mirror reversed in layout 2.0 (Table 9-1 in SKB 2014b) but the dimensions and the conceptualization of the geometrical domains remain unchanged.

2BMA vault (Figure 3-6): 2BMA is a vault for intermediate-level waste. It consists of thirteen separate concrete compartments, compared with fourteen in Abarca et al. (2013), placed directly on a floor of crushed rock. A highly permeable backfill surrounds each waste compartment. The inner walls are not resolved, and therefore, the waste inside each compartment is treated as a homogeneous block with no resistance to flow. The vault orientation is mirrored with respect to layout 1.5 and its dimensions are redefined according to layout 2.0 (Table 5-1 in SKB, 2014b). There is an increase in the thickness of the concrete walls, floor and lid. In addition, a gas evacuation system (Elfwing et al. 2017, von Schenck et al. 2018) formed by 6 gas evacuation channels per waste compartment is included (Figure 3-7).

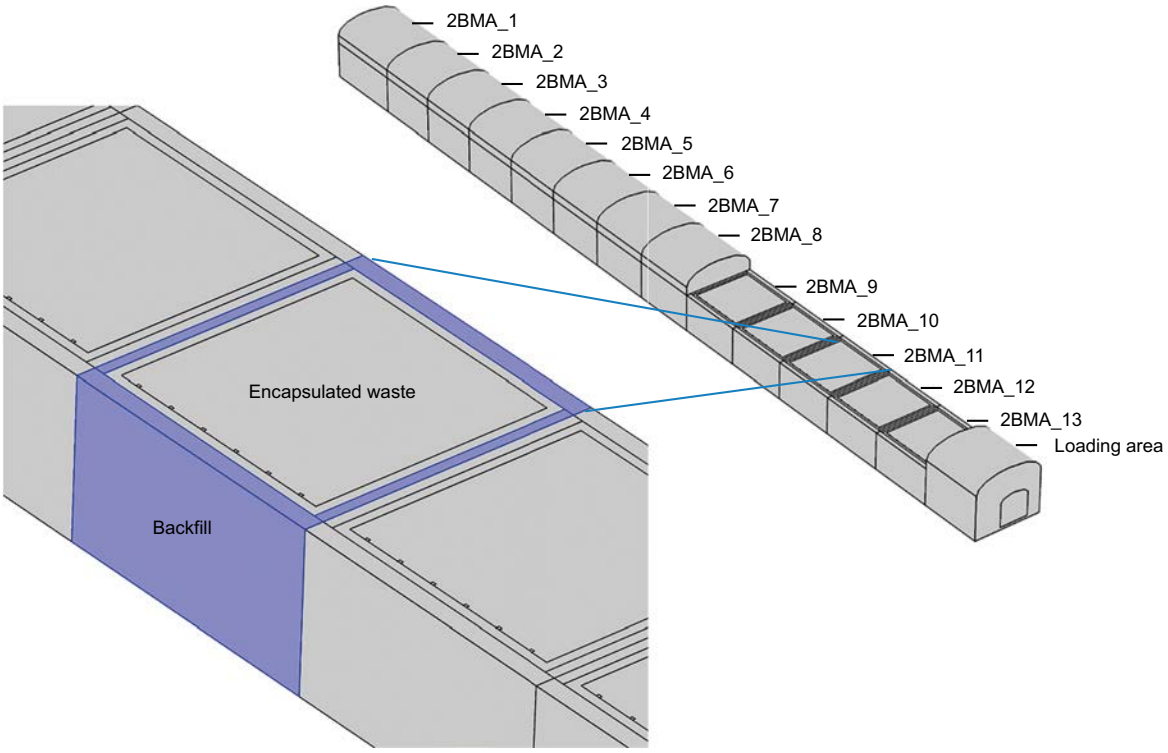

Figure 3-6. *Geometry of the 2BMA vault in the SFR 3 repository scale model including the gas evacuation channels (GEC).*

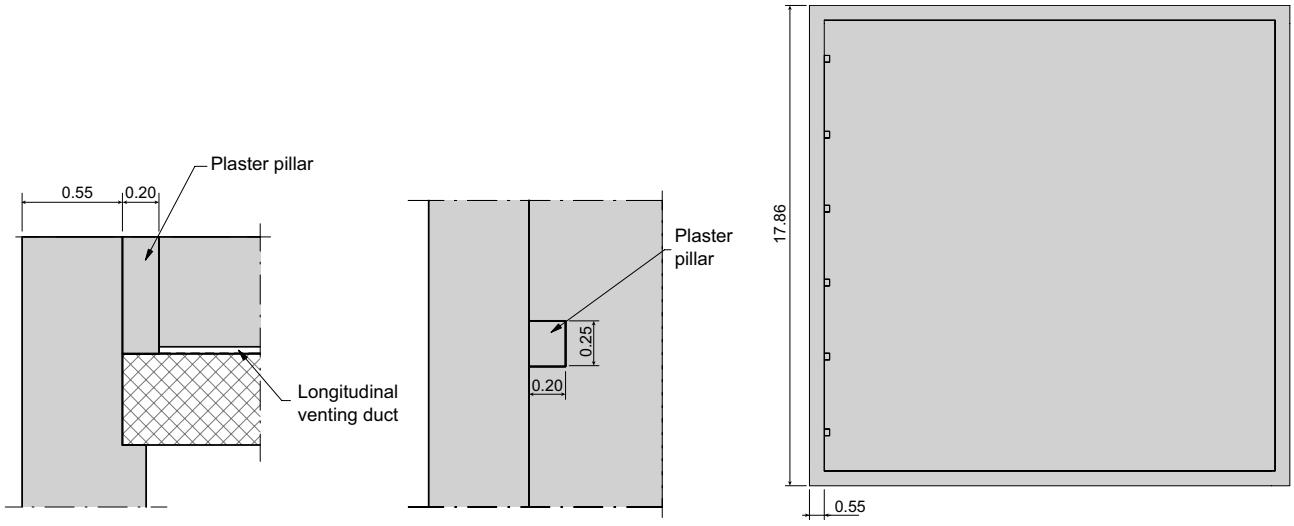

Figure 3-7. *The gas evacuation system in each of the waste compartments of 2BMA: (left) vertical cross-section; (centre) plan view and dimensions of a single evacuation channel and (right) plan view of a waste compartment showing the locations of the six gas evacuation channels (GEC).*

3.4 Partitioning of vaults for radionuclide transport simulations

A shared discretization of the vaults for the groundwater flow and the radionuclide transport models has been used.

The following control volumes were implemented for the SFR 1 repository:

- The SFR 1 vault ends (loading areas) that are not part of the other control volumes are considered as separate control volumes for each tunnel. These control volumes are named N Loading area and S Loading area.
- 1BMA:
  - Each of the 13 large waste compartments is considered a control volume. The two small ones, labelled 14 and 15 in Abarca et al. (2013, 2014), are now integrated into a single control volume labelled as EW_14_15. These control volumes are referred to as Encapsulated Waste (EW) and include the reinforced concrete barriers and the homogenized waste, which integrates the waste and the existing concrete structures (i.e. concrete floor, walls and lid). The concrete wall shared between two compartments is integrated as part of the southern control volume.
  - The flows through the top surface of each large EW is discriminated into the flow through each gas evacuation channel (GEC) and the remaining top surface. In the case of EW_14_15, the top surface has two GEC, one per small waste compartment, and the remaining surface.
  - The volumes are numbered from 1 in the south to 14 in the north.
  - Around each encapsulated waste control volume there are 3 backfill control volumes (top, east and west), see Figure 3-8.
  - Underlying each encapsulated waste control volume there is a foundation domain.

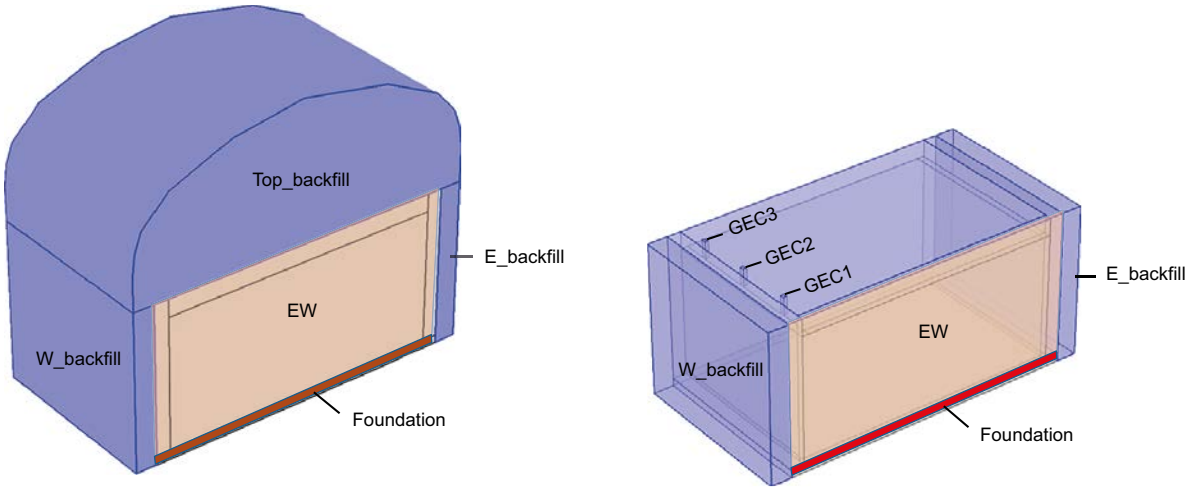

Figure 3-8. *Control volumes of the 1BMA vault in the SFR 1 repository as implemented in the repository-scale model. The orange volume corresponds to the encapsulated waste (EW) that includes the reinforced concrete walls. The waste compartments rest on a foundation formed by a gravel layer (macadam) injected with grout.*

- 1BTF and 2BTF: The control volume definition is the same as in Abarca et al. (2013).
- 1BLA: The control volume definition has been simplified in the BLA vaults. In Abarca et al. (2013), 1BLA was divided longitudinally into 10 sections. Here, these 10 control volumes are integrated together into a single section. Also, two control volumes were defined in each longitudinal section: one for the foundation and one for the rest of the vault. Here the foundation is included in the same section as the waste domain. Therefore, a single control volume is defined for the part of the 1BLA vault occupied by the waste. As for the rest of the SFR vaults, there are two additional control volumes for the north and south loading areas.
- Silo: The control volume definition in Abarca et al. (2013) is maintained.

For SFR 3, the subdivision into control volumes is done in the following way:

- In Abarca et al. (2013), the SFR 3 vaults end to the north were considered as a control volume (loading area). Here, only 2BMA has a control volume defining the loading area. Also, due to the change in the directions of the vaults in layout 2.0, it is now located at the south end of the vault.
- BRT: As in Abarca et al. (2013), the entire waste storage domain is considered as a single control volume and the entire tunnel area is considered as a single control volume (backfill).
- 2–5BLA: The control volume definition has been simplified. The 3 control volumes (waste, backfill and loading area) defined in Abarca et al. (2013), have been integrated into one per each of the BLA vaults.
- 2BMA:
  - Longitudinally, there are 13 encapsulated waste control volumes (Figure 3-9). There were 14 in the previous layout. Each waste compartment is delimited by a concrete barrier on top, bottom, and lateral sides. These outer concrete walls define the waste control volumes. The waste control volumes are numbered from 1 in the north to 13 in the south. There are also 13 sections of crushed rock backfill surrounding the waste control volumes. The limits of each section are chosen exactly at the mid point between two waste volumes. For similarity with 1BMA, each of the sections of backfill has been divided into 6 control volumes (top, bottom, south, north, east and west).
  - The flow through the top surface of each EW is discriminated into the flow through each gas evacuation channel (GEC) and through the remaining top surface.

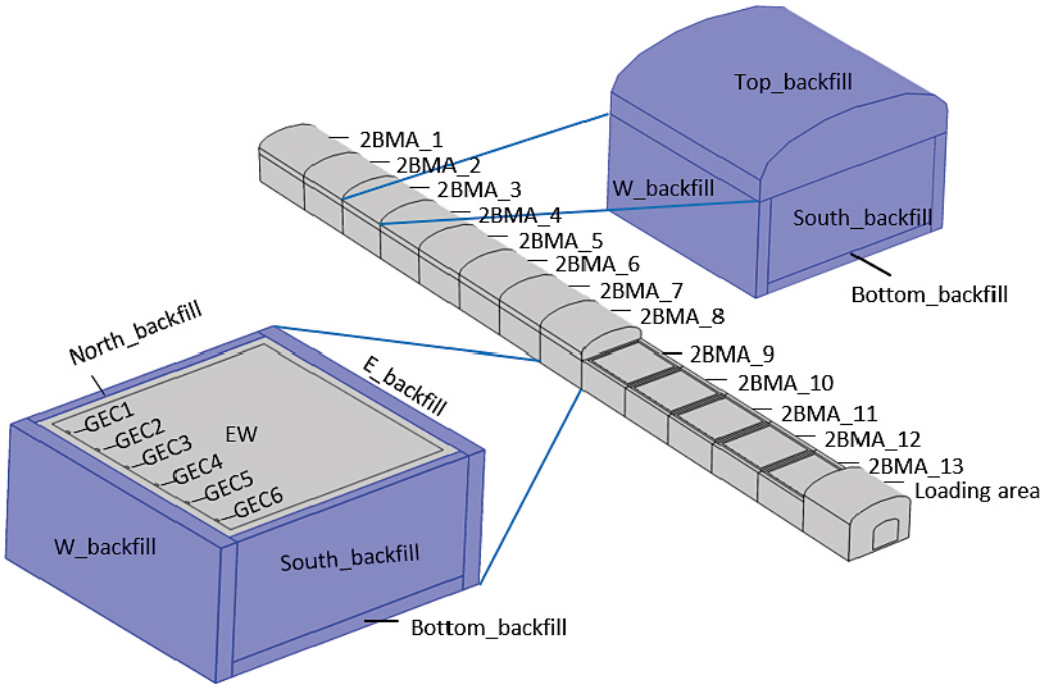

Figure 3-9. *Representation of 2BMA control volumes for Ecolego: numbering and details of control volume definition.*

The following conventions are used to name the flows:

The flows at the south side of the control volumes are indicated as y+,

The flows at the north side of the control volumes are indicated as y−,

The flows at the west side of the control volumes are indicated as x+,

The flows at the east side of the control volumes are indicated as x−.

Although the control volumes for the Silo do not line up completely with the north–south and east–west axes, the above naming scheme was applied here as well for simplicity.

3.5 Representation of the tunnels

The access ramps and tunnels were obtained directly from the CAD geometry except for the connection between the ramps of SFR 3 and SFR 1, which was directly specified in the COMSOL model (see Figure 3-1). The closure of the repository has been implemented according to Luterkort et al. (2012) as in Abarca et al. (2013). The only change relates to the material properties of the southern structural plug of the 1BLA vault. This structural plug was considered a support plug in the previous repository scale model with a hydraulic conductivity value of 1×10^{-6} m/s. Here the assumption has been changed to a gravel backfill having a hydraulic conductivity of 1×10^{-3} m/s.

3.6 Initial state of the repository materials

The hydraulic conductivities of the materials in the vaults of the SFR 1 and SFR 3 repositories are described in Table A-1 in Appendix A. The base case considers the material properties at their initial state. Almost all the assumptions underlying the selected values can be found in Abarca et al. (2013). One exception is the value of the concrete hydraulic conductivity (8.3×10^{-10} m/s in Abarca et al. 2013), which has been approximated to 1×10^{-9} m/s following the general comment after PSU-15. This impacts the value of the hydraulic conductivity of the grout and waste, that is computed as a function of the concrete conductivity. Thus, the hydraulic conductivity of the grout at initial state is 1×10^{-8} m/s, i.e., 10 times the value of the structural concrete. It also affects the hydraulic conductivity of the 1–2BTF waste domain, which depends on the hydraulic conductivities of both the waste and the concrete. The homogenized values of the hydraulic conductivities along the tunnels and perpendicular to the tunnels for the 1–2BTF waste domains were calculated based on the homogenization formulation proposed by Holmén and Stigsson (2001). The new approximation of the concrete and grout hydraulic conductivities, leads to an increase by 20 % in the hydraulic conductivity of the 1–2BTF waste domain.

Other changes with respect to the previously defined values concern mainly the configuration of 1BMA. The design of 1BMA has matured during the PSU project to accommodate construction-related requirements to improve the flow barrier properties of the concrete structure (von Schenck et al. 2015) and to incorporate the gas release systems planned for 2BMA (Elfwing et al. 2017). As a result, the internal structure of 1BMA in the present work incorporates the following features additional to those included in the preceding analysis for SR-PSU (Abarca et al. 2013):

- Reinforcement walls for the concrete structures in 1BMA (Mårtensson and Pettersson 2015).
- The foundation of grouted gravel in 1BMA that is assigned a hydraulic conductivity of 1×10^{-9} m/s on the basis of Elfwing et al. (2016).
- The grout filling the gas evacuation channels of 1BMA and 2BMA that is assigned a hydraulic conductivity of 5×10^{-9} m/s (Table 4-2 in Elfwing et al. 2017).

The rest of the material properties remain unchanged from those given in Abarca et al. (2013).

3.7 Properties of the host rock

The SFR repository is located at Forsmark, situated in crystalline rock. Groundwater moves preferentially through deformation zones and small-scale fractures. The distribution, connectivity and transmissivity of these features determine the hydraulic properties of the rock mass. The hydraulic conductivity field data were extracted from the regional hydrogeology model. These data correspond to the Case 1 (Base_Case1_DFN_R85), presented in Öhman and Odén (2018). The regional model in Öhman and Odén (2018) has the same rock properties (discrete fracture network and stochastic realization) as in the previous regional model by Odén et al. (2014). Therefore, there are no changes in the rock conductivity field reported in the previous repository-scale model. More detailed information can be found in Abarca et al. (2013).

3.8 Governing equations

3.8.1 Groundwater flow

The groundwater flow in porous media is modelled using the Subsurface Flow Module of COMSOL Multiphysics (COMSOL 2017). The water mass conservation is written as:

$$\frac{\partial(\rho\phi)}{\partial t} = -\nabla \cdot (\rho \boldsymbol{q}) + Q, \qquad \text{Equation 3-1}$$

where, $\boldsymbol{q}$ is the Darcy velocity (m/s), ρ is the water density (kg/m^3), ϕ is the porosity of the medium (–) and Q represents a sink/source term (kg/m^3/s). The Darcy velocity can be expressed as:

$$\boldsymbol{q} = -k/\mu\,(\nabla p), \qquad \text{Equation 3-2}$$

where k is the rock permeability (m^2), μ the dynamic viscosity (Pa·s) and p is the driving pressure (Pa), defined as the difference between the liquid pressure and the hydrostatic contribution ($\rho \cdot g \cdot z$), with $g = -9.81$ m/s^2 and z the elevation (negative in the present model). In this work, the repository scale simulations are performed under steady-state conditions, so that the time derivative is equal to zero. Furthermore, constant water density is assumed, and no sink/source terms are considered. As a result, Equation 3-1 reduces to its divergence free form:

$$\nabla \cdot \boldsymbol{q} = 0. \qquad \text{Equation 3-3}$$

3.8.2 Boundary conditions

Driving pressures and groundwater velocities from the regional hydrogeological simulations were extracted by means of the iDC interface (Abarca et al. 2013) and used as boundary conditions for the repository scale model. A linear interpolation function onto the domain mesh was used to impose the boundary conditions in COMSOL. As described in Abarca et al. (2013), a combination of boundary conditions was used in both the SFR 1 and SFR 3 models. A pressure field was specified on the surfaces corresponding to rock material. In addition, flux boundary conditions were specified where access tunnels intersect the model boundary. Both the pressure field and the Darcy velocity fields used as boundary conditions came from the same solution of the regional-scale model. Therefore, they are consistent in the intersection. According to Holmén and Stigsson (2001), the groundwater flow though the access ramp is limited by the groundwater divide upstream of the repository and it is not expected to increase due the presence or absence of plugs in the access ramp or to changes in the properties of the repository materials.

Four descriptions of the top boundary in DarcyTools serve as input to produce the boundary conditions for the repository scale models (Figure 3-10). These descriptions outline the time-evolution of the groundwater flow and correspond to four different positions of the shoreline relative to the repository:

- Shoreline position 1 (in the global warming and early periglacial climate cases, this position would correspond to the situation at 2000 AD): corresponds to a submerged repository.
- Shoreline position 2 (in the global warming and early periglacial climate cases, this position would correspond to the situation at 2500 AD): the shoreline is located right over the SFR 1 and 3 repositories. Parts of the repositories are situated below a small emerged peninsula. This situation was not considered in Abarca et al. (2013).
- Shoreline position 3 (in the global warming and early periglacial climate cases, this position would correspond to the situation at 3500 AD): corresponds to an intermediate case in which the shoreline has moved north away from the repository.
- Shoreline position 4 (in the global warming and early periglacial climate cases, this position would correspond to the situation at 5000 AD): corresponds to a retreating shoreline position, well removed from the repository.

The different shoreline positions are illustrated in Figure 3-10 below. Note that there is no correspondence between the shoreline position number here and in Abarca et al. (2013). There, three shoreline positions were analysed labelled shoreline positions 1, 2 and 3 that corresponded to 2000 AD, 3000 AD and 5000 AD, respectively. Therefore, to avoid misunderstandings, in this report we refer to the different shoreline positions by the time associated with them in the global warming and early periglacial climate cases. Thus, shoreline positions 1 and 3 of Abarca et al. (2013) correspond to the shoreline positions at times 2000 AD and 5000 AD, whereas the other two shoreline positions corresponding to 2500 AD and 3500 AD have no direct correspondence with the shoreline positions in Abarca et al. (2013). More information about the climate cases can be found in SKB (2014a).

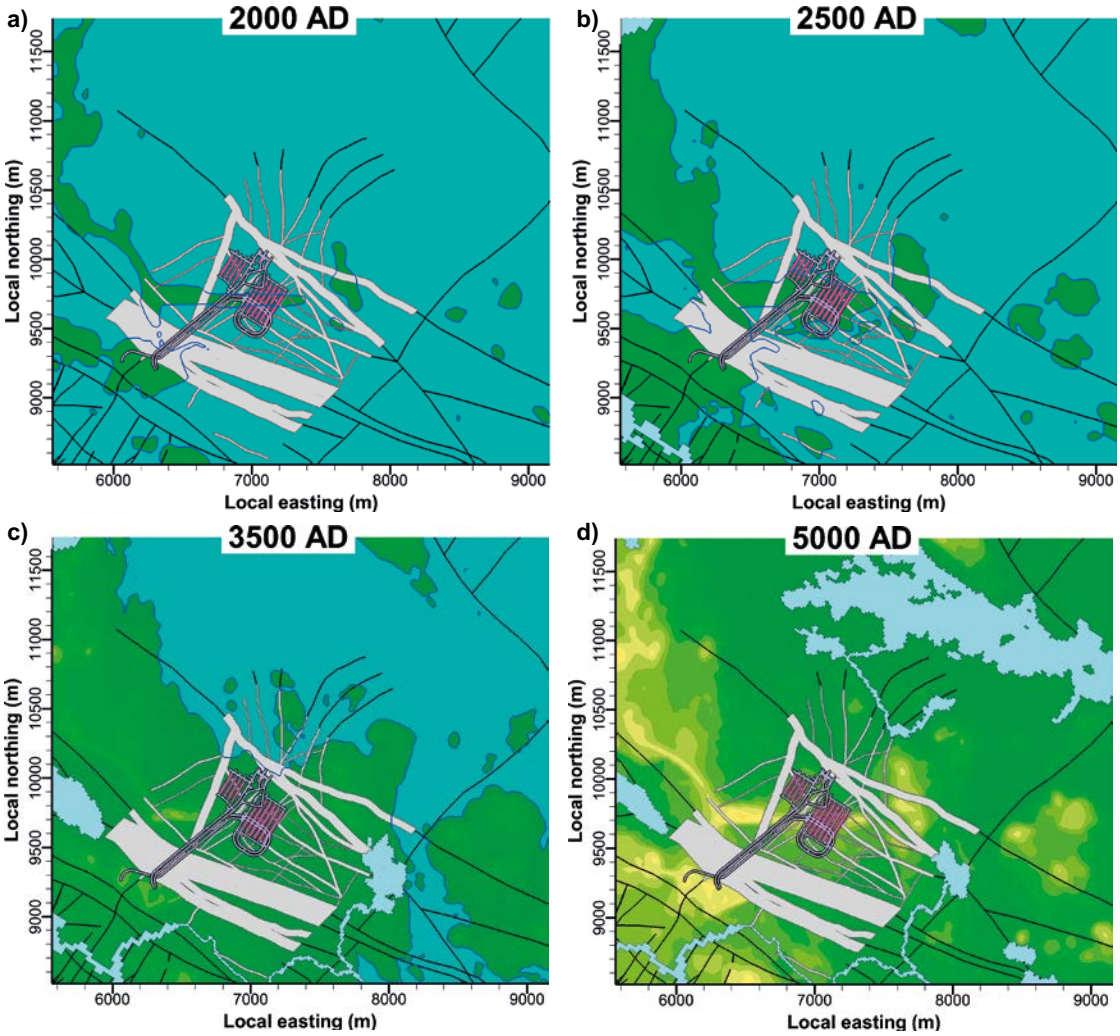

Figure 3-10. *Four shoreline positions with respect to the SFR repository used as boundary conditions for regional hydrological simulations (Odén et al. 2014).*

4 SFR 1 Calculation cases

4.1 Base case

This section presents the results of the Base case for four different shoreline positions (Figure 3-10). The Base case refers to a given set of hydraulic properties for the engineered barriers (Table A-1 in Appendix A) and to a given rock permeability field. The rock permeability field corresponds with the Base_Case1_DFN_R85 in Öhman and Odén (2018). Four DarcyTools simulations, with different top boundary conditions, of the regional hydrogeology serve as input to the repository-scale model. These simulations relate to the different shoreline positions (for more details see Section 3.8.2). Streamlines were generated to illustrate the flow field around the repository. The streamline is a curve everywhere tangent to the steady state Darcy velocity field.

4.1.1 Groundwater flow field at 2000 AD

At 2000 AD, the repository is situated below the regional groundwater discharge area (Figure 3-10). This situation corresponds to shoreline position 1 in Abarca et al. (2013). The streamlines showing the paths followed by the groundwater reaching and leaving each individual vault are illustrated in Figure 4-1. No differences are found with respect to the flow field described in Abarca et al. (2013) for shoreline position 1. Groundwater flows vertically upwards from deformation zone ZFM871 towards the repository vaults and from there towards the surface.

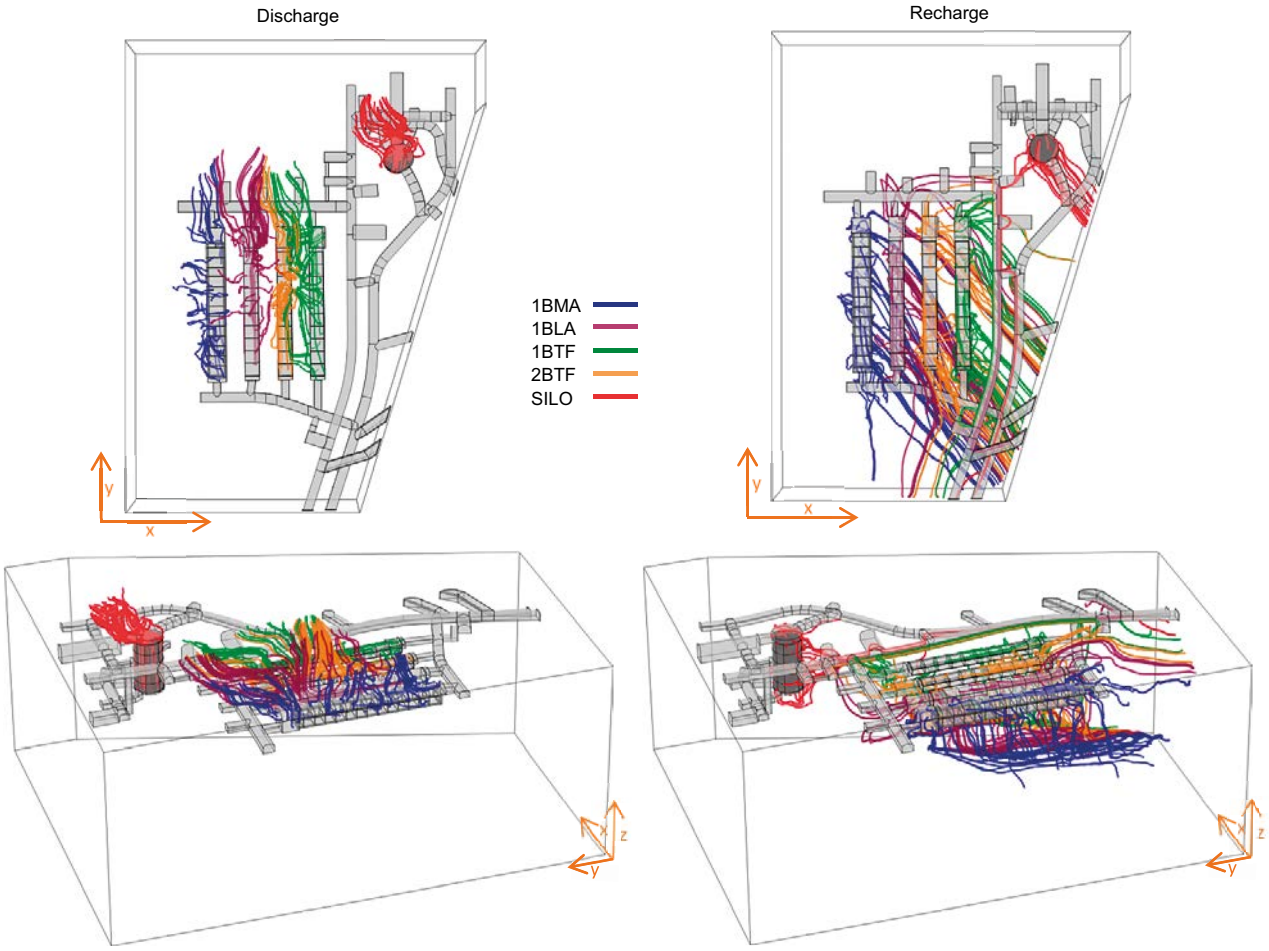

Figure 4-1. *Groundwater streamlines leaving (left) and reaching (right) individual vaults (colour tubes) for the Base case at 2000 AD. The x- and y-arrows point to the east and north, respectively.*

4.1.2 Groundwater flow field at 2500 AD

At 2500 AD, the shoreline is located right over the SFR 1 repository. The southernmost part of the repository is situated below a small emerged peninsula, whereas its northern part is located under the sea (Figure 3-10). This situation was not considered in Abarca et al. (2013). The streamlines (Figure 4-2) illustrate an inversion in flow direction with respect to 2000 AD. Groundwater recharge from the emerged peninsula reaches the vaults at their southern part. The water leaving the vaults can be differentiated according to the streamlines. Part of the water flows down and, when it reaches the deformation zone ZFM871, it flows towards the northwest and leaves the model domain through its lateral boundary. However, there is another portion that moves upwards from the vaults and discharges above the repository. In this case, the recharge and discharge areas of the water reaching the repository are very close. This implies a very local flow system with relatively short travel times from the surface to the vaults and vice versa.

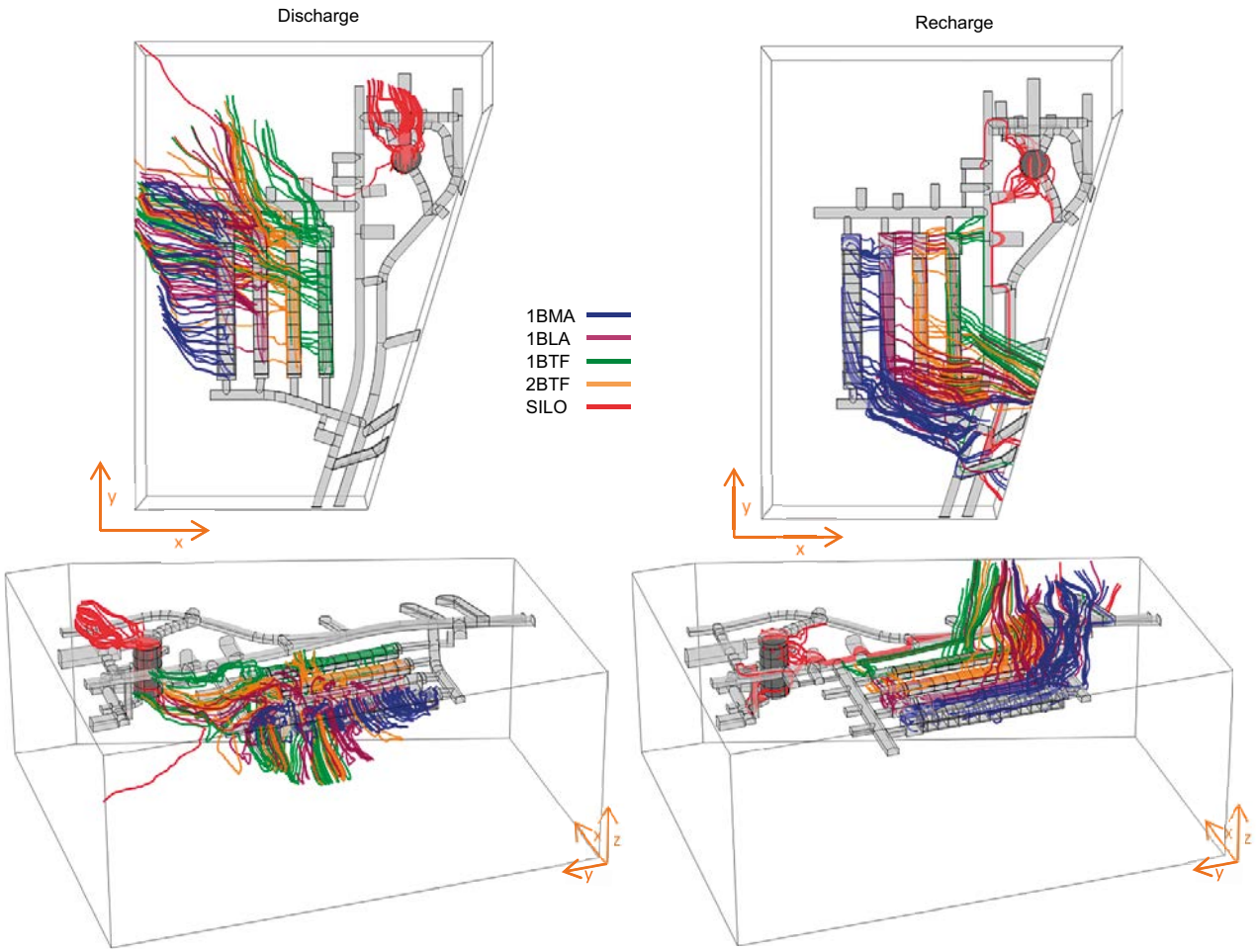

Figure 4-2. *Groundwater streamlines leaving (left) and reaching (right) individual vaults (colour tubes) for the Base case at 2500 AD. The x- and y-arrows point to the east and north, respectively.*

4.1.3 Groundwater flow field at 3500 AD

At 3500 AD, the shoreline is located north of the repository. The repository is situated below a groundwater recharge area (Figure 3-10). There is no corresponding shoreline position in Abarca et al. (2013). However, the observed flow field is similar to the one described in Abarca et al. (2013), for shoreline position 2, which corresponded to 3000 AD.

The groundwater flow paths to each individual vault are illustrated in Figure 4-3 (right). At 3500 AD, the groundwater reaching the vaults originates at the top boundary, south of the repository and reaches the east side of the vaults 1BMA, 1BLA, 1BTF and 2BTF through the deformation zone ZFMNNW120. Groundwater reaches the Silo dome mainly through the access tunnels. Outflow from the vaults (Figure 4-3, left) moves downwards through ZFMNNW1209 and northwest towards ZFMNNE0869. A portion of the Silo discharge flows north towards the model boundary.

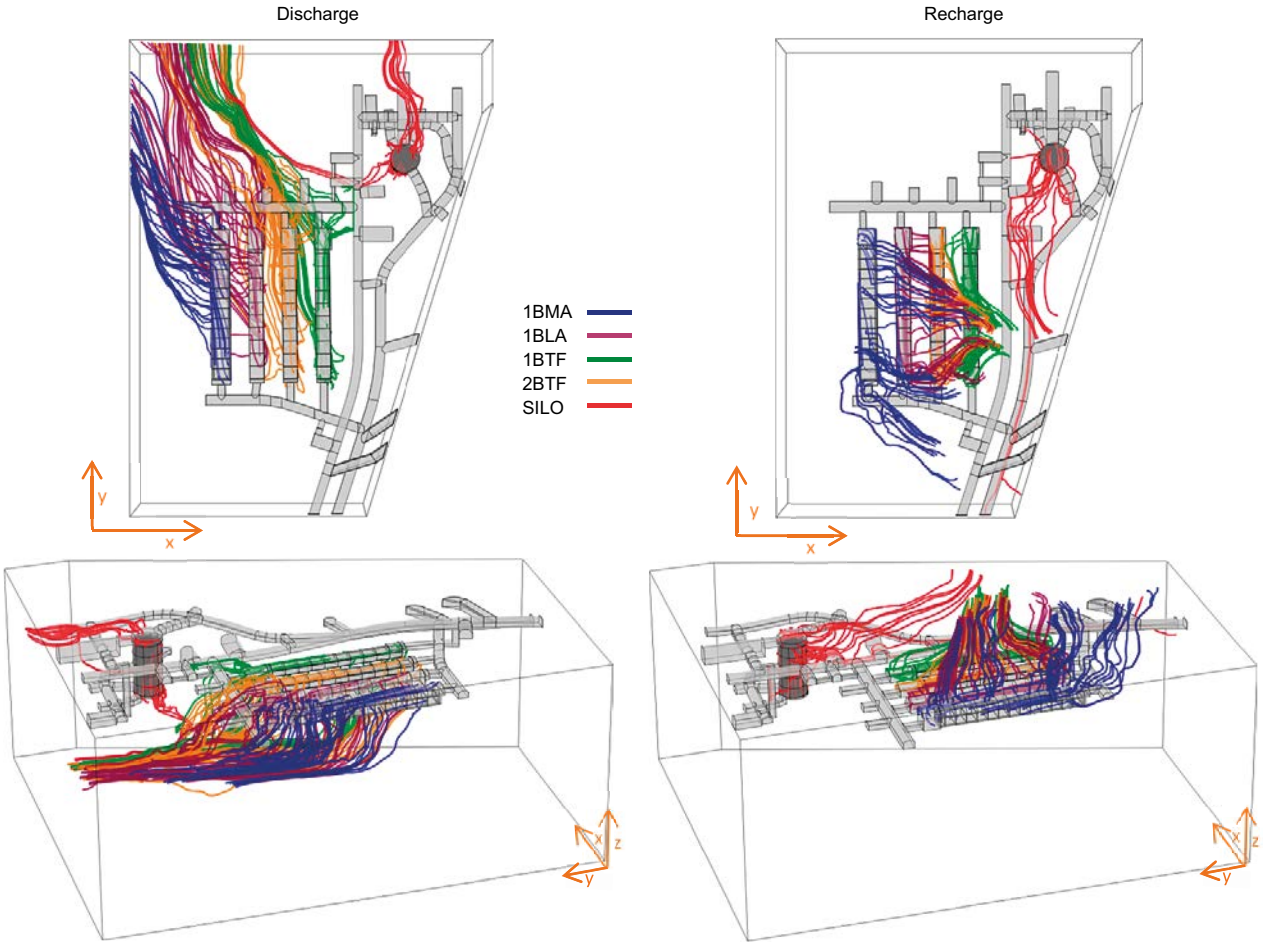

Figure 4-3. *Groundwater streamlines leaving (left) and reaching (right) individual vaults (colour tubes) for the Base case at 3500 AD. The x- and y-arrows point to the east and north, respectively.*

4.1.4 Groundwater flow field at 5000 AD

At 5000 AD, the repository is situated below a groundwater recharge area with the shoreline 1 km further north (Figure 3-10). This situation corresponds to shoreline position 3 in Abarca et al. (2013). No substantial differences are found in the flow field around the repository (Figure 4-4). A distributed recharge from the top boundary penetrates vertically through the deformation zone ZFMNNW1209 and other minor fractures towards the repository. The outflow moves downwards vertically from the vaults until the sub-horizontal deformation zone ZFM871 is reached and then moves north from the repository (Figure 4-4 left). The flow field is similar to that computed for 3500 AD but streamlines show deeper and longer pathways within the model domain, indicating that the main recharge zone has moved south, and the discharge zone is further north.

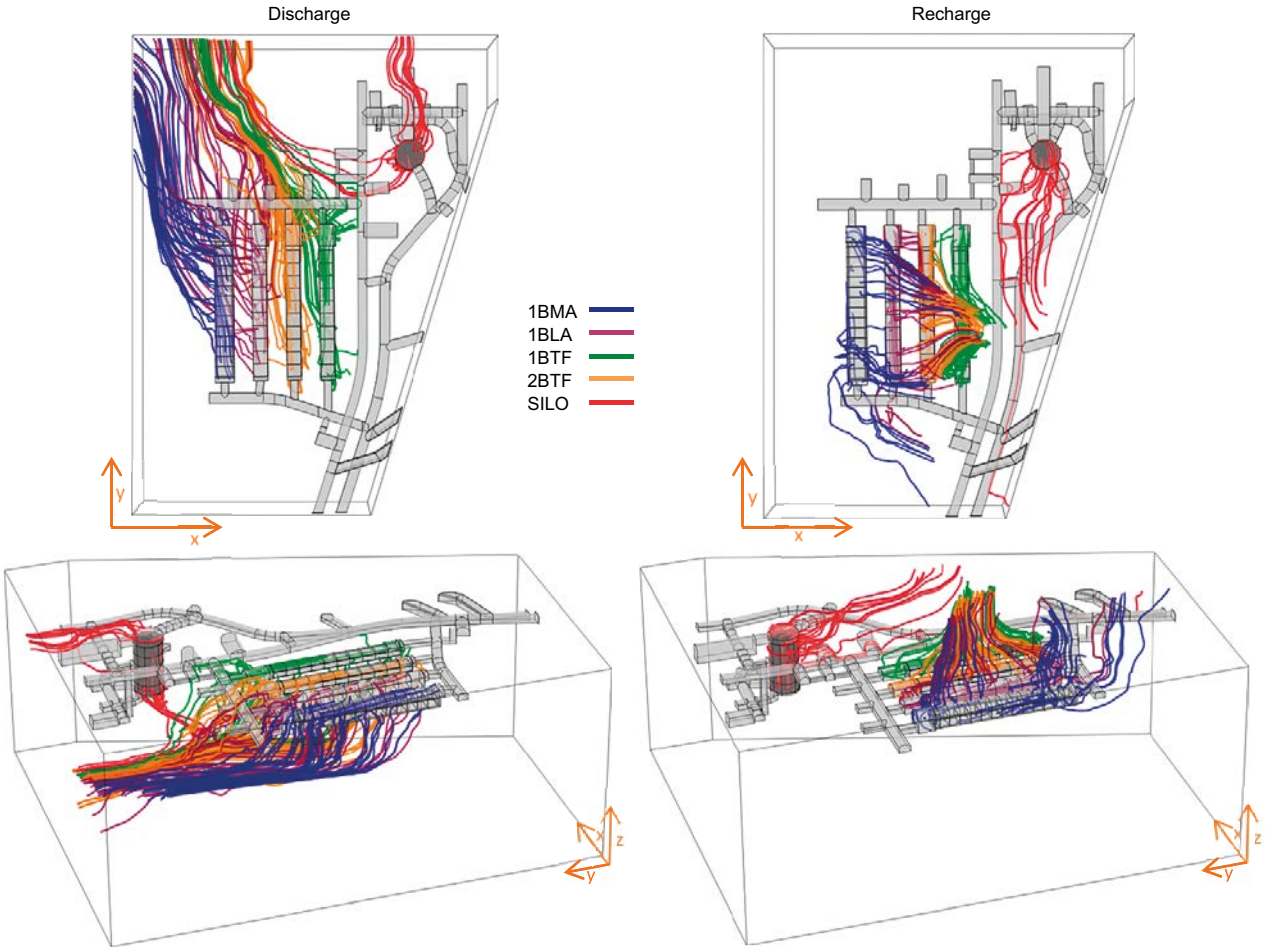

Figure 4-4. *Groundwater streamlines leaving (left) and reaching (right) individual vaults (colour tubes) for the Base case at 5000 AD. The x- and y-arrows point to the east and north, respectively.*

4.1.5 Total flow through the vaults and waste

The total flow through the vaults and through the waste domains is presented for each shoreline position. The total flow for a given waste or vault volume (m^3/year) is calculated as the sum of the total flow across each of the surfaces *i* defining the volume *v*:

$$\text{Total flow}_i = 0.5 \cdot (\text{abs(inflow)} + \text{abs(outflow)}) \qquad \text{Equation 4-1}$$

$$\text{Total flow}_v = \sum_i \text{Total flow}_i \qquad \text{Equation 4-2}$$

Table 4-1 shows the calculated total flow through the vaults and waste domains for the four shoreline positions. The flow through the vaults increases with time as the shoreline position recedes. The largest increase expressed as a percentage of the original flow occurs between 2000 and 2500 AD when the flow increases up to 2 orders of magnitude in 1BTF. This increase corresponds to the passage of the shoreline position over the repository and the change from being below a discharge area to being below a recharge area. The shorelines positions at 3500 AD and 5000 AD yield similar flow values. The flow at the model boundaries through the rock and through the ramp sections and the ratio between them is computed (Table 4-1). The results indicate that the flow through the ramp is at most 3 % for all shoreline positions. The largest percentage (3 %) is obtained for 2000 AD, when the total flow is much lower than for the rest of the shoreline positions. Therefore, the main source of groundwater recharge to the repository is infiltration through the rock in all cases.

The water flows through the wastes follow the trend observed for the flows through the vaults. The largest increase expressed as a percentage of the original flow occurs from 2000 AD to 2500 AD, but the proportion of flow that enters the waste with respect to the flow that enters the vault decreases. The ratio waste/vault flow approaches 1 in the vaults with similar waste and vault domains (1BLA and Silo). Note that the waste and vault domains in 1BLA differ uniquely in the volume occupied by the loading area. For the rest of the vaults, the ratio indicates the performance of the EBS. Ratios of 0.33 and 0.21 are obtained in 1BTF and 2BTF, respectively at 2000 AD, when the groundwater flow around the repository has an upwards component. The ratio remains equal or lower than 0.16 in the vaults with EBS for the rest of the shoreline positions. The ratio is 0.16 for 1BMA at 2000 AD and goes down to 0.04–0.06 for the rest of the shoreline positions. This ratio is close to the values computed for BTF and evidences the low efficiency of the hydraulic cage in 1BMA when the foundation is grouted.

Table 4-1. Total flows through the SFR 1 vaults and waste domains (m^3/year) for the Base case.

Total flow (m^3/year)		2000 AD	2500 AD	3500 AD	5000 AD
Boundaries	Rock	12.47	685.02	9690	11750
	Ramp	0.39	14.22	64.65	123.39
	Total	12.52	699.24	9755	11873
	Ratio Ramp/Total	0.03	0.02	0.007	0.01
Vaults	1BMA	0.0435	2.67	55.9	58.3
	1BLA	0.122	5.82	122	133
	1BTF	0.0288	2.84	21.7	24.5
	2BTF	0.0429	3.24	40.5	45
	Silo*	0.00459	0.178	0.933	1.3
Waste	1BMA	0.00691	0.102	2.94	3.57
	1BLA	0.118	5.39	120	131
	1BTF	0.00943	0.328	3.52	3.98
	2BTF	0.00921	0.213	4.58	5.1
	Silo	0.00446	0.168	0.88	1.29
Ratio waste/vault	1BMA	0.16	0.04	0.05	0.06
	1BLA	0.97	0.93	0.98	0.98
	1BTF	0.33	0.12	0.16	0.16
	2BTF	0.21	0.07	0.11	0.11
	Silo	0.97	0.94	0.94	0.99

* The Silo vault does not include the gravel dome.

The comparison with the results from previous simulations reported in Abarca et al. (2013) is presented in Table 4-2. The flows through 1BMA are compared against the case of low conductivity beams in Abarca et al. (2014). In both cases, there is not a perfect hydraulic cage configuration. Only the two comparable shoreline positions, i.e., 2000 AD (shoreline position 1 in Abarca et al. 2013) and 5000 AD (shoreline position 3 in Abarca et al. 2013) are reported. In general, the new configuration leads to similar flow results. A maximum increase of 37 % is found in 1BTF and of 3 % in neighbouring 2BTF. The flow though the waste follows the increase in flow through the 1BTF vault. The increase in flow in the 1–2BTF depends on the value of the homogenized hydraulic conductivity of the waste domain (see Section 3.6), which is 20 % larger than in Abarca et al. (2013). The waste domain occupies most of the vault and the flow changes almost linearly with the increase in the homogenised conductivity. The increase is larger in 1BTF, which is located upstream from the rest of the vaults (see Figure 4-1 and Figure 4-4). As explained in Abarca et al. (2013), there is a redistribution of flow between the vaults. An increase in flow in the vaults upstream is compensated by a decrease in the flow through the vaults located downstream. This is the case here, where the flow increase in the 1–2BTF is compensated by a flow decrease in the rest of the vaults. Besides the change in the hydraulic conductivity of 1–2BTF, there are two other changes with respect to the models reported in Abarca et al. (2014) that could potentially impact the flows. One of them is the change in the material properties of the southern structural plug of 1BLA, whose hydraulic conductivity has been modified from 1×10^{-6} m/s to 1×10^{-3} m/s. This change does not have an impact on the flow through the 1BLA vault. The other change is the connection of the SFR 3 ramp with the existing tunnels according to layout 2.6. The impact of this change alone has been evaluated by Öhman and Odén (2018) to be around 0.1 % for the individual vaults in SFR 1 at 5000 AD.

Table 4-2. Ratios of the total flow through the SFR 1 vaults with respect to the Base case in Abarca et al. (2013). Ratios lower than one indicate a reduction in the total flow with respect to the flows reported in Abarca et al. (2013).

Ratio		2000 AD	5000 AD
Vaults	1BMA	0.95	0.88
	1BLA	0.92	0.91
	1BTF	1.03	1.37
	2BTF	0.91	1.03
	Silo*	0.92	0.88
Waste	1BMA	0.86	1.04
	1BLA	0.96	0.94
	1BTF	1.05	1.14
	2BTF	1.02	1.12
	Silo	0.89	0.95

* The Silo vault does not include the gravel dome.

4.2 Barrier degradation

4.2.1 Concrete degradation

This section explores the effect of concrete barrier degradation on the total flow entering the tunnels and waste compartments of the SFR 1 vaults for the four shoreline positions (2000 AD, 2500 AD, 3500 AD and 5000 AD). As in Abarca et al. (2013), this effect has been studied with a set of three simulations referred to as moderate (MCD), severe (SCD), and complete (CCD) concrete degradation. The hydraulic conductivities of the different degradation states are defined in Appendix A. The hydraulic conductivity values of the degraded concrete and grout are selected to cover the range of values suggested to be used for different time periods and for different parts of SFR in SR-PSU (SKB 2014b). The three stages of degradation are defined between the hydraulic conductivity at

initial state and a case of complete failure with a hydraulic conductivity of 1×10^{-3} m/s. Moreover, the hydraulic conductivity of the waste (K_{waste}, m/s) has been selected considering the safety functions assumed for the waste packages and concrete structures of the repository. A safety function is a property by means of which a component contributes to the long-term safety of the repository. The concrete structures of the Silo and the BMA vaults, as well as the concrete tanks of the BTF vault, are considered to be flow barriers with the safety function to minimize advective flow. This safety function is not assigned to the waste packages, which are therefore not assumed to restrict groundwater flow. To represent these assumptions in the models the hydraulic conductivity of the waste has been set to a value 1 000 times greater than the hydraulic conductivity of the associated concrete structure ($K_{concrete}$, m/s). When concrete degradation is considered, this permeability ratio is also maintained. However, an upper limit for the hydraulic conductivity of the waste has been set to 1×10^{-3} m/s, such that no hydraulic contrast exists in a vault when the concrete is assumed to be completely degraded.

The flows through the boundaries of the rock and ramp sections have been calculated for all the degradation cases. The variation with respect to the base case (Table 4-1) is less than 1 ‰, which demonstrates that the boundary conditions are not affected by the change in the hydraulic conductivity of the concrete barriers. The flows through the vaults and waste for the concrete degradation cases are tabulated in Table B-2, Table B-3, Table B-4, Table B-5 in Appendix B, for 2000 AD, 2500 AD, 3500 AD and 5000 AD, respectively. Graphically, the flows are illustrated in Figure 4-5, Figure 4-6, Figure 4-7 and Figure 4-8. The colour of the bars refers to the Base case (BC) simulation and the three degradation cases MCD, SCD and CCD. The total bar height indicates the vault flow whereas the heights of the coloured portions illustrates the flow through the waste. Thus, the grey portion of the bar corresponds to the vault flow that does not enter the waste domain. The table of flow values (m^3/year) in the figures indicates the flow through the waste.

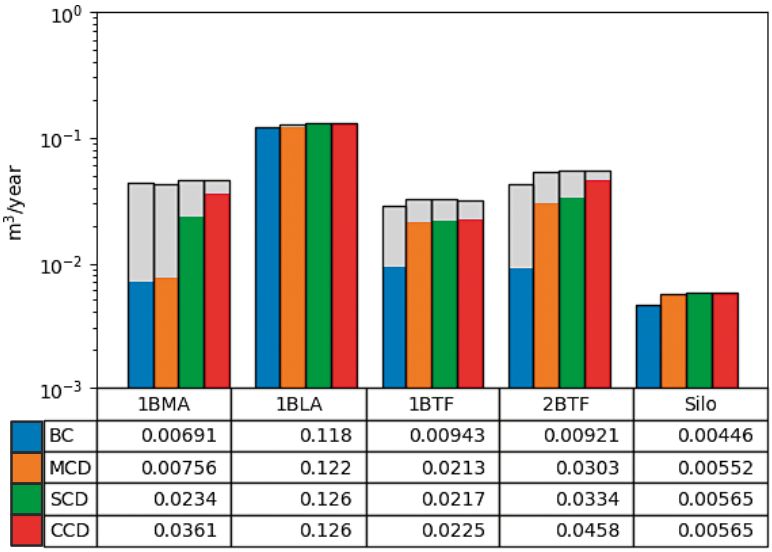

	1BMA	1BLA	1BTF	2BTF	Silo
BC	0.00691	0.118	0.00943	0.00921	0.00446
MCD	0.00756	0.122	0.0213	0.0303	0.00552
SCD	0.0234	0.126	0.0217	0.0334	0.00565
CCD	0.0361	0.126	0.0225	0.0458	0.00565

Figure 4-5. *Total flow (m^3/year) through the waste for the base case and three concrete degradation cases, studied at 2000 AD. The total bar height illustrates the vault flow whereas the height of the coloured portion illustrates the flow through the waste. Thus, the grey portion of the bar corresponds to the vault flow outside the waste compartment. The table gives the flow values through the waste (m^3/year).*

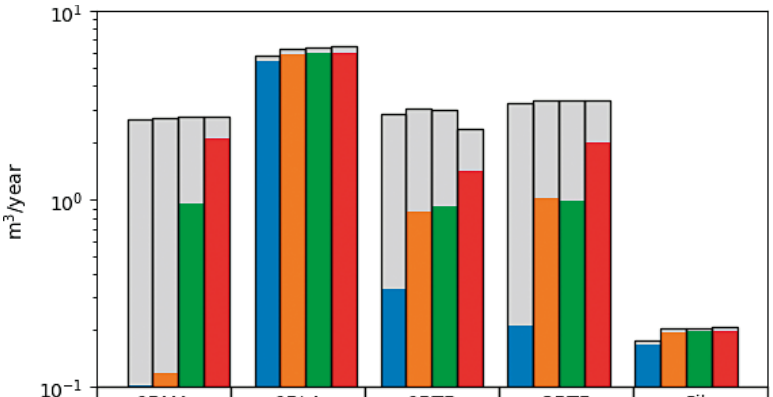

	1BMA	1BLA	1BTF	2BTF	Silo
BC	0.102	5.39	0.328	0.213	0.168
MCD	0.119	5.88	0.867	1.02	0.196
SCD	0.946	6.02	0.924	0.982	0.198
CCD	2.09	6.02	1.43	1.99	0.2

Figure 4-6. *Total flow (m^3/year) through the waste for the base case and three concrete degradation cases, studied at 2500 AD. The total bar height illustrates the vault flow whereas the height of the coloured portion illustrates the flow through the waste. Thus, the grey portion of the bar corresponds to the vault flow outside the waste compartment. The table gives the flow values through the waste (m^3/year).*

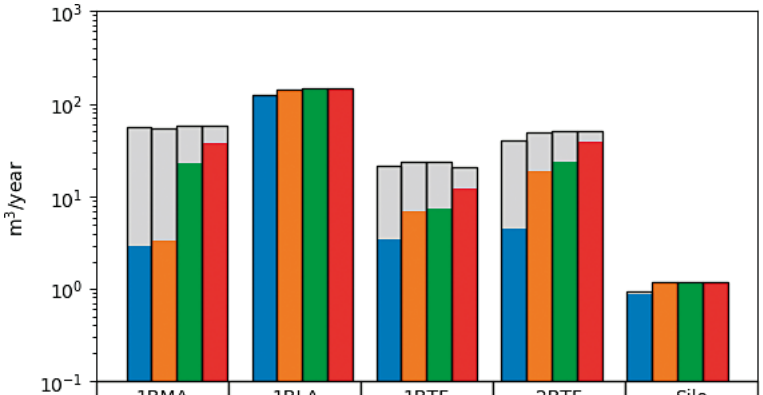

	1BMA	1BLA	1BTF	2BTF	Silo
BC	2.94	120	3.52	4.58	0.88
MCD	3.34	138	6.91	18.9	1.15
SCD	22.7	145	7.57	23.6	1.17
CCD	38.3	145	12.3	39.2	1.18

Figure 4-7. *Total flow (m^3/year) through the waste for the base case and three concrete degradation cases, studied at 3500 AD. The total bar height illustrates the vault flow whereas the height of the coloured portion illustrates the flow through the waste. Thus, the grey portion of the bar corresponds to the vault flow outside the waste compartment. The table gives the flow values through the waste (m^3/year).*

The results show that concrete degradation affects the flows through the wastes in vaults with concrete barrier systems, i.e., 1BMA and 1–2BTF. The flow increases when increasing the hydraulic conductivity of the concrete barriers. In 1BMA, the flow through the waste for the MCD case is only 10 % higher than for the BC. However, an abrupt increase in the flow occurs from the moderate to the severe concrete degradation case, i.e., when the hydraulic conductivity of the concrete increases from 1×10^{-7} to 1×10^{-5} m/s.

The 1–2BTF vaults contain grout as EBS. In these vaults, the sharpest increase in flow occurs between the BC and the MCD. This interval corresponds to a change in the hydraulic conductivity of the grout from 1×10^{-8} to 1×10^{-6} m/s. The results from the 1BMA and 1–2BTF vaults show consistently the loss of the hydraulic barrier effect when the hydraulic permeability of the concrete barrier reaches 1×10^{-6} m/s.

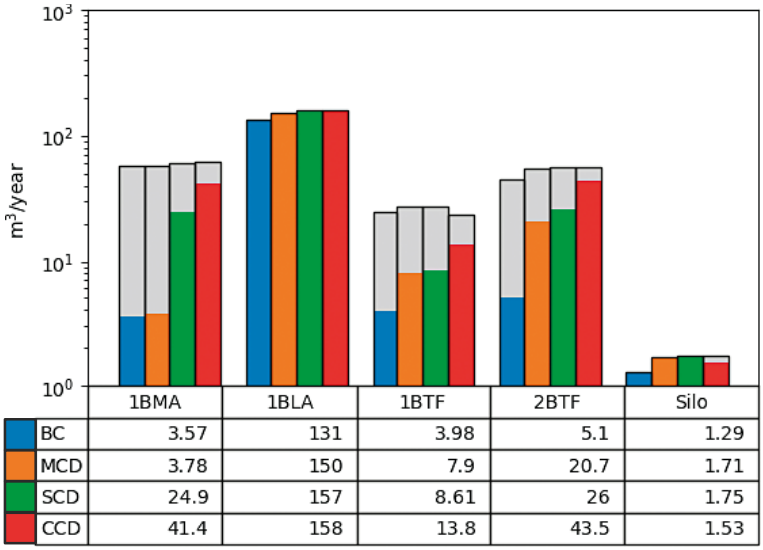

	1BMA	1BLA	1BTF	2BTF	Silo
BC	3.57	131	3.98	5.1	1.29
MCD	3.78	150	7.9	20.7	1.71
SCD	24.9	157	8.61	26	1.75
CCD	41.4	158	13.8	43.5	1.53

Figure 4-8. *Total flow (m^3/year) through the waste for the base case and three concrete degradation cases, studied at 5000 AD. The total bar height illustrates the vault flow whereas the height of the coloured portion illustrates the flow through the waste. Thus, the grey portion of the bar corresponds to the vault flow outside the waste compartment. The table gives the flow values through the waste (m^3/year).*

Table 4-3 shows the ratios of the total flow through the SFR 1 vaults for the concrete degradation cases with respect to the base case. The ratios illustrate that the concrete degradation does not affect substantially the total flow through the vaults. The degradation of the concrete barriers does not impact the flow through the vault because the active flow barriers are the rock and the bentonite plugs. Both restrain the flow that reach the vaults independently of the inner vault structure. However, the impact on the flow through the waste is substantial. The maximum impact of concrete degradation to the flow through the waste in 1BMA and 1–2BTF occurs at 2500 AD. In the CCD case, the flow through the waste increases one order of magnitude in 2BTF and it increases to up to 20 times the flow in the base case for 1BMA.

Table 4-3. Ratio of the total flow through the SFR 1 vaults for the concrete degradation cases with respect to the Base case.

		2000 AD			2500 AD			3000 AD			5000 AD		
		MCD	SCD	CCD	MCD	SCD	CCD	MCD	SCD	CCD	MCD	SCD	CCD
Vaults	1BMA	0.98	1.06	1.06	1.01	1.03	1.03	0.98	1.04	1.05	0.98	1.05	1.05
	1BLA	1.04	1.07	1.07	1.08	1.11	1.11	1.15	1.20	1.20	1.14	1.20	1.20
	1BTF	1.14	1.14	1.09	1.07	1.05	0.83	1.11	1.10	0.95	1.11	1.10	0.96
	2BTF	1.24	1.28	1.27	1.04	1.04	1.04	1.23	1.26	1.26	1.22	1.26	1.25
	Silo	1.22	1.24	1.25	1.15	1.16	1.16	1.24	1.25	1.26	1.32	1.35	1.35
Waste	1BMA	1.09	3.39	5.22	1.17	9.27	20.49	1.14	7.72	13.03	1.06	6.97	11.60
	1BLA	1.03	1.07	1.07	1.09	1.12	1.12	1.15	1.21	1.21	1.15	1.20	1.21
	1BTF	2.26	2.30	2.39	2.64	2.82	4.36	1.96	2.15	3.49	1.98	2.16	3.47
	2BTF	3.29	3.63	4.97	4.79	4.61	9.34	4.13	5.15	8.56	4.06	5.10	8.53
	Silo	1.24	1.27	1.27	1.17	1.18	1.19	1.31	1.33	1.73	1.33	1.36	1.19

4.2.2 Plug degradation

This section describes the effect of plug degradation on the groundwater flow and on the total flow entering the tunnels and waste compartments of the SFR 1 vaults. Three different degradation states, besides the intact state of the Base case, were considered for 5000 AD. They are referred to as moderate plug degradation (MPD), severe plug degradation (SPD) and complete plug degradation (CPD). The hydraulic conductivity of the plugs for each degradation state is presented in Appendix A.

The flows through the boundaries of the rock and ramp sections have been calculated for all the plug degradation cases. In the CPD case, the change with respect the Base case (Table 4-1) is less than 2 %, demonstrating a minimal impact on the boundary conditions following the extreme change in the hydraulic conductivity of the plugs. The flows through the vaults and wastes for the plug degradation cases at 5000 AD are tabulated in Table B-6 in Appendix B. Graphically, the flows are illustrated in Figure 4-9. Table 4-4 shows the ratio of the total flow through the SFR 1 vaults for the plug degradation cases with respect to the Base case.

Table 4-4. Ratio of the total flow through the SFR 1 vaults for the plug degradation cases with respect to the Base case.

		MPD	SPD	CPD
Vaults	1BMA	1.01	1.19	1.73
	1BLA	1.02	1.11	4.41
	1BTF	1.05	1.98	27.22
	2BTF	1.03	1.74	11.04
	Silo	0.97	1.34	1.62
Waste	1BMA	1.00	1.26	1.76
	1BLA	1.01	1.11	4.31
	1BTF	0.98	0.55	0.47
	2BTF	0.99	0.78	0.44
	Silo	0.97	1.33	1.60

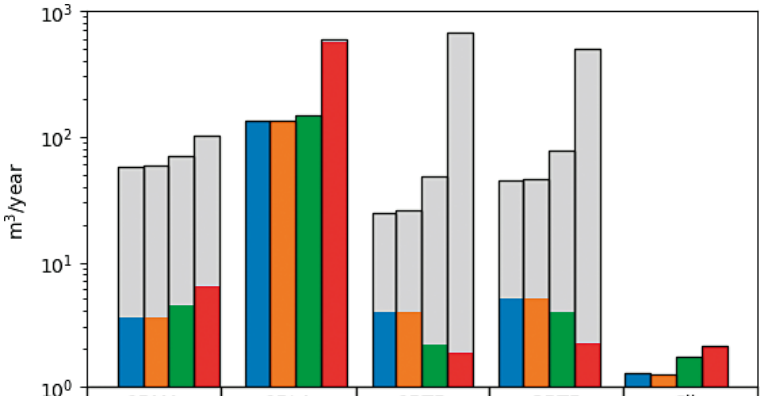

	1BMA	1BLA	1BTF	2BTF	Silo
BC	3.57	131	3.98	5.1	1.29
MPD	3.57	132	3.9	5.03	1.25
SPD	4.49	145	2.18	3.98	1.71
CPD	6.27	564	1.88	2.25	2.06

Figure 4-9. *Total flow (m^3/year) through the waste for the base case and three plug degradation cases, studied at 5000 AD. The total bar height illustrates the vault flow whereas the height of the coloured portion illustrates the flow through the waste. Thus, the grey portion of the bar corresponds to the vault flow outside the waste compartment. The table gives the flow values through the waste (m^3/year).*

The plug degradation impacts the total flow through the vaults. However, the computed flow increase is small for the BC and MPD case. When the hydraulic conductivity of the plugs gets higher than 1×10^{-6} m/s (CPD) there is a substantial increase in the total flow through the vaults (Table 4-4). The sensitivity of the vaults to the plug degradation is explained by their relative location with respect to the flow direction. The most sensitive vaults to the complete degradation of the plugs are those located upstream. As illustrated in Figure 4-10, the downwards recharge has a component from east to west. Thus, the maximum increase in the flow through the vaults occurs in 1BTF, followed by 2BTF and 1BLA. The flow through 1BMA, which is located furthest downstream, increases, in the CPD case, by 73 % with respect to the Base case.

The increase in vault flow is accompanied by an increase in the flow through the waste. This increase is more pronounced in 1BLA, which does not have other flow barriers. The 1–2BTF vaults are an exception. In these vaults, the flow through the waste decreases as the flow through the tunnel increase. The degradation of the plugs facilitates the connection between the north and south access tunnels through the backfill. This creates a preferential flow path that prevents water being forced laterally from the rock through the waste.

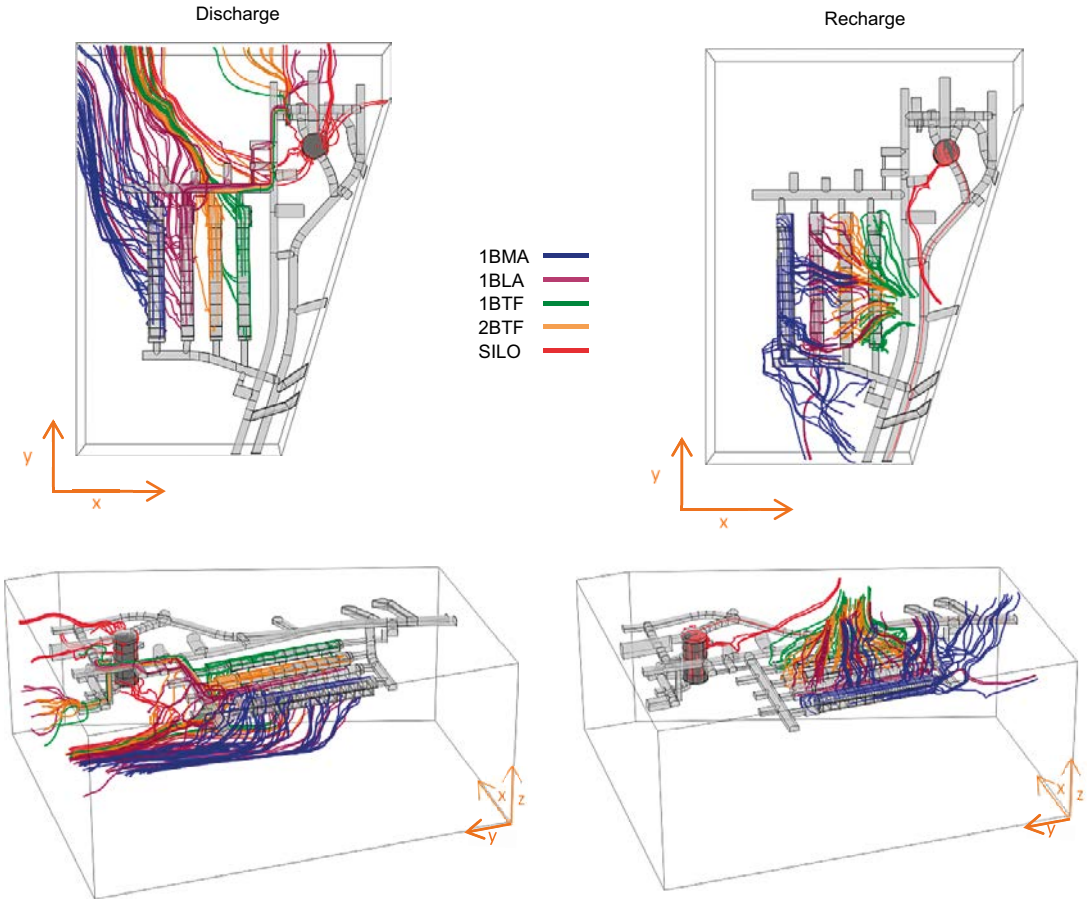

Figure 4-10. *Groundwater streamlines leaving (left) and reaching (right) individual vaults (colour tubes) for the case of complete plug degradation at 5000 AD. The x- and y-arrows point to the east and north, respectively.*

4.2.3 No barriers

This calculation case simulates the complete degradation of the concrete barriers and the bentonite barriers simultaneously. This case is a combination of the completely degraded concrete and the completely degraded plugs cases, in addition to the complete degradation of the Silo bentonite walls and the sand-bentonite top and bottom layers. All the concrete and bentonite domains have a conductivity of 10^{-3} m/s (Appendix A). This case has been evaluated for 5000 AD.

The flows through the vaults and wastes for the no barriers case for 5000 AD are tabulated in Table B-7, Appendix B. Graphically, the flows are illustrated in Figure 4-11. Table 4-5 shows the ratio of the total flow through the SFR 1 vaults for the no barrier case (NB) with respect to the Base case, and the complete plug degradation case presented in Section 4.2.2. The total flow through the repository is increased one order of magnitude in the no barriers case with respect to the Base case. The most affected vault is by far the Silo, for which the flow (vault and waste) is increased by almost three orders of magnitude with respect to the Base case and the complete plug degradation case. The reason why the increase is largest for the Silo is due to the effect of complete degradation of the bentonite walls and sand-bentonite top and bottom layers. In this situation, there is no flow barrier in the Silo, as opposed to the rest of the simulation cases. The Silo receives twice the flow of the rest of the vaults combined. This preferential flow through the Silo can be explained by a combination of the direction of the flow with respect to the vault direction and the surrounding rock permeability. At 5000 AD, there is a general downwards groundwater gradient. In the absence of barriers, the vertical Silo becomes a preferential flow path parallel to the groundwater gradient. Figure 4-12 shows the streamlines reaching and leaving the vaults for the case of no barriers. The recharge to the Silo occurs from the access tunnels (and even through 2BTF) but also through the rock. The recharge from the rock is concentrated in an area of high rock permeability located south of the Silo (Figure 4-13) that connects to a deformation zone parallel to the access tunnels (ZFMNE0870). The repository without barriers connects the flow from the west and east of this deformation zone which does not occur in the presence of barriers. The discharge flow lines indicate that in the absence of barriers there is a connection between the northern part of the vaults and the Silo. There is discharge from the 1–2BTF vaults reaching the plugs north of the Silo. This occurred to a lesser extent in the case of complete plug degradation (Figure 4-10). In other cases, the Silo is well isolated from the rest of the vaults. Compared with the Base case, apart from the Silo, the degree of effect inversely correlates with the vault distance to the access ramp. This impact is consistent with the results obtained for the complete plug degradation case. The flow increase is due to divergence of flow only, i.e. flow in the rock is diverted to paths with less resistance through the repository whereas the global driving pressure and flux to the repository is constant.

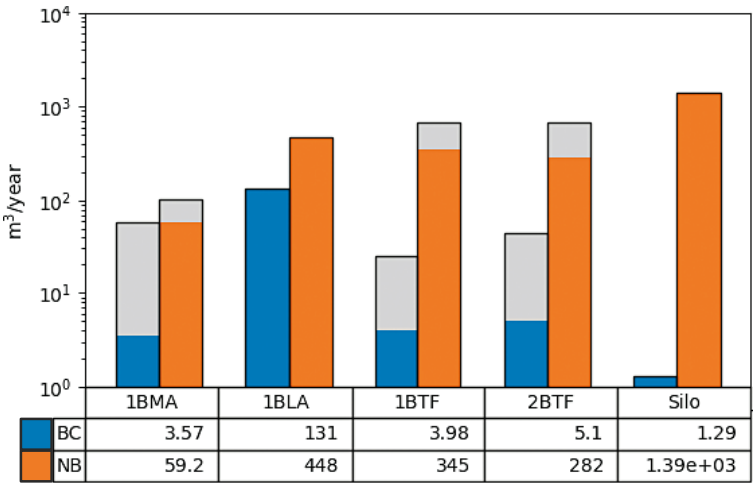

Figure 4-11. *Total flow (m^3/year) through the waste in the No Barriers case (NB) compared with the Base case (BC), studied at 5000 AD. The total bar height illustrates the vault flow whereas the height of the coloured portion illustrates the flow through the waste. Thus, the grey portion of the bar corresponds to the vault flow outside the waste compartment. The table of flow values (m^3/year) gives the flow through the waste.*

Table 4-5. Total flow through the SFR 1 vaults (m^3/year) for the No barriers case (NB) and ratio with respect to the Base case (BC), Complete plug degradation case (CPD) and No barriers case (NB*) reported in Abarca et al. (2013).

		No barriers	Ratio NB/BC	Ratio NB/CPD	Ratio NB/NB*
Vaults	1BMA	103	1.45	1.02	0.32
	1BLA	465	3.00	0.79	1.39
	1BTF	672	18.82	1.01	0.87
	2BTF	678	11.28	1.36	1.35
	Silo	1410	839.29	671.43	0.84
	Total	3328	10.28	1.80	1.09
Waste	1BMA	59.2	13.36	9.44	0.21
	1BLA	448	2.95	0.79	1.37
	1BTF	345	82.34	183.51	0.55
	2BTF	282	52.32	125.33	0.70
	Silo	1390	885.35	674.76	0.85
	Total	2524.2	15.06	4.38	1.30

* Abarca et al. (2013).

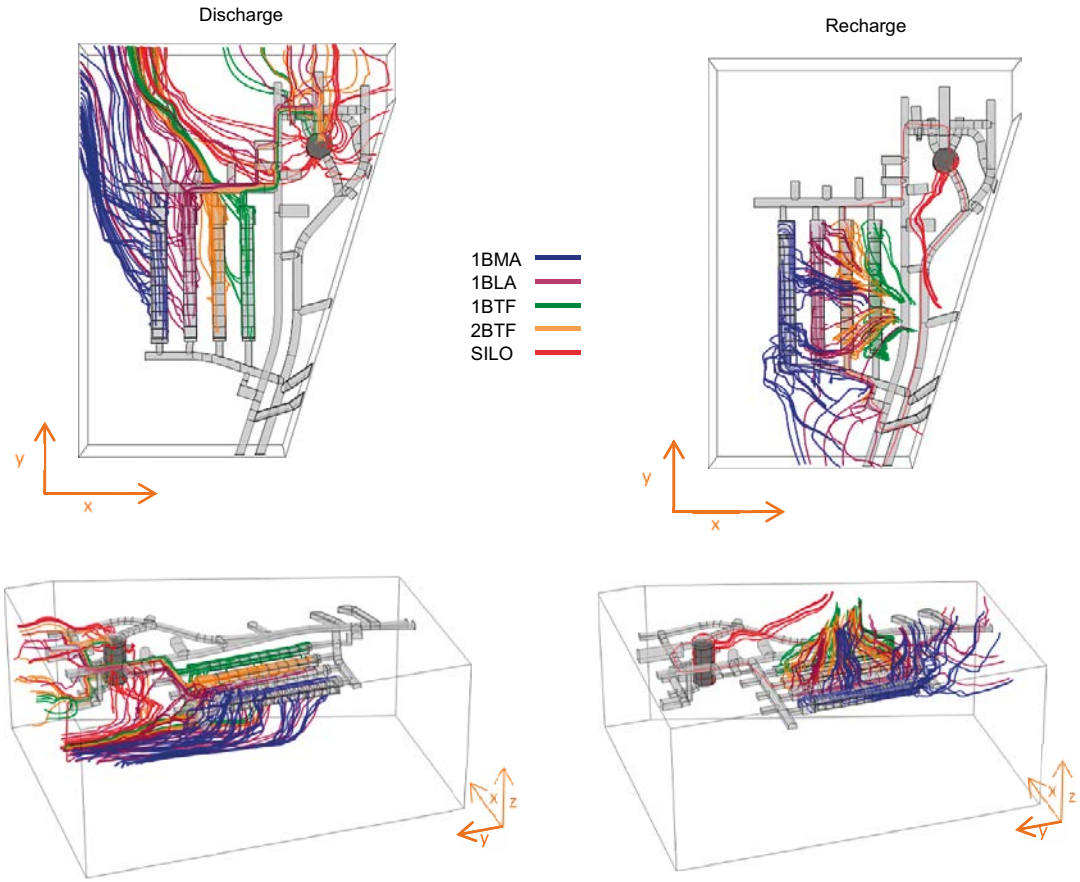

Figure 4-12. Groundwater streamlines leaving (left) and reaching (right) individual vaults (colour tubes) for the case of no barriers at 5000 AD.

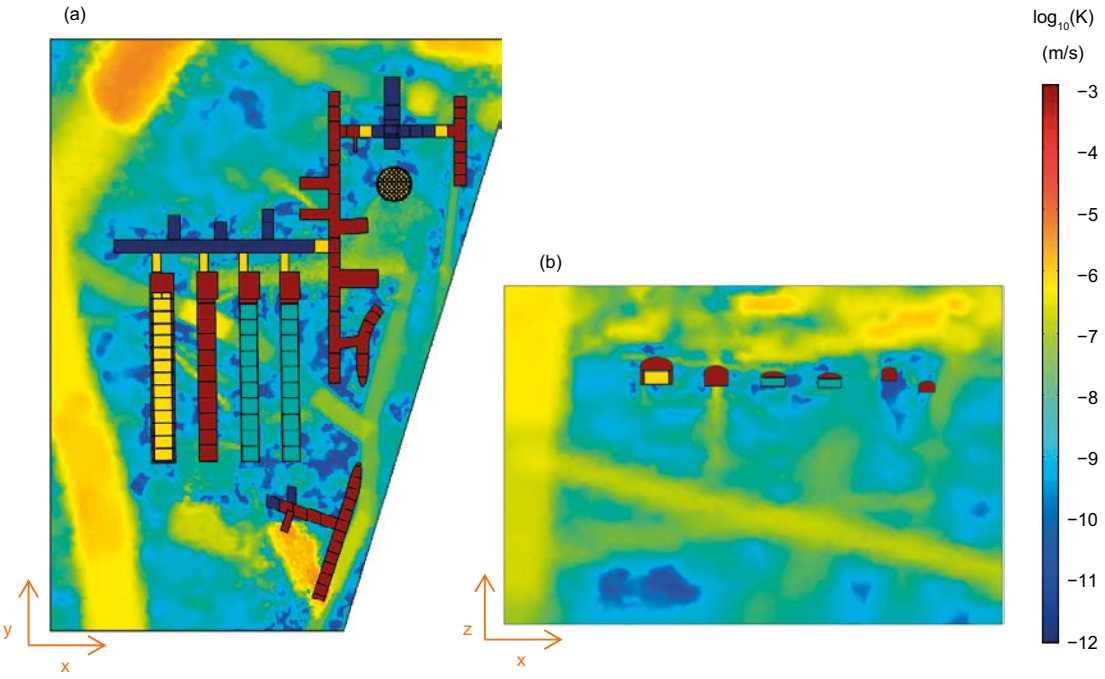

Figure 4-13. *Hydraulic conductivity of the rock and the repository materials for the base case at z = −82.5 m (a) and x = 10 050 m).*

The flow through the waste increases due to the increase in total flow through the vaults caused by the lack of plugs and the increase in the proportion of flow through the waste caused by the absence of concrete barriers. In the vaults with concrete barriers (1BMA and 1–2BTF), these two effects can be discriminated if the no barrier case is compared with the completely plug degradation (CPD) case presented in Section 4.2.2. In 1BMA, the effect of the absence of concrete barriers can be estimated by the comparison of the flow ratios NB/BC and NB/CPD (Table 4-5). The ratio NB/BC is 40 % larger than the NB/CPD. Therefore, it can be estimated that the absence of concrete barriers accounts for 40 % of the flow increase in the no barriers case. In the BTF vaults, the cumulative effect of the absence of plugs and grout, results in the amplification of the impact of the absence of plugs. Note that the complete plug degradation case reduced the flow through the waste in the BTF vaults. That beneficial effect is lost when the grout does not act as a flow barrier.

The flows are also compared with the No barriers case in Abarca et al. (2013) (Table 4-5). In this scenario, the flow through the repository was not limited by the engineered barriers but by the groundwater flow the rock can provide (see Table 4-1). Therefore, a substantial change in the total flow through the repository in the No barriers case reported in Abarca et al. (2013) should be interpreted as driven by the interaction between the rock and the change in the access ramp. When adding the total flow through all the repository vaults, the flow is the same for the two cases (ratio with respect to Abarca et al. (2013) close to 1 in Table 4-5). However, when looking at the results for the individual vaults, the flow increases in 1BLA and 2BTF and it is reduced in the other vaults. Therefore, there is a redistribution between the vaults, but the flow provided by the rock remains constant.

4.2.4 Ice lens

This calculation case explores the effect of an ice lens, formed as permafrost reaches Silo depth on the local groundwater flow. The ice lens is assumed to cause degradation of a section of the outer bentonite wall of the Silo. In the model, the degradation of the bentonite has been simulated by a 10.67 m thick ring of high hydraulic conductivity (10^{-3} m/s) in the Silo walls (see Abarca et al. 2013 for details), at mid-height of the waste domain. The rest of the material properties are the same as in the Base case (see Appendix A). This case has been evaluated for 5000 AD.

The degradation of the bentonite ring results in an increase of the total flow through the Silo (Figure 4-14). An increase of total flow into the waste domain by more than 300 % with respect to the Base case occurs in the Silo. The rest of the vaults remain unaffected.

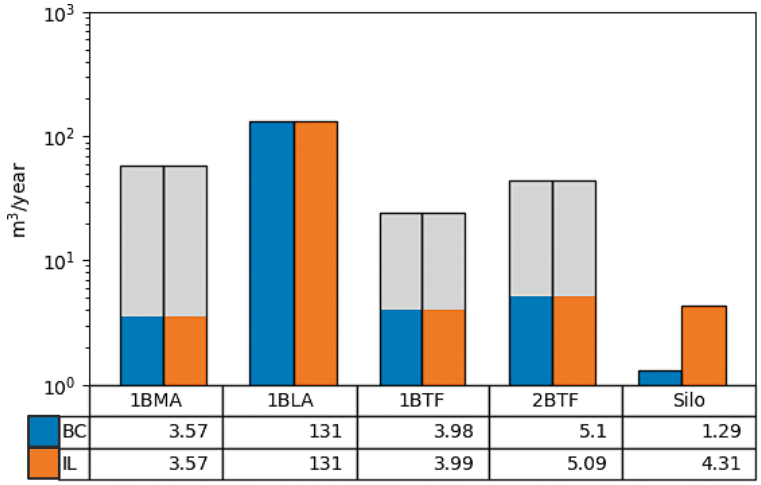

Figure 4-14. *Total flow (m^3/year) through the waste in the Ice Lens case (IL) and in the Base case (BC) at 5000 AD. The grey area illustrates the vault flow outside the waste compartment.*

4.3 Estimation of uncertainty associated with the geosphere

Two realizations of the rock permeability were used to assess the range of variability in the computed flows due to the uncertainties in the geosphere hydraulic description. These realizations are considered as representative of two cases that lead to a higher and a lower average tunnel flow with respect to the Base case. For this reason, hereafter, they are referred to as High (HFC) and Low (LFC) flow realizations (see Table 4-6 for correspondence with respective DarcyTools simulations). This case is evaluated at 2000 AD and 5000 AD.

Table 4-6. Nomenclature of the three realizations of the rock permeability field in the repository-scale model and the regional-scale model (Odén et al. 2014).

Repository-scale model	Case number in regional-scale model	Regional-scale model
Base case	Case 1	Base_Case1_DFN_R85
High Flow Case	Case 11	nc_DEP_R07_DFN_R85
Low Flow Case	Case 15	nc_NoD_R01_DFN_R18

The High Flow case and the Base case share the same discrete fracture network (DFN) realization and thus the locations of the minor fractures affecting the vaults. The main difference between these two realizations is the higher connectivity between the deformation zones ZFMNNW1209 and ZFMNNE0869 west of 1BMA in the High flow case. The Low flow case corresponds to a different DFN realization. The main differences with the Base case are that, in general, the vaults are located in a lower permeability area and are not intersected by the high permeability structures above the vaults. Also, the minor fractures affecting 1BMA and 1BLA are not present. More details on the rock conductivity fields can be found in Abarca et al. (2013) and Öhman and Odén (2018).

The flows through the vaults and waste for the two additional realizations of the rock conductivity field are tabulated for 2000 AD and 5000 AD in Table B-8 and Table B-9 in Appendix B, respectively. Graphically, the flows are illustrated in Figure 4-15 and Figure 4-16. Table 4-7 shows the ratios of the total flow through the SFR 1 vaults for two realizations of the rock conductivity (LFC, HFC) with respect to the Base case.

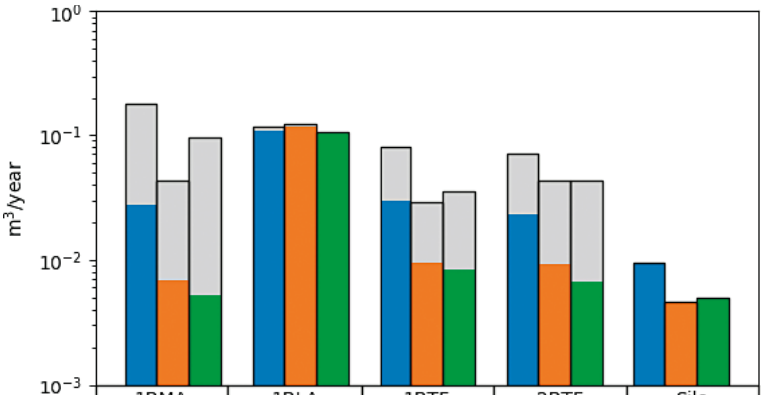

	1BMA	1BLA	1BTF	2BTF	Silo
LFC	0.0276	0.109	0.0299	0.0233	0.00942
BC	0.00691	0.118	0.00943	0.00921	0.00446
HFC	0.00522	0.102	0.00835	0.00666	0.00484

Figure 4-15. *Total flow (m^3/year) through the waste for three bedrock realizations, studied at 2000 AD. The grey area illustrates the vault flow outside the waste compartment.*

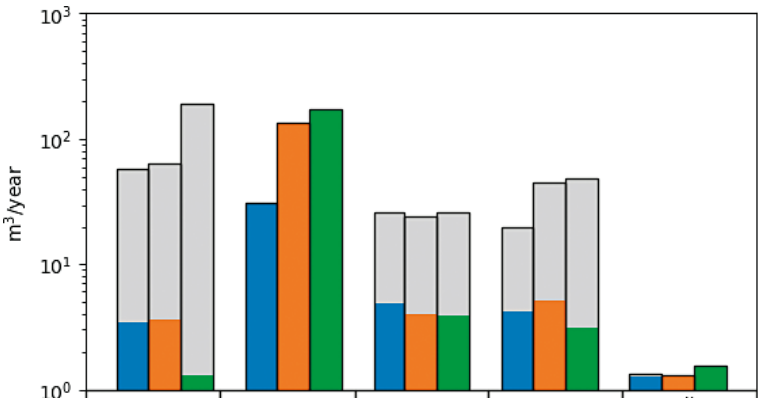

	1BMA	1BLA	1BTF	2BTF	Silo
LFC	3.41	30.6	4.88	4.17	1.28
BC	3.57	131	3.98	5.1	1.29
HFC	1.29	168	3.86	3.11	1.55

Figure 4-16. *Total flow (m^3/year) through the waste for three bedrock realizations, studied at 5000 AD. The grey area illustrates the vault flow outside the waste compartment.*

The different realizations of the rock conductivity fields have a large impact on the flow through the repository vaults. The computed flow values range from 0.25 to 4 times the values obtained from the base case (Table 4-7). The largest flow increases, with ratios higher than 3, are highlighted in red and the largest flow decreases, with ratios lower than 1/3, are highlighted in green. The LFC and HFC were ranked for times after 2000 AD (Öhman et al. 2014) using the total flow through all the vaults in SFR 1 and SFR 3. For 5000 AD the flows through the vaults for HFC increase systematically, as observed in Öhman et al. (2014). For 2000 AD, the flows do not systematically increase for a particular realization. The maximum and minimum relative change are calculated at 2000 AD and at 5000 AD, respectively, for the same realization (LFC). This results highlight the importance of the location and local connectivity of fractures around the individual repository vaults.

Table 4-7. Ratio of the total flow through the SFR 1 vaults for two realizations of the rock conductivity (LFC, HFC) with respect to the Base case. Ratios higher than 3 and lower than 1/3 are highlighted in red and green, respectively.

		2000 AD		5000 AD	
		Ratio LFC/BC	Ratio HFC/BC	Ratio LFC/BC	Ratio HFC/BC
Vaults	1BMA	4.00	2.21	1.10	2.67
	1BLA	0.96	0.86	0.25	1.29
	1BTF	2.81	1.23	0.94	1.10
	2BTF	1.67	1.01	0.49	1.03
	Silo	2.09	1.08	1.08	1.18
Waste	1BMA	3.99	0.76	1.00	0.37
	1BLA	0.92	0.86	0.25	1.28
	1BTF	3.17	0.89	1.42	0.94
	2BTF	2.53	0.72	1.06	0.68
	Silo	2.11	1.09	1.14	1.15

The results of these simulations are compared against the same simulations performed with the previous repository parameterization and layout reported in Abarca et al. (2013). The values of the flow ratios are given in Table 4-8. The ratios are close to 1 for the computed flows at 2000 AD, indicating that the flow through the vaults is not sensitive to the changes in the repository at that shoreline position. The range of ratio broadens at 5000 AD. For this shoreline position, the impact of the changes is noticeable in 1BMA, 1BTF and the Silo. The increase in flow in the 1–2BTF vaults is due to the increase in the value of the homogenized hydraulic conductivity of the waste domain (see Section 3.6), which is 20 % larger than in Abarca et al. (2013). The effect is larger in 1BTF, which is located upstream from the rest of the vaults. An increase in flow in the vaults upstream is compensated by a decrease in the flow through the vaults located downstream (Abarca et al. 2013). This is the case here, where the flow increase in 1BTF is compensated with a flow decrease, in particular in 1BMA, which is the vault located furthest downstream from 1BTF. These results are consistent with the comparison between the base case and the results from previous simulations reported in Abarca et al. (2013), see Section 4.1.5.

Table 4-8. Ratio of the total flow through the SFR 1 vaults for two realizations of the rock conductivity (LFC, HFC) with respect to the same realizations reported in Abarca et al. (2013).

		2000 AD		5000 AD	
		Ratio LFC	Ratio HFC	Ratio LFC	Ratio HFC
Vaults	1BMA	0.88	1.02	0.74	0.89
	1BLA	0.91	0.88	1.01	0.85
	1BTF	0.95	0.93	1.17	1.26
	2BTF	0.94	0.92	1.05	1.01
	Silo	0.96	0.99	1.35	0.81
Waste	1BMA	1.02	0.87	1.18	1.04
	1BLA	0.98	0.91	1.06	0.87
	1BTF	1.00	1.04	1.20	1.13
	2BTF	0.93	1.11	1.13	1.10
	Silo	0.94	0.97	1.45	0.87

4.4 Summary of the calculation cases

The results presented for all the barrier degradation and/or configuration cases at 5000 AD are summarized in Figure 4-17 and Table 4-9. The reason to restrict the analysis to 5000 AD is that some cases have only been calculated with this shoreline position.

The no barriers case is by far the most unfavourable situation of all the calculation cases considered, with total flows in the waste domains of around two to three orders of magnitude higher than for the Base case. According to the model predictions, the Silo is the most sensitive structure of the repository to the no barrier degradation case, which is the only case in which the Silo bentonite walls are completely degraded.

The 1BMA vault is the least sensitive vault to the degradation cases. Even for the no barriers case, the increase in flow is lower than the flow variability due to the uncertainty in the local rock conductivity field. This vault is located the furthest from the access ramp, and therefore, protected by the other vaults in the case of a repository failure.

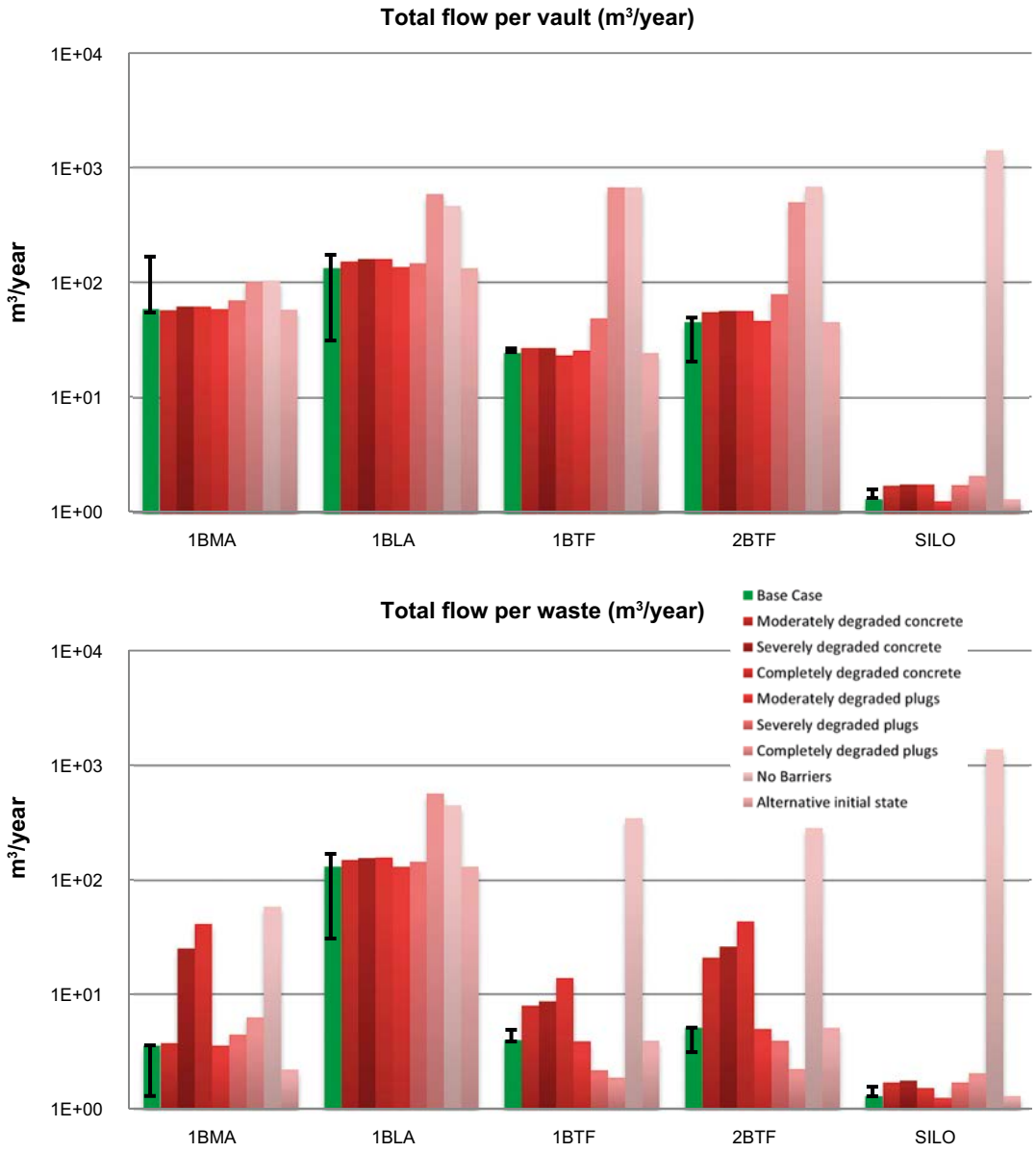

Figure 4-17. *Total flow (m^3/year) for the different vaults and waste domains in the SFR 1 repository for the shoreline at 5000 AD. The black line accompanying the Base case bar indicates the uncertainty interval for each vault due to the studied variability in the geosphere. The vertical axis is logarithmic.*

The 1BLA and 2BTF vaults show a trade-off in the no barrier and the completely degraded plugs case. For the 2BTF vault, located closer to the access ramp, flow increases for the no barriers case, whereas 1BLA is less affected by the no barriers case than by the case of completely degraded plugs.

Regarding the flow through the wastes, the flow increase in the vaults without concrete barriers is similar to that of the vault flow. Therefore, the no plugs and no barriers cases are the worst-case scenarios for the 1BLA vault and the Silo, resulting in the highest flows. For the 1BMA and 1–2BTF vaults, which have concrete barriers, the no barriers case followed by the severely and completely degraded concrete cases represent the worst-case scenarios. The 1–2BTF vaults are also strongly impacted by moderate degradation of concrete.

Table 4-9. Summary of the results of total flow (m^3/year) in each vault for all the barrier degradation cases at 5000 AD.

		1BMA	1BLA	1BTF	2BTF	Silo
Vaults	Base case	58.3	133	24.5	45	1.3
	Moderately degraded concrete	57.1	152	27.3	55	1.72
	Severely degraded concrete	61.2	159	27	56.6	1.75
	Completely degraded concrete	61.3	160	23.5	56.3	1.75
	Moderately degraded plugs	58.7	135	25.8	46.5	1.26
	Severely degraded plugs	69.4	147	48.5	78.3	1.74
	Completely degraded plugs	101	586	667	497	2.1
	No Barriers	103	465	672	678	1410
	Alternative initial state	57.8	133	24.5	45	1.3
Waste	Base case	3.57	131	3.98	5.1	1.29
	Moderately degraded concrete	3.78	150	7.9	20.7	1.71
	Severely degraded concrete	24.9	157	8.61	26	1.76
	Completely degraded concrete	41.4	158	13.8	43.5	1.53
	Moderately degraded plugs	3.57	132	3.9	5.03	1.25
	Severely degraded plugs	4.49	145	2.18	3.98	1.71
	Completely degraded plugs	6.27	564	1.88	2.25	2.06
	No Barriers	59.2	448	345	282	1390
	Alternative initial state	2.21	131	3.98	5.1	1.29

5 SFR 3 Calculation cases

5.1 Base case

This section presents the results of the Base case for the SFR 3 at four different shoreline positions (Figure 3-10). The Base case refers to a given set of hydraulic properties for the engineered barriers (Table A-1 in Appendix A). The rock permeability field corresponds to the Base_Case1_DFN_R85 in Öhman and Odén (2018). Streamlines were generated to illustrate the flow field around the repository in four simulations that relate to the different shoreline positions (for more details see Section 3.8.2).

5.1.1 Groundwater flow field at 2000 AD

At 2000 AD, the repository is situated below the regional groundwater discharge area (Figure 3-10). This situation corresponds to shoreline position 1 in Abarca et al. (2013). The streamlines showing the paths followed by the groundwater reaching and leaving each individual vault are illustrated in Figure 5-1.

Groundwater flows upwards from the south through a deformation zone reaching the bottom of the vaults (Figure 5-1 right). Outflow from the vaults (Figure 5-1 left) can roughly be divided into two zones. At the south end of the vaults, there is vertical upward outflow from all vaults. The loop of the ramp located above the vaults disturbs this upwards flow towards the surface. In the new layout the loop is wider, and the upwards flow paths are less disturbed than with the smaller loop of layout 1.5 (see Abarca et al. 2013). The northern part of the vaults has a diffuse outflow upwards with a NW direction. The exceptions are the 2BMA vault that also discharges towards the NE and the BRT vault whose north end discharges downwards. This is one of the main differences with respect to the flow field described in Abarca et al. (2013) for shoreline position 1 and it is due to the elongation of the BRT vault in the new layout.

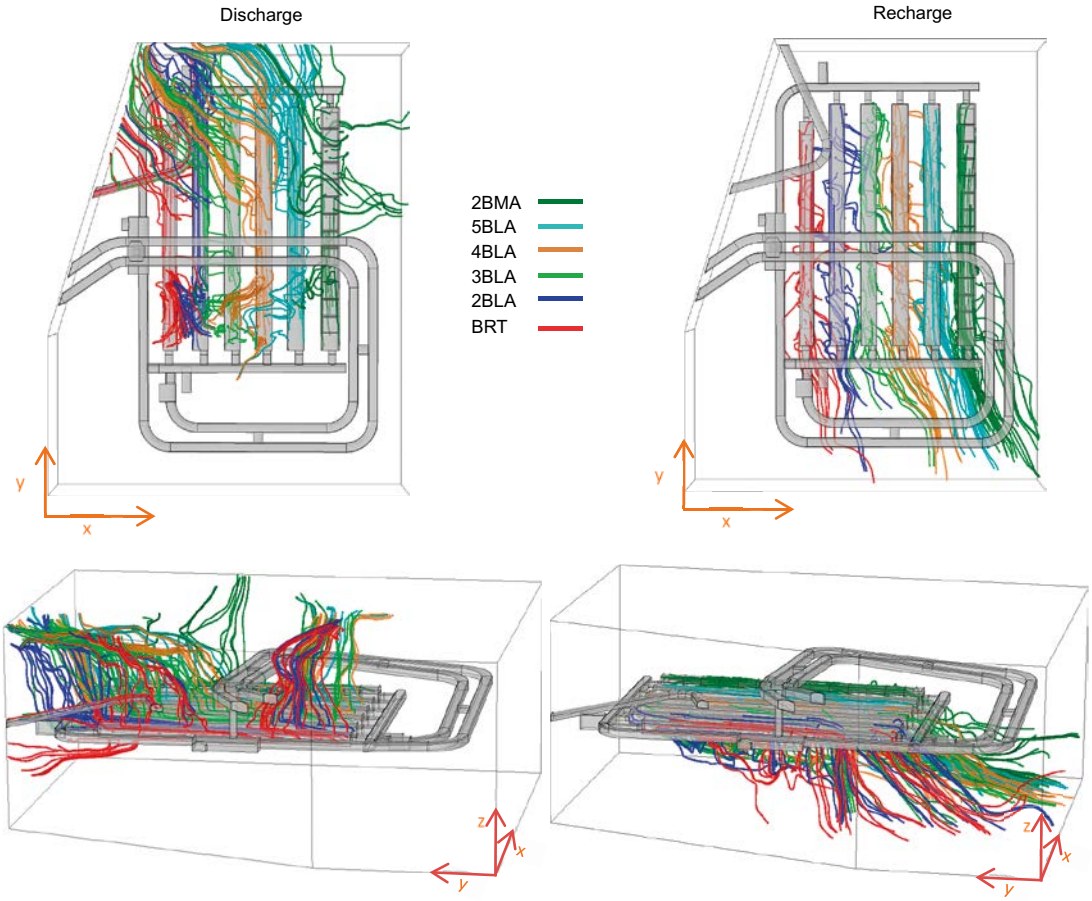

Figure 5-1. *Groundwater streamlines leaving (left) and reaching (right) individual vaults (colour tubes) of the SFR 3 repository for the Base case at 2000 AD. The x- and y-arrows point to the east and north, respectively.*

5.1.2 Groundwater flow field at 2500 AD

At 2500 AD, the shoreline is located right over the SFR 3 repository. The repository is situated below a small emerged peninsula (Figure 3-10). This shoreline position was not considered in Abarca et al. (2013). The streamlines (Figure 5-2) illustrate the inversion in flow direction with respect to 2000 AD. Groundwater recharge from the emerged peninsula reaches the vaults vertically through two vertical deformation zones. One deformation zone affects all vaults in their northern parts and the other one affects the rock inside the loop of the access ramp and the vaults in their southern parts. Part of the water infiltrating through this deformation zone reaches the loop of the access ramp at its eastern part. It descends through the ramp and penetrates into the rock again to reach vertically the 2BMA vault. The flow direction of the water leaving the vaults depends on the water origin. The water that infiltrated from the rock inside the loop of the access ramp flows first downwards from the repository vaults and later towards the west following a deformation zone leaving the model domain through its lateral boundary. The water that infiltrated in the northern part of the vaults leaves the vaults vertically downwards and flows horizontally towards the north leaving the domain through its north boundary.

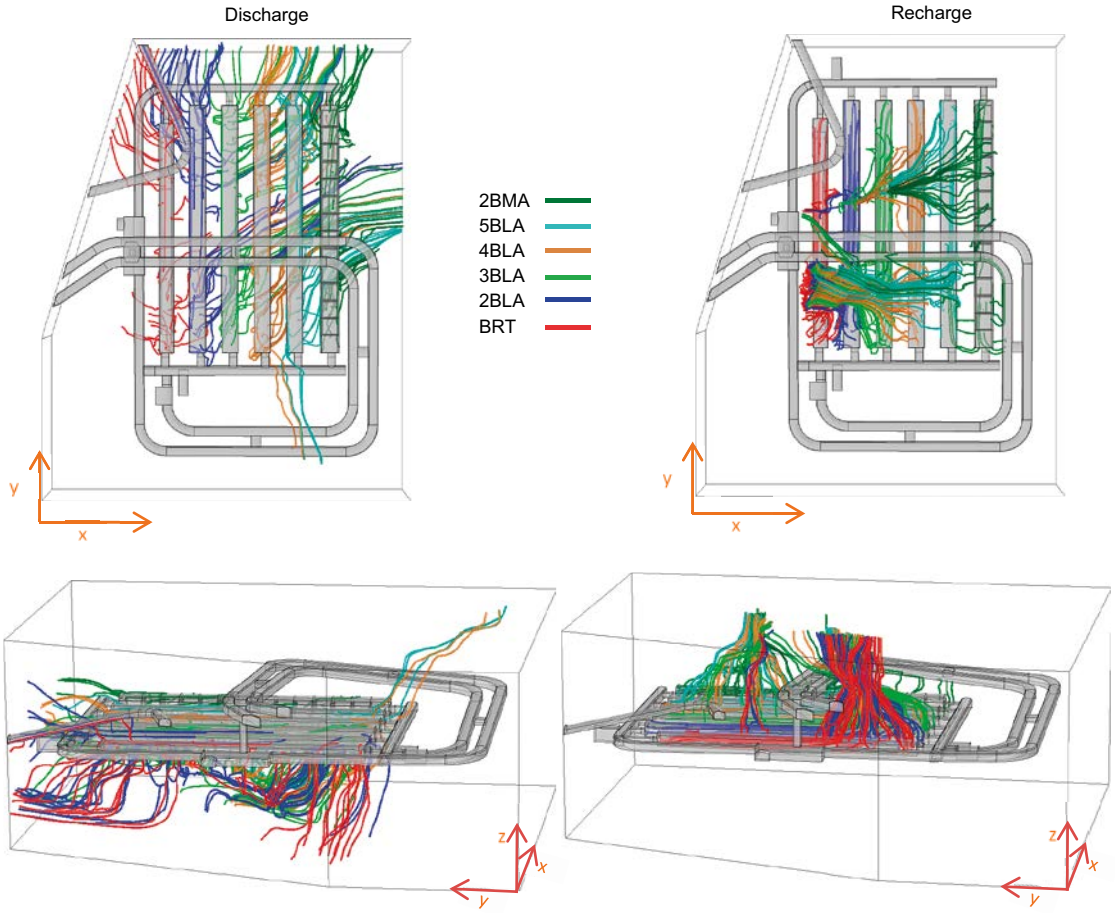

Figure 5-2. *Groundwater streamlines leaving (left) and reaching (right) individual vaults (colour tubes) of the SFR 3 repository for the Base case at 2500 AD. The x- and y-arrows point to the east and north, respectively.*

5.1.3 Groundwater flow field at 3500 AD

At 3500 AD, the shoreline is located north of the repository. The repository is situated below a groundwater recharge area (Figure 3-10). The observed flow field is similar to the one described for shoreline position 2 in Abarca et al. (2013). The groundwater flow paths to and from each individual vault are illustrated in Figure 5-3. Inflow from the top of the domain is localized mainly over the half southern part of the repository. Most of the water reaches the vaults from a deformation zone area circumscribed by the loop in the access ramp. A lower portion of streamlines reaches the vaults from the rock outside of the loop. Groundwater discharge flows downwards vertically through a vertical fracture until reaching ZFM871 and then moves north following a main subhorizontal deformation zone.

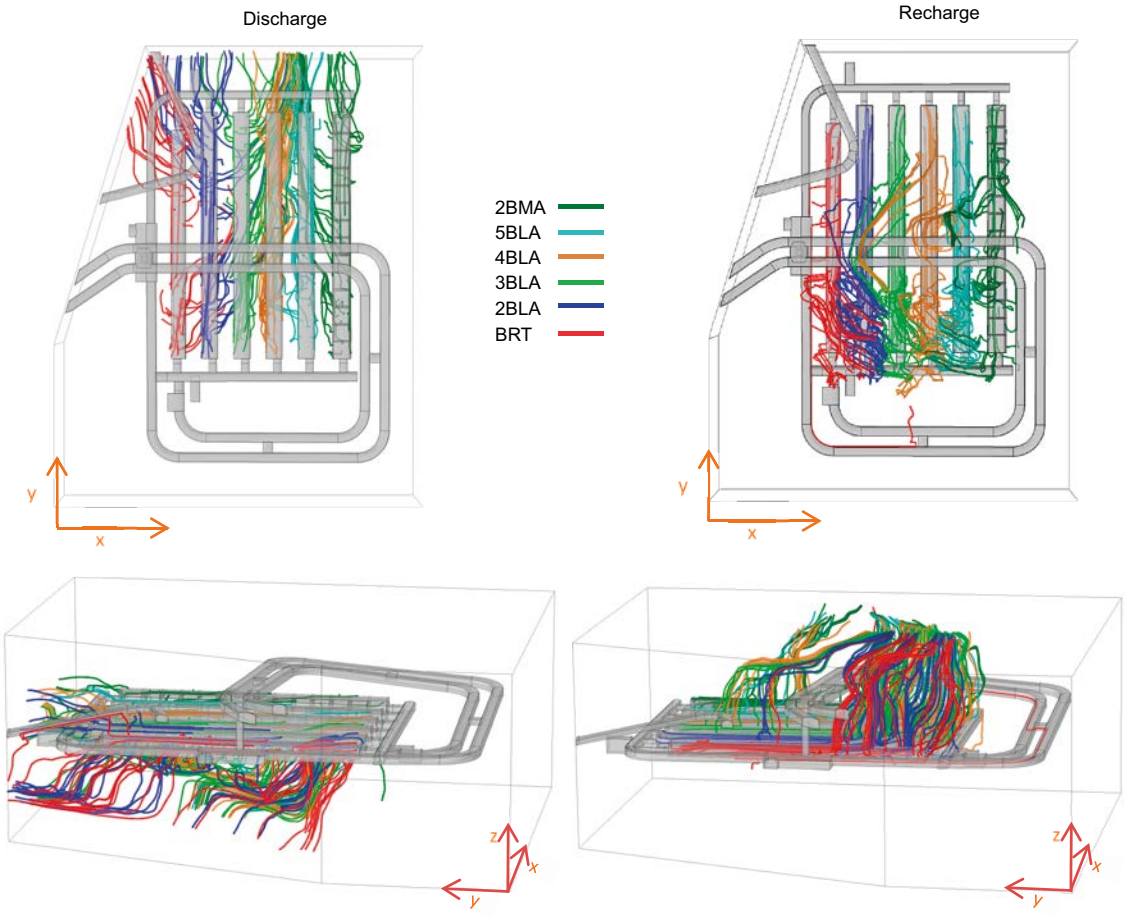

Figure 5-3. *Groundwater streamlines leaving (left) and reaching (right) individual vaults (colour tubes) of the SFR 3 repository for the Base case at 3500 AD. The x- and y-arrows point to the east and north, respectively.*

5.1.4 Groundwater flow field at 5000 AD

At 5000 AD, the repository is situated below a groundwater recharge area with the shoreline 1 km further north (Figure 3-10). This situation corresponds to shoreline position 3 in Abarca et al. (2013). The streamlines (Figure 5-4) show no substantial differences with respect to the flow field described for 3500 AD (Figure 5-3).

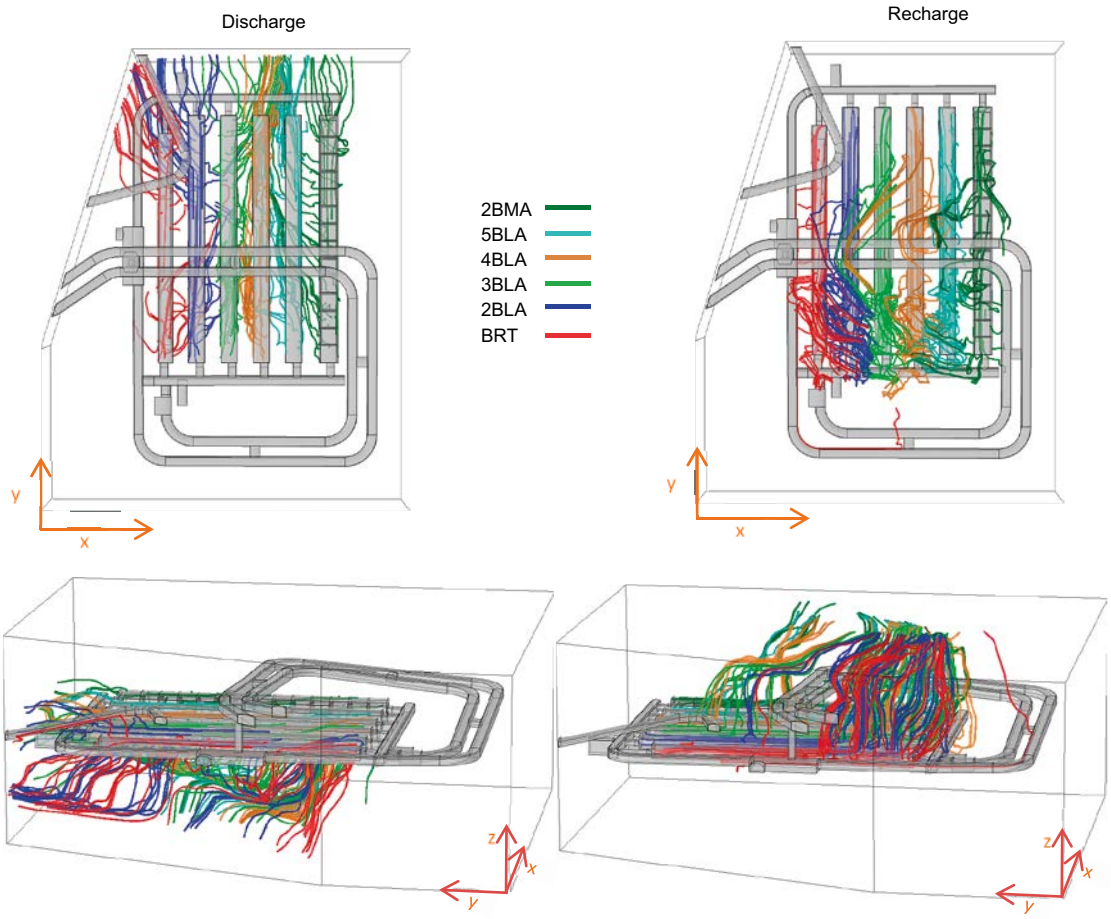

Figure 5-4. *Groundwater streamlines leaving (left) and reaching (right) individual vaults (colour tubes) of the SFR 3 repository for the Base case at 5000 AD. The x- and y-arrows point to the east and north, respectively.*

5.1.5 Total flow through the vaults and waste

Table 5-1 shows the calculated total flow through the SFR 3 vaults and waste domains for the four shoreline positions. Consistent with the results for the SFR 1 vaults (see Section 4.1.5), the flow through the vaults increases with time as the shoreline position recedes. The largest proportionate increase occurs between 2000 and 2500 AD when the flow increases more than one order of magnitude in all vaults. This increase corresponds to the passage of the shoreline position over the repository and the change from being located under a discharge area to becoming located under a recharge area. The flow increases by almost another order of magnitude from 2500 AD to 3500 AD. The calculations for 3500 AD and 5000 AD yield similar flow values. The flows at the model boundaries through the rock and through the ramp sections and the ratio between them are computed (Table 4-1). The results indicate that the flow through the ramp is less than 1 % for all shoreline positions. Therefore, the main source of groundwater recharge to the repository is infiltration through the rock in all cases.

The highest flows through the vaults are obtained in 2BMA, which is the vault with the largest volume (see dimensions in Table 3-1). This result is consistent with the results reported in Abarca et al. (2013). The flow values for the rest of the vaults are quite similar to the ones reported in Abarca et al. (2013).

The flow through the waste is not reported for the BLA vaults, since the waste domain is defined identically to the vault domain. The increase in the vault flow as the shoreline position recedes affects the flow through the waste in BRT and 2BMA. The relative increase in the flow through the waste is of the same order as the increase in the vault flow. The proportion of flow that enters the waste with respect to the flow that enters the vault decreases and is defined by the ratio waste/vault flow in Table 5-1. That ratio remains between 0.12 and 0.18 for BRT. These values are very similar to the ones obtained for the grouted 1–2BTF vaults in SFR 1 (see Section 4.1.5). The ratio waste/vault flow for 2BMA remains extremely low (under 1×10^{-5}) for all shoreline positions. This low ratio evidences the high efficiency of the hydraulic cage effect achieved by the 2BMA configuration.

Table 5-1. Total flow through the SFR 3 vaults and waste domains (m^3/year) for the Base case.

		2000 AD	2500 AD	3500 AD	5000 AD
Boundaries	Rock	62.72	1557.6	5930.3	6003.8
	Ramp	0.0	0.0	33.5	36.5
	Total	62.72	1557.6	5963.9	6040.4
	Ratio Ramp/Total	0.0	0.0	0.006	0.006
Vaults	2BLA	0.126	3.44	23.7	24.4
	3BLA	0.108	4.38	30.2	31
	4BLA	0.0994	3.57	24.3	24.9
	5BLA	0.107	1.68	16.6	17.3
	BRT	0.122	3.3	20.8	21.8
	2BMA	0.262	4.78	33.8	32.9
Waste	BRT	0.0147	0.528	3.8	4.02
	2BMA	2.42×10^{-6}	3.6×10^{-5}	0.000292	0.000282
Ratio waste/vault	BRT	0.12	0.16	0.18	0.18
	2BMA	9.24×10^{-6}	7.53×10^{-6}	8.64×10^{-6}	8.57×10^{-6}

The comparison with the results from previous simulations reported in Abarca et al. (2013) is presented in Table 5-2. At 2000 AD, there is a general increase in the values of flows through the vaults, except for 2BMA. The largest increase occurs in BRT, both in terms of vault and waste flow. This increase is due to the larger dimensions of BRT in the new layout. At 5000 AD, the flow values are very similar to those reported in Abarca et al. (2013), even for BRT. There is an increase in the flow through the waste. In BRT it is interpreted as a result of the larger dimensions of the waste domain and in 2BMA, due to the presence of gas evacuation channels in the waste compartments. This increase occurs at 5000 AD, when the flow in the vaults is mainly from south to north and it is minimized at 2000 AD, when the flow is vertical and upwards.

Table 5-2. Ratio of the total flow through the SFR 3 vaults with respect to the Base case in Abarca et al. (2013). Ratios lower than one indicate a reduction in the total flow with respect to the flows reported in Abarca et al. (2013).

Ratio		2000 AD	5000 AD
Vaults	2BLA	1.024	0.900
	3BLA	1.293	1.030
	4BLA	1.112	1.051
	5BLA	1.079	0.844
	BRT	1.681	1.095
	2BMA	0.858	1.058
Waste	BRT	1.123	1.426
	2BMA	0.945	1.410

5.2 Barrier degradation

5.2.1 Concrete degradation

This section explores the effect of concrete barrier degradation on the total flow entering the tunnels and waste compartments of the SFR 3 vaults for the four shoreline positions (2000 AD, 2500 AD, 3500 AD and 5000 AD). As in Section 4.2.1, this effect has been studied with a set of three simulations referred to as moderate, severe, and complete concrete degradation. The hydraulic conductivities of the different degradation states are defined in Appendix A**.**

The flows through the vaults and wastes for the concrete degradation cases are tabulated in Table B-15, Table B-16, Table B-17 and Table B-18 in Appendix B, for 2000 AD, 2500 AD, 3500 AD and 5000 AD, respectively. Graphically, the flows are illustrated in Figure 5-5, Figure 5-6, Figure 5-7 and Figure 5-8.

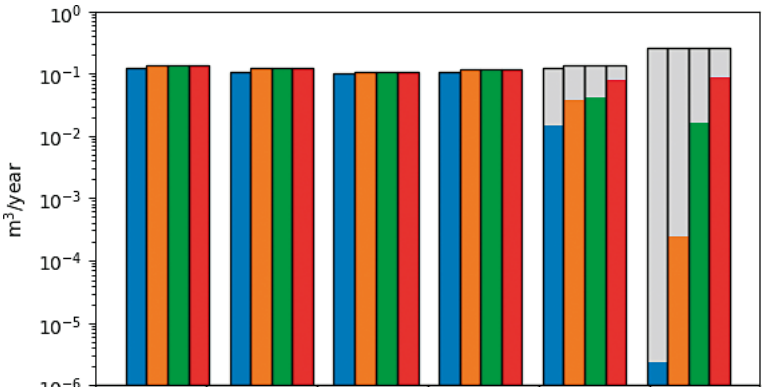

	2BLA	3BLA	4BLA	5BLA	BRT	2BMA
BC	0.126	0.108	0.0994	0.107	0.0147	2.42e-06
MCD	0.135	0.121	0.106	0.117	0.0372	0.000241
SCD	0.138	0.122	0.107	0.119	0.0422	0.0166
CCD	0.139	0.122	0.107	0.119	0.0784	0.0883

Figure 5-5. *Total flow (m^3/year) through the waste for the base case and three concrete degradation cases, studied at 2000 AD. The total bar height illustrates the vault flow whereas the height of the coloured portion illustrates the flow through the waste. Thus, the grey portion of the bar corresponds to the vault flow outside the waste compartment. The table gives the flow values through the waste (m^3/year).*

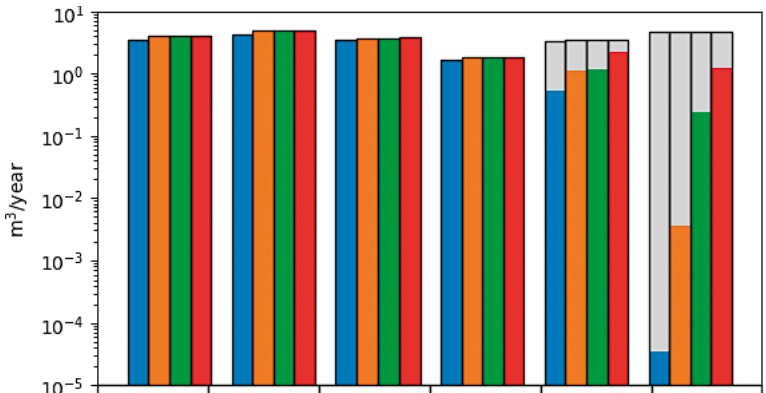

	2BLA	3BLA	4BLA	5BLA	BRT	2BMA
BC	3.44	4.38	3.57	1.68	0.528	3.6e-05
MCD	4.04	4.87	3.72	1.83	1.11	0.00358
SCD	4.14	4.91	3.78	1.84	1.19	0.243
CCD	4.14	4.92	3.79	1.85	2.28	1.24

Figure 5-6. *Total flow (m^3/year) through the waste for the base case and three concrete degradation cases, studied at 2500 AD. The total bar height illustrates the vault flow whereas the height of the coloured portion illustrates the flow through the waste. Thus, the grey portion of the bar corresponds to the vault flow outside the waste compartment. The table gives the flow values through the waste (m^3/year).*

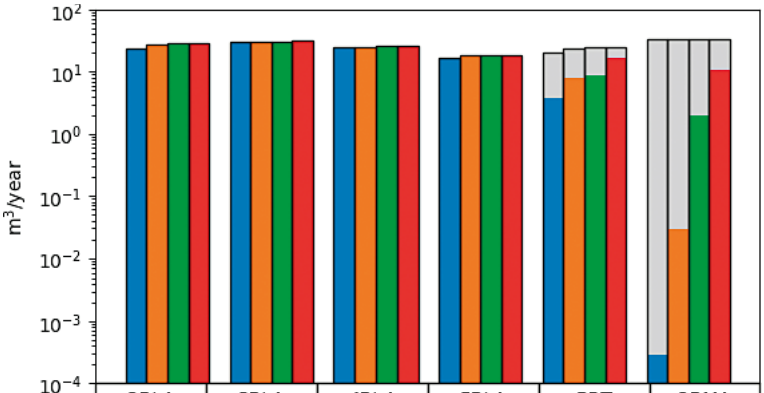

	2BLA	3BLA	4BLA	5BLA	BRT	2BMA
BC	23.7	30.2	24.3	16.6	3.8	0.000292
MCD	27.9	30.8	25.4	18.1	7.85	0.029
SCD	28.7	31	25.8	18.3	8.71	1.99
CCD	28.7	31.1	25.9	18.3	16.9	10.5

Figure 5-7. *Total flow (m^3/year) through the waste for the base case and three concrete degradation cases, studied at 3500 AD. The total bar height illustrates the vault flow whereas the height of the coloured portion illustrates the flow through the waste. Thus, the grey portion of the bar corresponds to the vault flow outside the waste compartment. The table gives the flow values through the waste (m^3/year).*

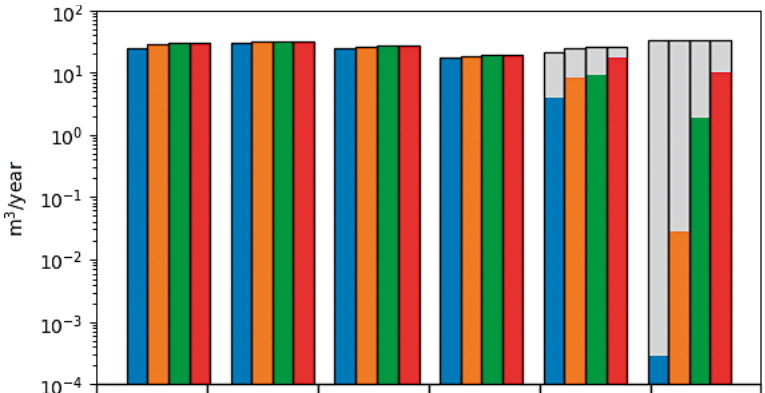

	2BLA	3BLA	4BLA	5BLA	BRT	2BMA
BC	24.4	31	24.9	17.3	4.02	0.000282
MCD	28.9	31.5	26.4	18.8	8.27	0.0279
SCD	29.7	31.6	26.8	19.1	9.16	1.91
CCD	29.7	31.7	26.8	19.1	17.8	10.1

Figure 5-8. *Total flow (m^3/year) through the waste for the base case and three concrete degradation cases, studied at 5000 AD. The total bar height illustrates the vault flow whereas the height of the coloured portion illustrates the flow through the waste. Thus, the grey portion of the bar corresponds to the vault flow outside the waste compartment. The table gives the flow values through the waste (m^3/year).*

The results show that concrete degradation slightly affects the BLA vaults because of their concrete floor degradation. The maximum effect occurs at 2BLA, which is the BLA vault closest to the access ramp. Note that for these type of vaults, the waste domain occupies the whole vault domain.

The flow through BRT increases by up to 17 % also due to the degradation of the concrete floor (Table 5-3). However, this increase occurs already at the moderate concrete degradation state and does not substantially increase as the degradation advances. The waste of BRT is grouted. Therefore, the flow through the BRT waste is quite sensitive to the grout degradation. It doubles from the base case in the moderate concrete degradation case (MCD). This interval corresponds to a change in the hydraulic conductivity of the grout from 1×10^{-8} to 1×10^{-6} m/s. It doubles again when the grout conductivity reaches 1×10^{-3} m/s (CCD).

The flow through the 2BMA vault is insensitive to the concrete degradation. However, the flow through the waste increases almost linearly when increasing the hydraulic conductivity of the concrete barriers. In 2BMA, the waste flow for the MCD is two orders of magnitude higher than for the base case (Table 5-3). The waste flow multiplies by 6 800 and by 36 000 when the hydraulic conductivity of the concrete increases to 1×10^{-7} m/s (SCD) and 1×10^{-5} m/s (CCD), respectively.

Table 5-3. Ratio of the total flow through the SFR 3 vaults for the concrete degradation cases with respect to the Base case.

		2000 AD			2500 AD			3000 AD			5000 AD		
		MCD	SCD	CCD	MCD	SCD	CCD	MCD	SCD	CCD	MCD	SCD	CCD
Vaults	2BLA	1.07	1.10	1.10	1.17	1.20	1.20	1.18	1.21	1.21	1.18	1.22	1.22
	3BLA	1.12	1.13	1.13	1.11	1.12	1.12	1.02	1.03	1.03	1.02	1.02	1.02
	4BLA	1.07	1.08	1.08	1.04	1.06	1.06	1.05	1.06	1.07	1.06	1.08	1.08
	5BLA	1.09	1.11	1.11	1.09	1.10	1.10	1.09	1.10	1.10	1.09	1.10	1.10
	BRT	1.10	1.12	1.12	1.06	1.07	1.07	1.15	1.17	1.17	1.15	1.17	1.17
	2BMA	1.00	1.00	1.00	1.00	0.99	0.99	0.99	0.99	0.99	0.99	0.99	0.99
Waste	BRT	2.53	2.87	5.33	2.10	2.25	4.32	2.07	2.29	4.45	2.06	2.28	4.43
	2BMA	100	6 860	36 488	99	6 750	34 444	99	6 815	35 959	99	6 773	35 816

5.2.2 Plug degradation

This section describes the effect of plug degradation on the groundwater flow and on the total flow entering the tunnels and waste compartments of the SFR 3 vaults. Three degradation states, referred to as moderate plug degradation (MPD), severe plug degradation (SPD) and complete plug degradation (CPD) are considered for 5000 AD. The hydraulic conductivity of the plugs for each degradation state is presented in Appendix A.

The flows through the vaults and wastes for the plug degradation cases are tabulated in Table B-19 in Appendix B. Graphically, the flows are illustrated in Figure 5-9. Table 5-4 shows the ratio of the total flow through the SFR 3 vaults for the plug degradation cases with respect to the base case.

The plug degradation affects the total flow through the vaults. The flow increases between 7 to 34 % from the BC to the SPD case. When the hydraulic conductivity of the plugs reaches 1×10^{-3} m/s (CPD) there is a substantial increase in the total flow through the vaults. BRT is affected the most and 2BMA the least (Table 5-4). The BRT and the 2BLA vaults receive water collected from the ramp loop as indicated by the recharge streamlines in Figure 5-10. The increase in the flow through BRT is not accompanied by an increase in the flow through the waste, which remains unaffected. The flow through the 2BMA waste reflects the slight increase in the flow through the vault.

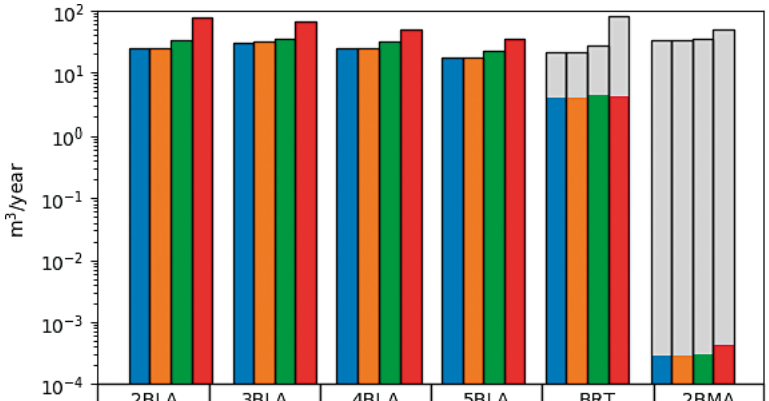

	2BLA	3BLA	4BLA	5BLA	BRT	2BMA
BC	24.4	31	24.9	17.3	4.02	0.000282
MPD	24.4	31.1	25	17.4	4.01	0.000282
SPD	32.7	35.8	32.1	23	4.31	0.000302
CPD	77	65.4	50	35.3	4.07	0.00043

Figure 5-9. *Total flow (m^3/year) through the waste for the base case and three plug degradation cases, studied at 5000 AD. The grey area illustrates the vault flow outside the waste compartment.*

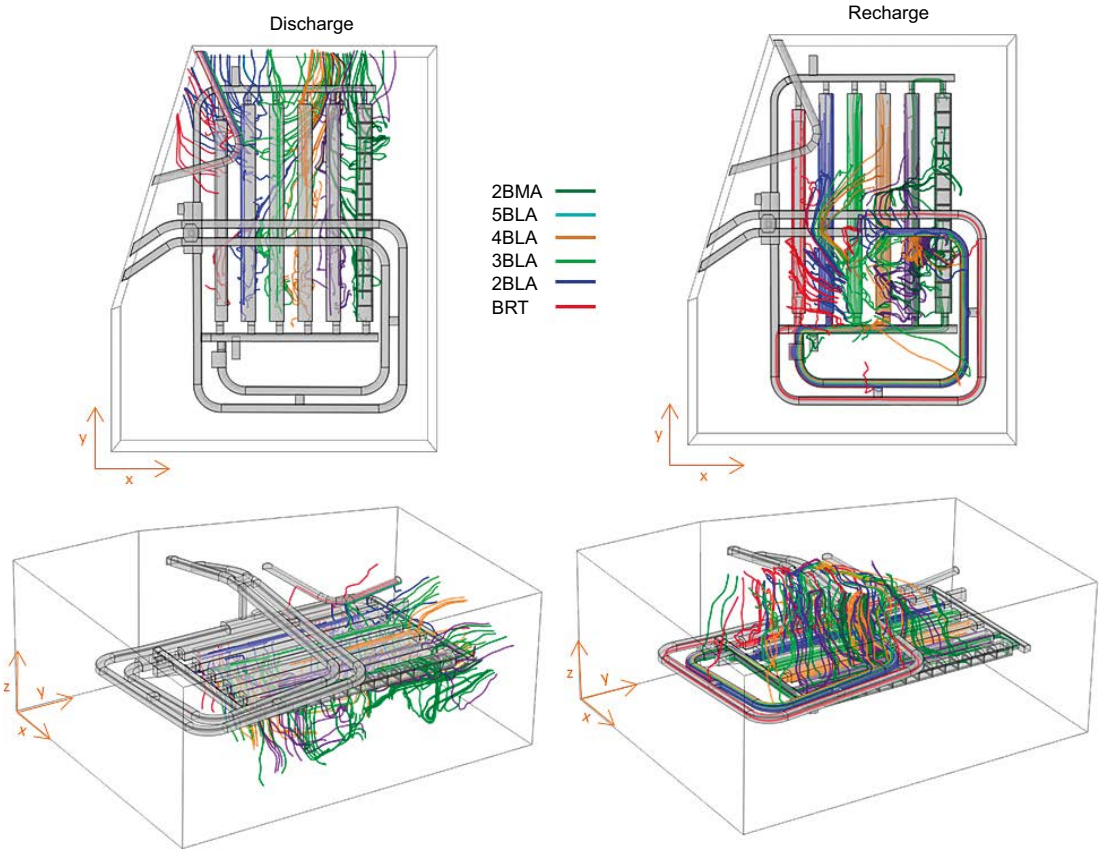

Figure 5-10. *Groundwater streamlines leaving (left) and reaching (right) individual vaults (colour tubes) of the SFR 3 repository for the case of complete plug degradation at 5000 AD. The x- and y-arrows point to the east and north, respectively.*

Table 5-4. Ratio of the total flow through the SFR 3 vaults for the plug degradation cases with respect to the Base case.

		MPD	SPD	CPD
Vaults	2BLA	1.00	1.34	3.16
	3BLA	1.00	1.15	2.11
	4BLA	1.00	1.29	2.01
	5BLA	1.01	1.33	2.04
	BRT	1.00	1.23	3.75
	2BMA	1.00	1.07	1.53
Waste	BRT	1.00	1.07	1.01
	2BMA	1.00	1.07	1.52

5.2.3 No barriers

This calculation case simulates the simultaneous and complete degradation of the concrete and bentonite barriers in SFR 3. This case is a combination of the completely degraded concrete and the completely degraded plugs cases. All the concrete and bentonite domains have a conductivity of 10^{-3} m/s (Appendix A). This case has been evaluated for 5000 AD.

The flows through the vaults and wastes for the plug degradation cases for 5000 AD are tabulated in Table B-20, Appendix B. Graphically, the flows are illustrated in Figure 5-11. Table 5-5 shows the ratio of the total flow through the SFR 3 vaults for the no barrier case with respect to the base case, and with respect to the complete plug degradation case presented in Section 5.2.2.

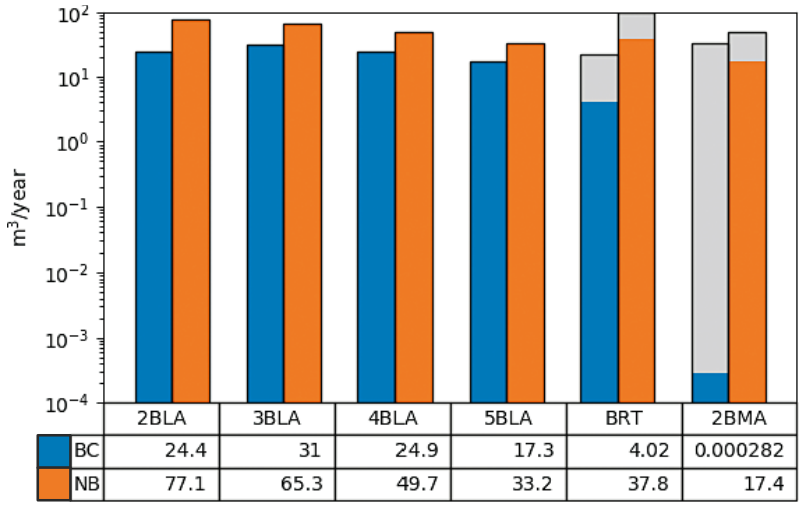

Figure 5-11. *Total flow (m^3/year) through the waste in the No Barriers case (NB) compared with the Base case (BC), studied at 5000 AD. The grey area illustrates the vault flow outside the waste compartment.*

The total flow through the repository is doubled with respect to the base case (Table 5-5). The most affected vault is by far BRT. The degree of effect decreases with the vault distance to the access ramp. This impact is consistent with the results obtained for the complete plug degradation case. In fact, the ratio between the cases of no barriers (NB) and with completely degraded plugs (CDP), are close to one for the flow through all vaults (Table 5-5). This indicates that the increase in the flow through the vaults in the no barriers case is solely due to the absence of plugs.

The flow through the waste increases in the two vaults with concrete barriers (2BMA and BRT). In BRT, it is multiplied by 9 with respect to the flow for the Base case (Table 5-5). The combined effect of the degradation of the plugs and the concrete barriers doubles the impact of the complete concrete degradation alone (see Table 5-3). The combined effect also enhances the increase of flow through the 2BMA waste. The no barriers case yields an additional 12 % of flow increase if compared with the effect of the complete concrete degradation alone (Table 5-3).

The flows are also compared with the No barriers case in Abarca et al. (2013), Table 5-5. There is a total increase of 18 % that is mainly concentrated in BRT and 2BMA. The change in BRT is not surprising since it has larger dimensions in the new layout. The new layout increases the flow in 2BMA by 28 %. The BLA vaults have a moderate increase in flow (between 8 and 18 %).

Table 5-5. Total flow through the vaults (m^3/year) for the No barriers (NB) case and ratio with respect to the Base case (BC), the Complete plug degradation case (CPD) and the No barriers case (NB*) reported in Abarca et al. (2013) at 5000 AD. Ratios lower than one indicate a reduction in flow.

		No barriers	Ratio NB/BC	Ratio NB/CPD	Ratio NB/NB*
Vaults	2BLA	77.1	3.08	1.00	1.08
	3BLA	65.3	2.00	1.00	1.14
	4BLA	49.7	1.80	0.99	1.18
	5BLA	33.2	1.68	0.94	1.09
	BRT	96.1	3.31	1.18	1.29
	2BMA	49.7	1.23	0.99	1.28
	Total	**371.10**	**2.13**	**1.03**	**1.18**
Waste	BRT	37.80	8.63	9.29	1.07
	2BMA	17.40	48333.33	40465.12	1.41

* Abarca et al. (2013).

5.3 Estimation of uncertainty associated with the geosphere

Two additional realizations of the rock permeability were used to assess the range of variability in the computed flows due to the uncertainties in the geosphere hydraulic description. These realizations are considered as representative of two cases that lead to a higher and a lower average tunnel flow with respect to the Base case. For this reason, hereafter, they are referred to as High (HFC) and Low (LFC) flow realizations (see Table 4-6 for the correspondence with respective DarcyTools simulations).

The Base case and the High flow realization represent the same structures affecting the repository. There are basically three high permeability zones. The first one is the deformation zone ZFMWNW8042, a thin fracture zone crossing all the vaults and 2BMA. The second one is a high permeability zone affecting the rock between vaults BRT and 5BLA. The third structure is the deformation zone ZFMWNW0835, a thick deformation zone crossing 2BMA, which also affects the 4BLA and 5BLA vaults. All these structures have a higher permeability in the High flow realization. There is also an increased presence of high permeability vertical structures in the High flow realization. The Low flow realization is characterized by a lower permeability zone in the areas of the access tunnels and the BRT vault and by thinner and less permeable fractures crossing the repository. There is a fourth permeable structure in the Low flow realization that crosses 2BMA and extends west affecting all the SFR 3 vaults. Details on the rock conductivity fields can be found in Abarca et al. (2013) and Öhman and Odén (2018).

This case was evaluated at 2000 AD and 5000 AD. The flows through the vaults and wastes for the two additional realizations of the rock conductivity field are tabulated for 2000 AD and 5000 AD in Table B-21 and Table B-22 in Appendix B, respectively. Graphically, the flows are illustrated in Figure 5-12 and Figure 5-13. Table 5-6 shows the ratio of the total flow through the SFR 3 vaults for two realizations of the rock conductivity (LFC, HFC) with respect to the Base case.

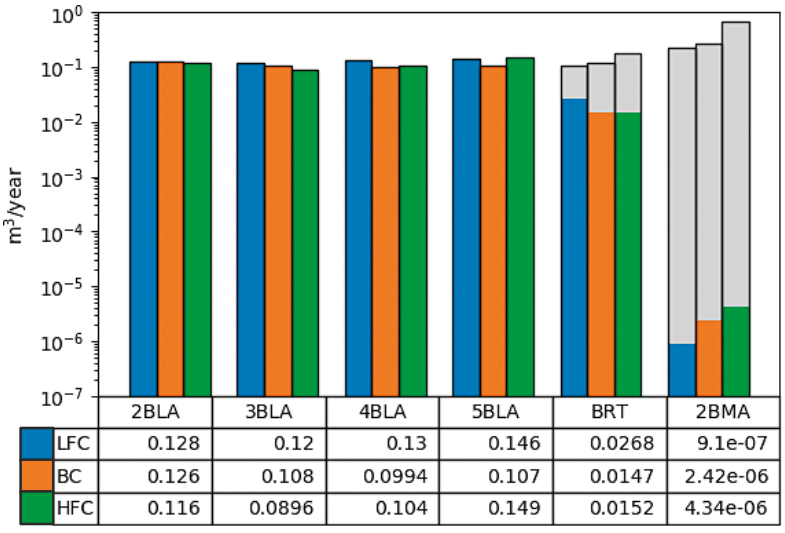

	2BLA	3BLA	4BLA	5BLA	BRT	2BMA
LFC	0.128	0.12	0.13	0.146	0.0268	9.1e-07
BC	0.126	0.108	0.0994	0.107	0.0147	2.42e-06
HFC	0.116	0.0896	0.104	0.149	0.0152	4.34e-06

Figure 5-12. *Total flow (m³/year) through the waste for three bedrock realizations, studied at 2000 AD. The grey area illustrates the vault flow outside the waste compartment.*

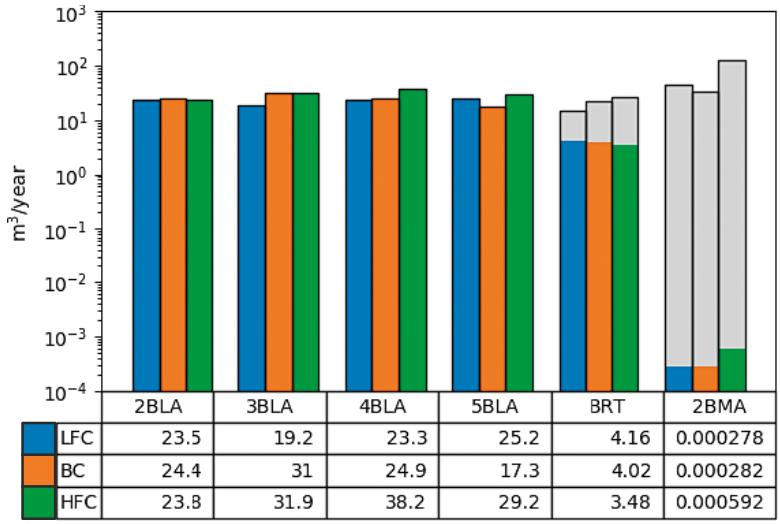

	2BLA	3BLA	4BLA	5BLA	BRT	2BMA
LFC	23.5	19.2	23.3	25.2	4.16	0.000278
BC	24.4	31	24.9	17.3	4.02	0.000282
HFC	23.8	31.9	38.2	29.2	3.48	0.000592

Figure 5-13. *Total flow (m^3/year) through the waste for three bedrock realizations, studied at 5000 AD. The grey area illustrates the vault flow outside the waste compartment.*

The different realizations of the rock conductivity fields condition the flow through the repository vaults. The computed flow values range from 0.62 and 4 times the values obtained for the base case (Table 5-6). The most sensitive vault is 2BMA, with a four times higher flow for the High Flow case at 5000 AD. This results highlight the importance of the location and local connectivity of fractures around the individual repository vaults.

Table 5-6. Ratio of the total flow through the SFR 3 vaults for the plug degradation cases with respect to the Base case.

		2000 AD		5000 AD	
		Ratio LFC/BC	Ratio HFC/BC	Ratio LFC/BC	Ratio HFC/BC
Vaults	2BLA	1.02	0.92	0.96	0.98
	3BLA	1.11	0.83	0.62	1.03
	4BLA	1.31	1.05	0.94	1.53
	5BLA	1.36	1.39	1.46	1.69
	BRT	0.86	1.46	0.66	1.21
	2BMA	0.87	2.57	1.33	3.92
Waste	BRT	1.82	1.03	1.03	0.87
	2BMA	0.38	1.79	0.99	2.10

The results of these simulations were compared against the same simulations performed with the previous repository and ramp layout reported in Abarca et al. (2013). The values of the flow ratios are given in Table 5-7. The ratios are in general larger than 1 at 2000 AD, indicating a consistent increase in the flows through the SFR 3 vaults with the new layout. The largest increase occurs in 2BMA and BRT. The increase in BRT is due to its larger dimensions in the new layout. The increase in flow in 2BMA in the HFC with the new layout is related to a change in its location relative to the local fracture zones. The maximum increase in the BLA vaults is 24 % for 5BLA at 2000 AD.

Table 5-7. Ratio of the total flow through the SFR 3 vaults (m^3/year) for two realizations of the rock conductivity (LFC, HFC) with respect to the same realizations reported in Abarca et al. (2013).

		2000 AD		5000 AD	
		Ratio LFC	Ratio HFC	Ratio LFC	Ratio HFC
Vaults	2BLA	0.98	0.89	1.01	0.81
	3BLA	1.20	0.90	1.09	0.95
	4BLA	1.18	0.95	1.08	1.09
	5BLA	1.22	1.24	1.03	0.98
	BRT	1.50	2.54	1.11	1.17
	2BMA	1.14	3.37	0.97	1.10
Waste	BRT	1.63	0.93	1.85	1.46
	2BMA	0.79	3.76	1.13	1.18

5.4 Summary of the calculation cases

The results presented for all the barrier degradation cases are summarized in Figure 5-14 and Table 5-8 at 5000 AD. This is the only set of boundary conditions for which all the calculation cases have been simulated. The comparison illustrates the variability of results over the calculation cases. The Base case is accompanied by a black line that indicates the variability in the flow associated with the uncertainty in the geosphere, as reported in Section 5.3. According to the model predictions, the most unfavourable cases are the completely degraded plugs case and the no barriers case. In those cases, the loop of the ramp that is located above the vaults collects the downwards flow from the rock and redirects the water through the ramp towards the vaults. Directly downstream of the ramp is BRT. The impact on the tunnel flow decreases with the distance to this ramp.

The most unfavourable case for BRT is the no barriers case. Most of the water circulates through this vault and prevents the increase of flow in the vaults situated east from BRT. For the rest of the vaults, the impact of the complete plugs degradation case and the no barrier case are equally severe. The impact of those two cases (no barriers and completely degraded plugs) is greater than the interval of variability due to the changes in the geosphere defined in Section 5.3, except for the 2BMA vault. The latter vault is extremely sensitive to the permeability of the different fracture zones intersecting it. The geosphere properties have a higher impact on the tunnel flows than the absence of plugs in the repository.

Regarding the water flow in the wastes, the critical cases are all the degraded concrete or no barrier cases. The concrete degradation impact is greater than the uncertainty interval associated with the geosphere variability, which is very small in the flows through the BRT and 2BMA wastes.

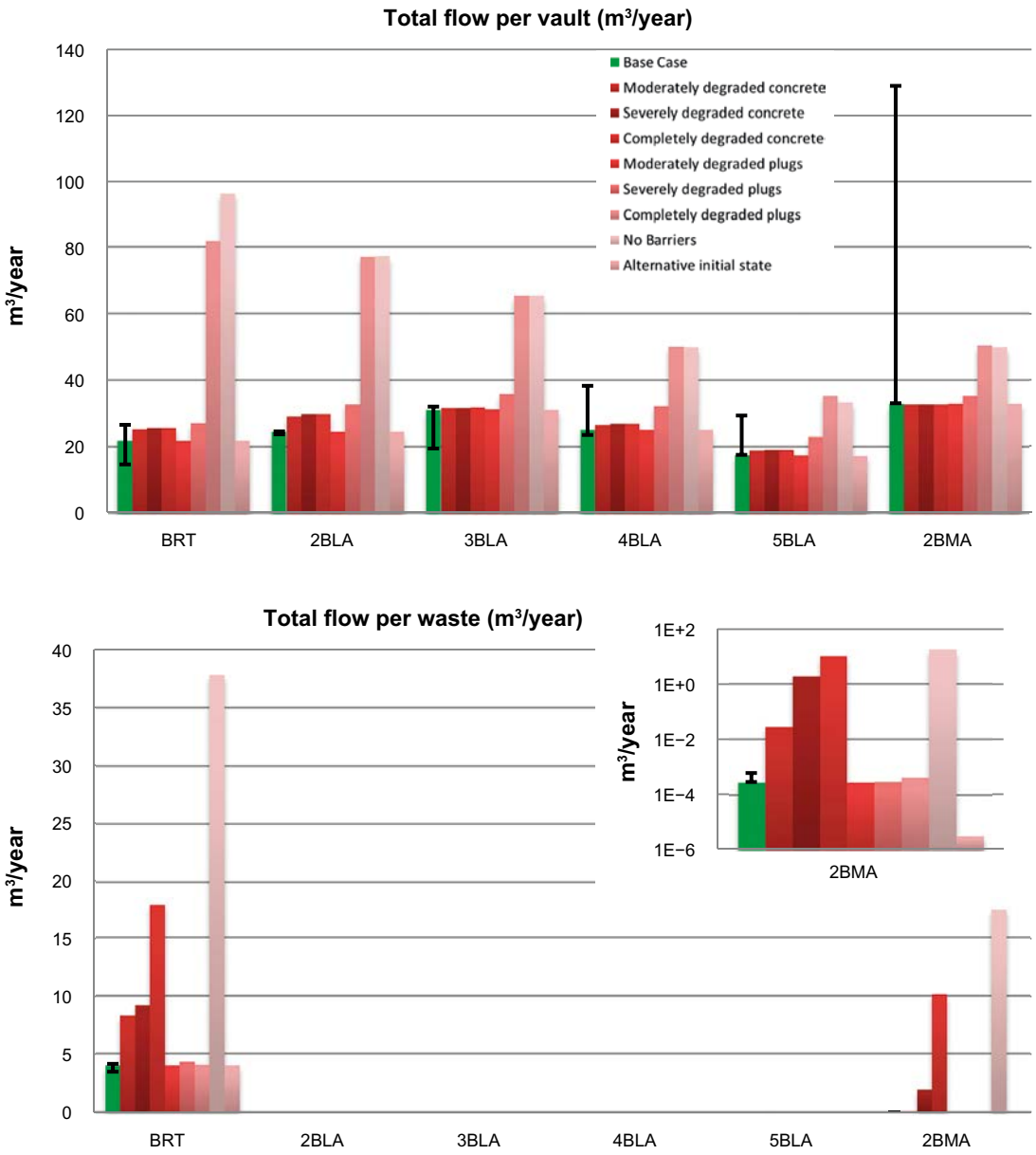

Figure 5-14. *Total flow (m^3/year) for the different vaults and waste domains in the SFR 3 repository for all the simulated cases at 5000 AD. The black line accompanying the Base case bar indicates the uncertainty interval for each vault due to the studied variability in the geosphere. The flow through the 2BMA waste ranges over many orders of magnitude, therefore it is also illustrated in logarithmic scale for clarity.*

Table 5-8. Summary of the results of total flow (m^3/year) in each vault for all the barrier degradation cases at 5000 AD.

		BRT	2BLA	3BLA	4BLA	5BLA	2BMA
Vaults	Base case	21.80	24.40	31.00	24.90	17.30	32.90
	Moderately degraded concrete	25.10	28.90	31.50	26.40	18.80	32.70
	Severely degraded concrete	25.50	29.70	31.60	26.80	19.10	32.70
	Completely degraded concrete	25.50	29.70	31.70	26.80	19.10	32.70
	Moderately degraded plugs	21.80	24.40	31.10	25.00	17.40	32.90
	Severely degraded plugs	26.90	32.70	35.80	32.10	23.00	35.30
	Completely degraded plugs	81.70	77.00	65.40	50.00	35.30	50.30
	No Barriers	96.10	77.10	65.30	49.70	33.20	49.70
	Alternative initial state*	21.80	24.40	31.00	24.90	17.30	32.90
Waste	Base case	4.02					2.82×10^{-4}
	Moderately degraded concrete	8.27					0.028
	Severely degraded concrete	9.16					1.910
	Completely degraded concrete	17.80					10.100
	Moderately degraded plugs	4.01					2.82×10^{-4}
	Severely degraded plugs	4.31					3.02×10^{-4}
	Completely degraded plugs	4.07					4.3×10^{-4}
	No Barriers	37.80					17.400
	Alternative initial state*	4.02					0.000

* The alternative initial state case is discussed in Section 6.

6 Alternative initial state for the 1BMA and 2BMA concrete

SKB is investigating a new engineered concrete (limestone concrete) that may improve the resistance to flow and increase the durability of the engineered barriers. This chapter analyses the potential reduction in flow through the 1BMA and 2BMA wastes assuming a high-performance construction concrete for 2BMA and for the reinforcement of 1BMA. A reduced hydraulic conductivity of 10^{-11} m/s is assumed for the alternative initial state of this new concrete. The rest of the repository materials have the properties assumed for the base case (see Appendix A).

Table 6-1 indicates the flow through the 1BMA and 2BMA vaults and waste domains for the alternative initial state case and the four shoreline positions. Table 6-2 presents the ratio of flows with respect to the Base case. The ratio of the vault flow is close to one for 1BMA and precisely one for 2BMA. Therefore, a high-performance concrete reduces minimally the flow through the 1BMA vault and does not alter the flow through 2BMA.

The impact of the high-performance concrete lies in the reduction of the flow through the waste. The reduction is of more than one order of magnitude with respect to the base case for 1BMA and of two orders of magnitude for 2BMA (Table 6-2). In the case of 2BMA, which has a perfect hydraulic cage configuration, the waste flow decrease is directly proportional to the reduction in the hydraulic conductivity of the concrete.

The change in the concrete properties in these two vaults has no effect in the rest of the repository vaults (see Appendix B and Appendix C).

Table 6-1. Total flow through the SFR 1 vaults and waste domains (m^3/year) for the Alternative Initial State for the 1BMA and 2BMA vaults.

		2000 AD	2500 AD	3500 AD	5000 AD
Vaults	1BMA	0.042	2.640	55.0	57.8
	2BMA	0.262	4.780	34	33
Waste	1BMA	0.0008	0.0144	0.3850	2.21
	2BMA	2.83×10^{-8}	4.16×10^{-7}	3.4×10^{-6}	3.27×10^{-6}

Table 6-2. Ratio of the total flow through the 1BMA and 2BMA vaults with respect to the Base case.

		2000 AD	2500 AD	3500 AD	5000 AD
Vaults	1BMA	0.966	0.989	0.984	0.991
	2BMA	1.000	1.000	1.000	1.000
Waste	1BMA	0.1169	0.1412	0.1310	0.6190
	2BMA	1.17×10^{-2}	1.16×10^{-2}	1.16×10^{-2}	1.16×10^{-2}

7 1BMA vault-scale model

Some specific questions concerning the effects and extent of concrete degradation of the 1BMA structure were investigated in more detail using the vault-scale model approach described in Abarca et al. (2014). A vault model was generated based on the repository scale model of SFR 1 described in Section 3. The objective was to extend the simulation cases to include an assessment of a reinforcement/repair case for 1BMA that does not rely on a foundation with injected cement.

7.1 Geometry of the 1BMA vault

The vault model includes all the improvements proposed for the 1BMA vault. To that end, it was necessary to modify the geometry of 1BMA with respect to the repository scale model described in Section 3. A new placement and thickness of the reinforced walls and lid were implemented following SR-PSU assumptions (Figure 7-1).

The new configuration includes:

- Modifications of the reinforced walls and lid. The thickness of the new walls is 0.3 m. The lid is divided into an inner lid of 0.4 m thickness and an outer lid of 0.8 m thickness.
- The new walls are supported by the rock floor.
- Drainage holes at the wall base ensure high permeability of the foundation domain.
- No injection of the foundation. In the numerical model, the foundation domain includes both the base of the new walls with drainage and the gravel layer (Figure 7-1).
- The vault scale model uses an updated geometry with respect to the repository scale model, but without considering the gas evacuation channels. The rock permeability field and boundary conditions from the repository scale model (Section 4.1) are implemented.

This configuration of 1BMA, with a high permeability foundation, is similar to the 1BMA vault with high permeability beams considered in Abarca et al. (2014) and to that of 2BMA. This configuration guarantees a more efficient hydraulic cage effect.

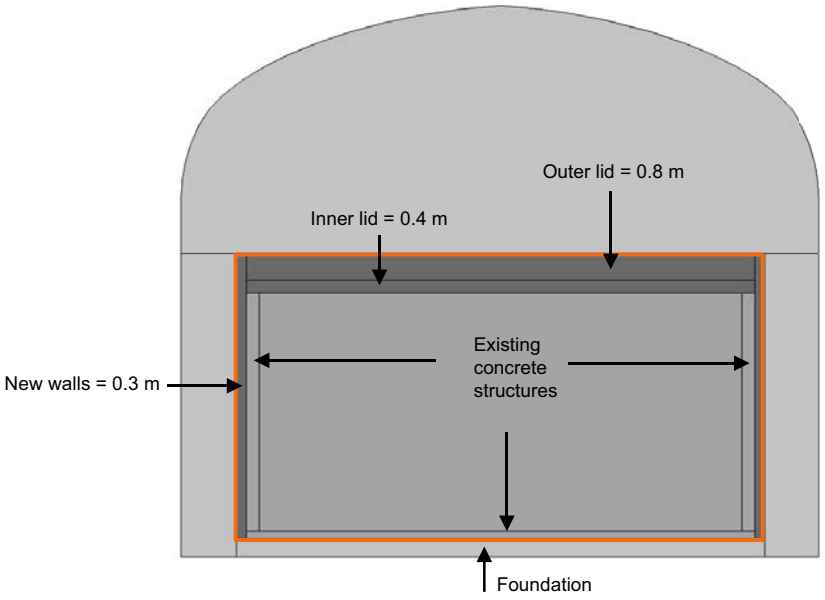

Figure 7-1. *Geometry of the 1BMA vault in the SFR 1 repository as implemented in the vault-scale model. The orange rectangle illustrates the encapsulated waste that serves as control volume to evaluate the flow through the waste. It is composed of the waste compartment surrounded by the existing concrete walls and new reinforcement walls and lid. The foundation includes the gravel layer (macadam) and the base of the new walls with drainage holes.*

7.2 Mesh

The resulting vault-scale model is illustrated in Figure 7-2. The dimensions of the vault together with vertex coordinates are presented in Table 7-1. The reference coordinate system (position and orientation) is consistent with the system used in the SDM report (SKB 2013).

Table 7-1. Dimensions of the 1BMA vault-scale model and coordinates of the corners.

Length	Width	Height	Xmin	Ymin	Zmin
175	38.56	38.4	6326.88	9977	−96

The mesh contains 4 147 043 tetrahedral elements (Figure 7-2).

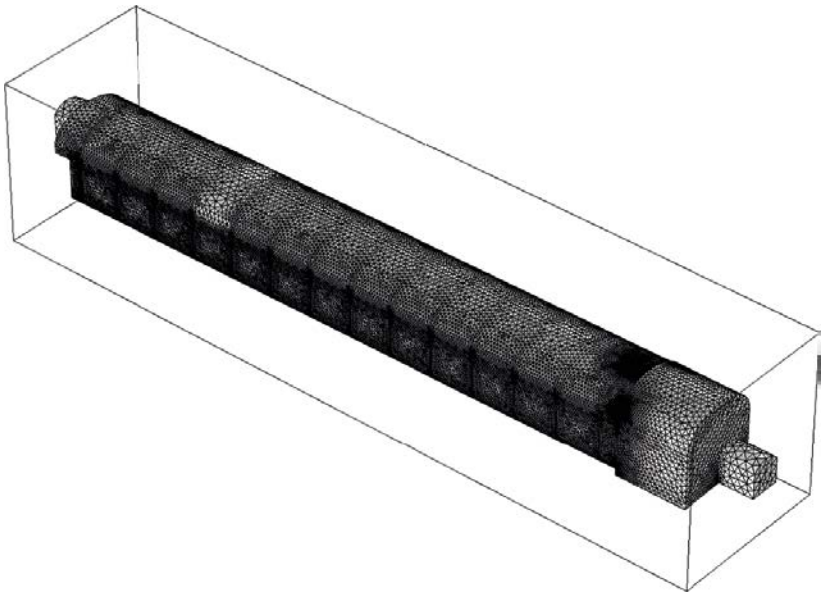

Figure 7-2. *Detail of the domain of the vault-scale model and mesh of tetrahedral elements in 1BMA.*

7.3 Boundary conditions and rock properties

The boundary conditions were extracted from the results for the Base case of the SFR 1 repository-scale model (Section 4.1). The fields of the calculated driving pressure at 2000 AD, 2500 AD, 3500 AD and 5000 AD were extracted and imposed at the vault-scale model boundaries. Even though the boundaries intersect the tunnel at the plug locations, a fixed pressure in the boundary conditions is justified because the repository-scale model and the vault-scale model are discretized with finite element meshes that adapt to the vault geometry. Therefore, the pressure field at the boundaries extracted from the repository scale model is fully consistent with the parameterization used in the vault-scale model. The boundaries are very close to the vault and the question arises as to whether the fixed pressure boundary conditions may be compromised. This has been tested and, as long as the backfill permeability is maintained, the boundary conditions of the vault-scale model are not affected by changes in the internal concrete structure of 1BMA. The backfill is crushed rock with no flow resistivity in this analysis. The large permeability of that backfill controls the pressure field around 1BMA and prevents impact on the boundaries. In some previous vault-scale models, in which alternative backfill materials were investigated, the boundary conditions had to be recomputed with the repository scale model using the same permeability of the backfill (von Schenck et al. 2018). In this case, this was not necessary.

The rock hydraulic conductivity field was imported into the vault-scale model using the same methodology as for the repository-scale models (see Section 3.8.2). The rock conductivity field corresponds to Case 1 (Base_Case1_DFN_R85) of the regional-scale model in DarcyTools, which is presented in more detail in Öhman and Odén (2018).

7.4 Calculation cases

The concrete evolution for the new walls and lid follows the Base case evolution for concrete as detailed in SKB (2015). However, the existing concrete structures (outer and inner walls and floor) follow the evolution of accelerated concrete degradation as detailed in SKB (2015). The supporting beams, base of new walls, and crushed rock in the foundation have the maximum conductivity (K = 10^{-3} m/s) as in SR-PSU. This large conductivity value represents the drainage system that is in place in the foundation.

The calculation cases reflect a one-time progression of four degradation states (Table 7-2 and Figure 7-3). To that end, IS and DS1 is simulated for all shoreline positions and, the advanced degradation states DS2 and DS3, only for the last shoreline position (5000 AD). The conductivity of the waste was assumed to be the maximum of the values for the Base case or the accelerated concrete degradation cases.

Table 7-2. Time progression of the four concrete degradation states for the reinforced and existing concrete structures.

	IS Initial state	DS1 2–22 kyr	DS2 22–52 kyr	DS3 52–102 kyr
Reinforced concrete walls and lids	8.3×10^{-10}	1.0×10^{-7}	1.0×10^{-5}	1.0×10^{-3}
Existing inner and outer walls and floor	1.0×10^{-5}	1.0×10^{-5}	1.0×10^{-3}	1.0×10^{-3}
Waste (max(K_acc_deg,K_waste_BC))	1.0×10^{-5}	1.0×10^{-4}	1.0×10^{-3}	1.0×10^{-3}

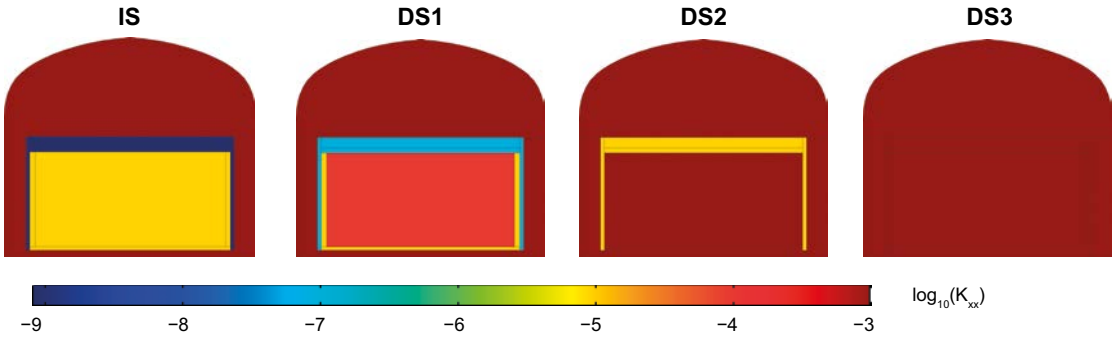

Figure 7-3. *Hydraulic conductivity of the 1BMA concrete barriers for the four concrete degradation states.*

7.4.1 Observables

Four observables were defined to quantify groundwater flow through 1BMA for the different cases. Two of them describe the flow at the scale of control volumes whereas the other two are integrated indicators at vault scale.

1. The groundwater flow through the control volume faces, Q_{face}, is calculated by taking the surface integral over each of the 6 faces of the control volume:

$$Q_{face} = \iint \left(u\, n_x + v\, n_y + w\, n_z\right) dA\,, \qquad \text{Equation 7-1}$$

where dA is a surface element, u, v and w are the Darcy flow components (m/s) in the x-, y- and z-directions, respectively and n_x, n_y and n_z are the components of the normal vector in the x-, y- and z-directions, respectively.

The COMSOL model produces tables of groundwater flow rates for all faces of thecontrol volumes of the 1BMA vault. These tables serve as input to the radionuclide transport model that is set up and solved in the commercial software Ecolego (SKB 2013).

2. The total inflow through a control volume ***i*** is computed by summing the inflow ($Q_{face} > 0$)through the 6 control volume faces. Correspondingly, the total outflow through a control volume *i* is computed by adding up the computed outflow ($Q_{face} < 0$) over its 6 faces. Thus, the total flow over the control volume is the average between the total inflow and outflow and the mass balance error is the difference between the inflow and outflow. The total flows (Qi) through the 15 waste control volumes (Figure 7-4) are computed and presented in this report to illustrate changes in the axial distribution of flow in the waste control volumes for the considered cases.

$$Q_{in_i} = \sum\left[\left(Q_{face}\right) > 0\right] \qquad \text{Equation 7-2}$$

$$Q_{out_i} = \sum\left[\left(Q_{face}\right) < 0\right] \qquad \text{Equation 7-3}$$

$$Q_i = \frac{Q_{in_i} - Q_{out_i}}{2} \qquad \text{Equation 7-4}$$

3. The total groundwater flow through the whole waste. The waste flow (m^3/year) is calculated as the summation, over all the faces defining the concrete/backfill interface (Figure 7-5), of the average of the inflow and outflow. This indicator is presented in the tables of this report. Note that the waste flow is not equal to adding the total flow of the 15 waste control volumes because the shared faces of the control volumes are not part of the concrete/backfill interface.
4. The total groundwater flow through the 1BMA vault**.** The vault flow (m^3/year) is calculated as the summation, over all the faces defining the rock/backfill interface (Figure 7-6), of the average of the inflow and outflow. This indicator is presented in the tables of the report.

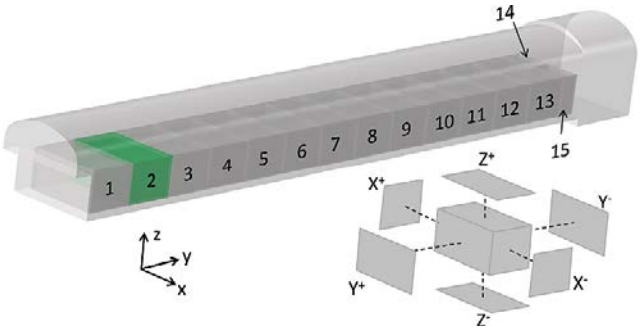

Figure 7-4. *Waste control volumes in the 1BMA model. For each individual control volume flow is computed in each of its 6 faces. Control volumes 14 and 15 are merged together in a control volume labelled 14_15.*

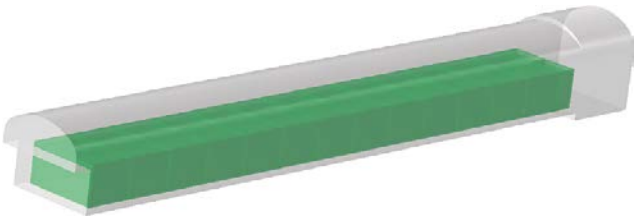

Figure 7-5. *Geometry of the 1BMA vault. The surface backfill/concrete where the waste flow is evaluated is shown in green.*

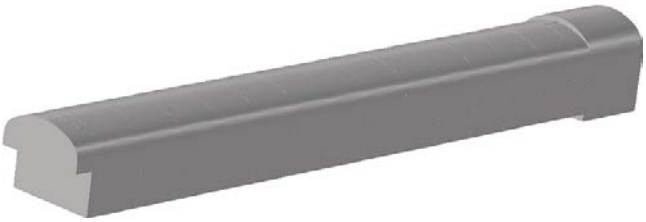

Figure 7-6. *Backfill/rock surface where the vault flow is evaluated.*

7.4.2 Groundwater flow through the 1BMA vault and waste

The results of the flow through the vault and the waste for the calculation cases are presented in Table 7-3. The simulation cases reflect a progression of four concrete degradation states (Table 7-2).

Table 7-3. Summary of total flow (m^3/year) through the vault and waste domains and the ratios with respect to initial state for the different degradation states and the 4 shoreline positions.

Degradation ID	Shoreline position	Vault Flow (m^3/y)	Waste Flow (m^3/y)	Waste flow/ Vault flow	Vault flow ratio wrt IS	Waste flow ratio wrt IS
IS	2000 AD	0.05	0.0005	0.010	-	-
	2500 AD	2.82	0.02	0.007	-	-
	3500 AD	65.76	0.47	0.007	-	-
	5000 AD	70.15	0.51	0.007	-	-
DS1	2000 AD	0.05	0.002	0.040	1.00	4.95
	2500 AD	2.82	0.08	0.028	1.00	5.03
	3500 AD	65.51	2.59	0.040	1.00	5.50
	5000 AD	69.87	2.83	0.041	1.00	5.50
DS2	5000 AD	69.14	25.46	0.368	0.99	49.48
DS3	5000 AD	69.64	47.56	0.683	0.99	92.43

For the initial state (IS), the vault and waste flows increase as the shoreline position advances, consistent with the results reported for the base case of the repository scale model (Section 4.1.5).

Comparing the concrete degradation states, it is observed that the vault flow is insensitive to the degradation state of the concrete barriers for all shoreline positions. However, the water flow in the waste increases following the concrete degradation. In the initial state, flow in the waste is less than 1 % of the vault flow for all shoreline positions. A slightly higher proportion of the vault flow enters the waste at 2000 AD, when groundwater flows upwards through 1BMA.The percentage of vault flow entering the waste increases as the degradation state advances. At degradation state 3, it reaches a maximum of around 68 %. The flow in the waste in that case is two orders of magnitude higher than the flow in the waste for the initial state.

The magnitude of the flow and the flow field for each degradation state on two transverse and one longitudinal sections of the 1BMA vault-scale model are shown in Appendix D and Appendix E, respectively. The plots illustrate the local change in the flow field around the repository for each degradation state.

7.4.3 Axial distribution of the water flow in the waste

The axial distribution of the flow in the waste has been analysed by means of the computed flow rates through the waste control volumes defined in Section 7.4.1. The encapsulated waste (EW) of 1BMA is divided into 14 inner sections (Figure 7-4). Note than in previous reports (Abarca et al. 2013, 2014), the waste in 1BMA was divided into 15 sections. Here, sections 14 and 15 are merged into a unique waste control volume.

- At 2000 AD (Figure 7-7), the flow increases from EW3 to EW9 and reaches a maximum in EW9–11. EW12 receives less water inflow because it is in a shadow zone between fractures affecting the neighbouring sections. Note that EW12 is located upstream of EW13, which is affected by the deformation zone ZFMNNW1209. Assuming the concrete barriers in degradation state 1 (DS1), the axial distribution is maintained although the overall flow increases.
- At 2500 AD (Figure 7-8) the axial profile is almost flat between EW1 and EW8 and between EW8 and EW14–15. Most of the inflow is concentrated in EW8. The degradation of the concrete to degradation state 1, results in a homogeneous increase in flow per control volume but the pattern in the axial profile is maintained.

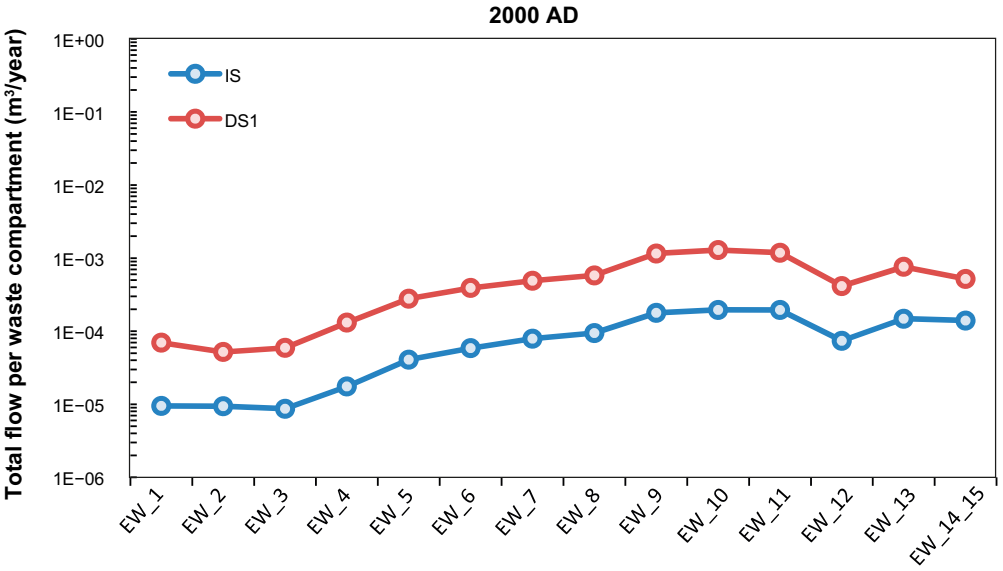

Figure 7-7. *Flow rates (m^3/year) through the encapsulated waste (EW) compartments of the repaired 1BMA for the Initial State (IS) and the Degradation Stage 1 (DS1) of the reinforced structures for the time 2000 AD.*

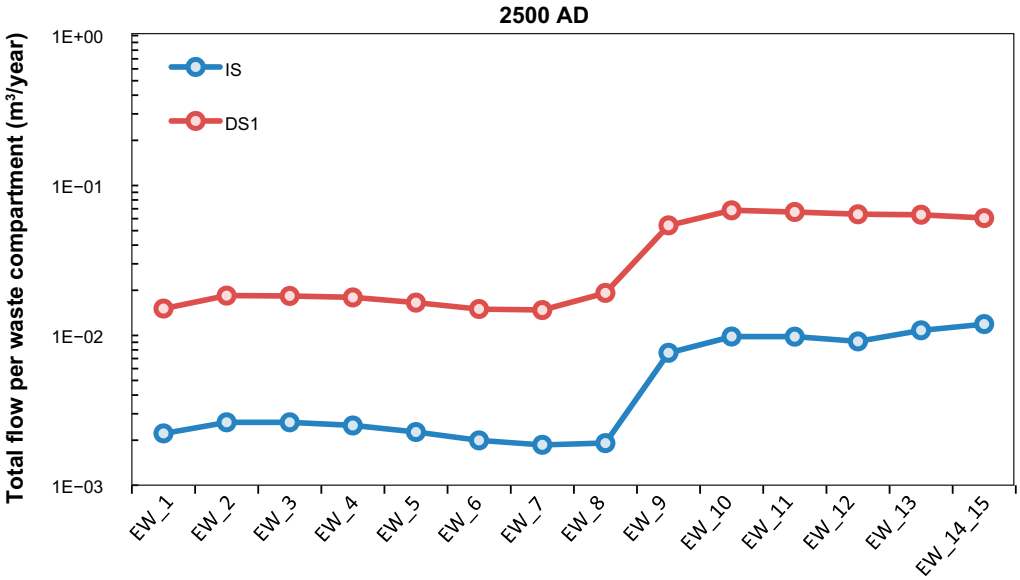

Figure 7-8. *Flow rates (m^3/year) through the encapsulated waste (EW) compartments of the repaired 1BMA for the Initial State (IS) and the Degradation Stage 1 (DS1) of the reinforced structures for the time 2500 AD.*

- The flow profiles at 3500 AD (Figure 7-9) and 5000 AD (Figure 7-10) have a similar pattern. The flow increases uniformly from south to north indicating inflow from the backfill in all sections. The flow has a maximum in EW13, influenced by the deformation zone ZFMNNW1209 that acts a preferential outflow zone. The pattern is maintained with the degradation of the concrete barriers, with a consistent increase in the flow through individual waste compartments with the concrete degradation.

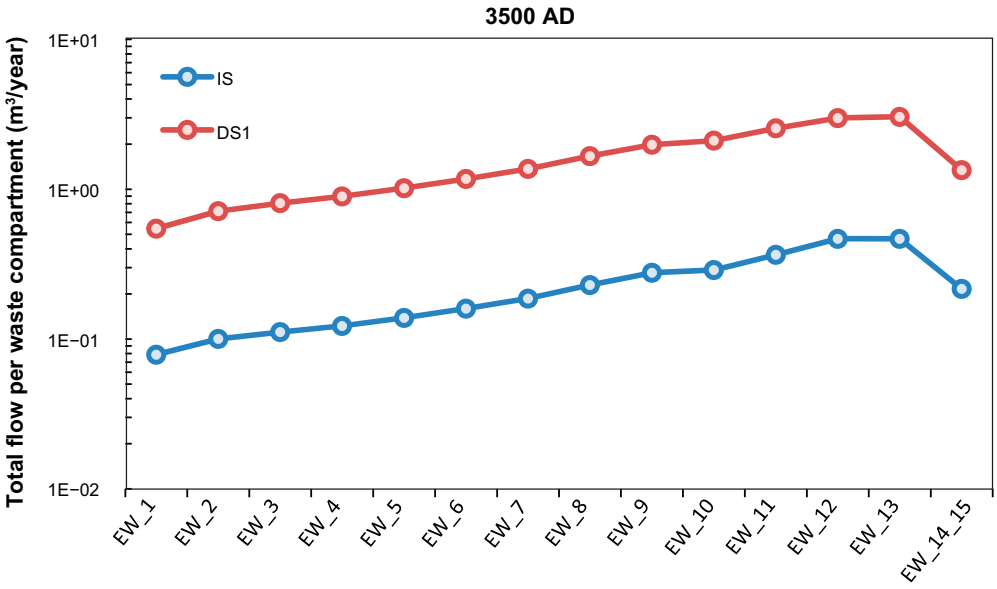

Figure 7-9. *Flow rates (m^3/year) through the encapsulated waste (EW) compartments of the repaired 1BMA for the Initial State (IS) and the Degradation Stage 1 (DS1) of the reinforced structures for the time 3500 AD.*

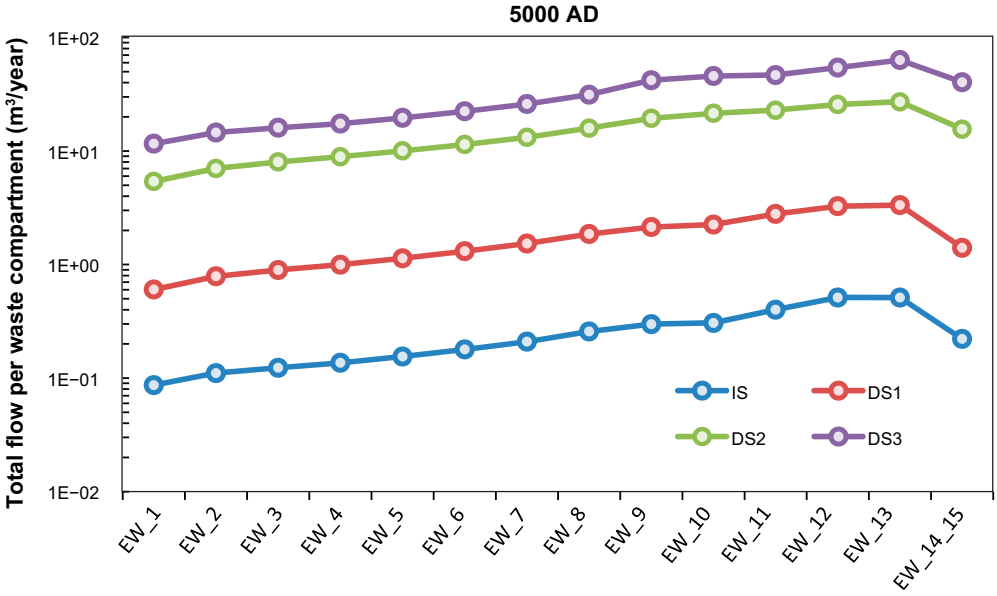

Figure 7-10. *Flow rates (m^3/year) through the encapsulated waste (EW) compartments of the repaired 1BMA for the Initial State (IS), the Degradation Stage 1 (DS1), the Degradation Stage 2 (DS2) and the Degradation Stage 3 (DS3) of the reinforced structures for the time 5000 AD.*

7.5 Summary of the calculation cases

The effect of the concrete barrier degradation on flow through the waste is summarized in Figure 7-11 corresponding to 5000 AD. The results show:

- For a concrete conductivity lower than 1×10^{-5} m/s, there is a linear log-log relationship between the hydraulic conductivity of the concrete barriers and the flow through the waste.
- For a concrete conductivity higher than 1×10^{-5} m/s, the flow through the waste approaches asymptotically the flow through the vault. In these cases, the hydraulic conductivity of the concrete barriers is higher than that of the host rock. Therefore, in these cases the main flow barrier is the rock that limits the flow towards the vault.
- The flow through the vault is not affected by the hydraulic properties of the concrete. That flow is limited by the host rock properties and the regional groundwater flow field, which changes with the movement of the shoreline position.

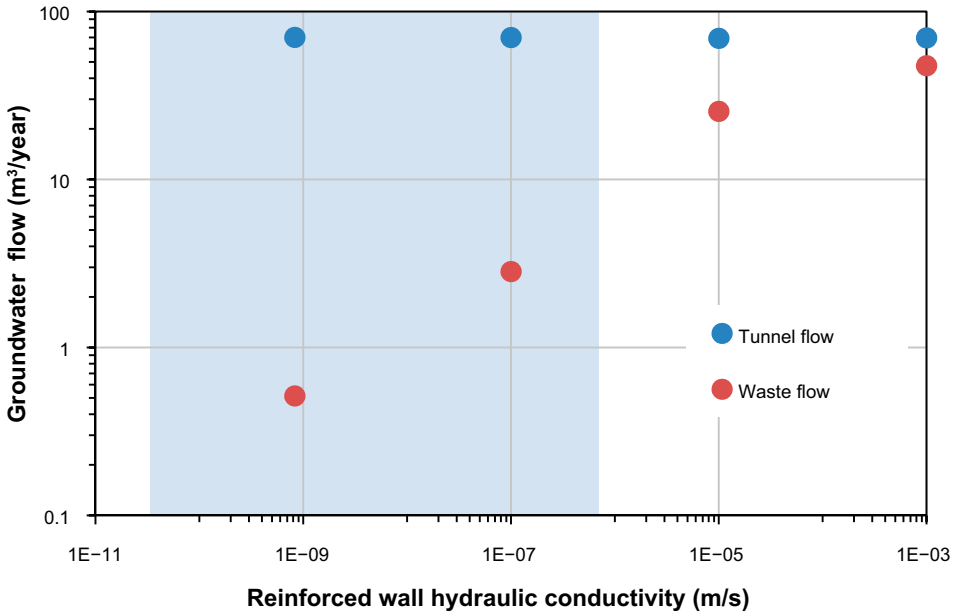

Figure 7-11. *Tunnel and waste flow (m^3/year) through the repaired 1BMA as a function of the hydraulic conductivity of the reinforced walls at shoreline position 4. The blue area delimitates the range of the rock hydraulic conductivity.*

References

SKB's (Svensk Kärnbränslehantering AB) publications can be found at www.skb.com/publications. SKBdoc documents will be submitted upon request to document@skb.se.

Abarca E, Idiart A, de Vries L M, Silva O, Molinero J, von Schenck H, 2013. Flow modelling on the repository scale for the safety assessment SR-PSU. SKB TR-13-08, Svensk Kärnbränslehantering AB.

Abarca E, Silva O, Idiart A, Nardi A, Font J, Molinero J, 2014. Flow and transport modelling on the vault scale for the safety assessment SR-PSU. SKB R-14-14, Svensk Kärnbränslehantering AB.

COMSOL, 2017. COMSOL Multiphysics® v. 5.3. COMSOL AB, Stockholm, Sweden.

Elfwing M, Mårtensson P, Pettersson A, von Schenck H, 2016. Fördjupad redovisning av förstärkningsmetod för betongkonstruktionen i 1BMA i SFR 1. SKBdoc 1534701 ver 2.0, Svensk Kärnbränslehantering AB. (In Swedish.)

Elfwing M, Lundin M, von Schenck H, 2017. Vidareutvecklad utformning av förvarsutrymmet 2BMA i utbyggd del av SFR. SKBdoc 1569813 ver 1.0, Svensk Kärnbränslehantering AB. (In Swedish.)

Facilia, 2015. Ecolego v6.2, http://ecolego.facilia.se.

Holmén J G, Stigsson M, 2001. Modelling of future hydrogeological conditions at SFR. SKB R-01-02, Svensk Kärnbränslehantering AB.

Luterkort D, Gylling B, Johansson R, 2012. Closure of the Spent Fuel Repository in Forsmark. Studies of alternative concepts for sealing of ramp, shafts and investigation boreholes. SKB TR-12-08, Svensk Kärnbränslehantering AB.

Mårtensson P, Pettersson A, 2015. Reparations- och förstärkningsåtgärder för 1B. SKBdoc 1467828 ver 2.0, Svensk Kärnbränslehantering AB. (In Swedish.)

Odén M, Follin S, Öhman J, Vidstrand P, 2014. SR-PSU Bedrock hydrogeology. Groundwater flow modelling methodology, setup and results. SKB R-13-25, Svensk Kärnbränslehantering AB.

SKB, 2013. Site description of the SFR area at Forsmark at completion of the site investigation phase. SDM-PSU Forsmark. SKB TR-11-04, Svensk Kärnbränslehantering AB.

SKB, 2014a. Climate and climate related issues for the safety assessment SR-PSU. SKB TR-13-05, Svensk Kärnbränslehantering AB.

SKB, 2014b. Initial state report for the safety assessment SR-PSU. SKB TR-14-02, Svensk Kärnbränslehantering AB.

SKB, 2015. Radionuclide transport and dose calculation for the safety assessment SR-PSU. Revised edition. SKB TR-14-09, Svensk Kärnbränslehantering AB.

Svensson U, Ferry M, Kuylenstierna H-O, 2010. DarcyTools version 3.4 – Concepts, methods and equations. SKB R-07-38, Svensk Kärnbränslehantering AB.

von Schenck H, Åstrand P-G, Abarca E, Sampietro D, 2015. Reparationsåtgärder för 1BMA utvärderade med modellering av närzonshydrologi och radionuklidtransport. Internal report SKBdoc 1480977 ver 2.0, Svensk Kärnbränslehantering AB. (In Swedish.)

von Schenck H, Åstrand P-G, Abarca E, Sampietro D, 2018. Inverkan av återfyllnadsmaterial på grundvattenflöde och radionuklidtransport i 2BMA. SKBdoc 1601117 ver 1.0, Svensk Kärnbränslehantering AB. (In Swedish.)

Öhman J, Odén M, 2018. SR-PSU (PSAR) Bedrock hydrogeology. TD18 – Temperate climate conditions. SKB P-18-02, Svensk Kärnbränslehantering AB.

Appendix A

Properties of the repository materials

Table A-1. Hydraulic conductivity (m/s) of the repository materials for all the simulated cases.

Repository components		Materials		Base case	Alternative initial state	Concrete degradation			Plug degradation			No barriers	Ice lens
						Moderate	Severe	Complete	Moderate	Severe	Complete		
		ID Simulation case		1–4; 26–29	5–8	9–12	13–16	17–20	21	22	23	24	25
Tunnels		Backfill		1.0×10^{-3}	1.0×10^{-3}	1.0×10^{-3}	1.0×10^{-3}	1.0×10^{-3}	1.0×10^{-3}	1.0×10^{-3}	1.0×10^{-3}	1.0×10^{-3}	1.0×10^{-3}
SFR1	Vaults	Concrete 1–2BTF, Silo, BRT		1.0×10^{-9}	1.0×10^{-9}	1.0×10^{-7}	1.0×10^{-5}	1.0×10^{-3}	1.0×10^{-9}	1.0×10^{-9}	1.0×10^{-9}	1.0×10^{-3}	1.0×10^{-9}
		Construction concrete reinforcement 1BMA		1.0×10^{-9}	1.0×10^{-11}	1.0×10^{-7}	1.0×10^{-5}	1.0×10^{-3}	1.0×10^{-9}	1.0×10^{-9}	1.0×10^{-9}	1.0×10^{-3}	1.0×10^{-9}
		Foundation 1BMA (injection concrete)		1.0×10^{-9}	1.0×10^{-9}	1.0×10^{-9}	1.0×10^{-5}	1.0×10^{-3}	1.0×10^{-9}	1.0×10^{-9}	1.0×10^{-9}	1.0×10^{-3}	1.0×10^{-9}
		Waste domain 1BMA (grouted waste + existing concrete structure)		1.0×10^{-6}	1.0×10^{-8}	1.0×10^{-4}	1.0×10^{-3}	1.0×10^{-3}	1.0×10^{-6}	1.0×10^{-6}	1.0×10^{-6}	1.0×10^{-3}	1.0×10^{-6}
		Concrete backfill (BTF vaults), grout		1.0×10^{-8}	1.0×10^{-8}	1.0×10^{-6}	1.0×10^{-4}	1.0×10^{-3}	1.0×10^{-8}	1.0×10^{-8}	1.0×10^{-8}	1.0×10^{-3}	1.0×10^{-8}
		Gas evacuation channels 1BMA		5.0×10^{-9}	5.0×10^{-9}	1.0×10^{-6}	1.0×10^{-5}	1.0×10^{-3}	5.0×10^{-9}	5.0×10^{-9}	5.0×10^{-9}	1.0×10^{-3}	5.0×10^{-9}
		Waste 1–2BTF vaults	Kx*	8.07×10^{-9}	8.07×10^{-9}	8.06×10^{-7}	7.54×10^{-5}	1.0×10^{-3}	8.07×10^{-9}	8.07×10^{-9}	8.07×10^{-9}	1.0×10^{-3}	8.07×10^{-9}
			Ky*	4.58×10^{-9}	4.58×10^{-9}	4.58×10^{-7}	4.48×10^{-5}	1.0×10^{-3}	4.58×10^{-9}	4.58×10^{-9}	4.58×10^{-9}	1.0×10^{-3}	4.58×10^{-9}
			Kz*	6.35×10^{-9}	6.35×10^{-9}	6.35×10^{-7}	6.07×10^{-5}	1.0×10^{-3}	6.35×10^{-9}	6.35×10^{-9}	6.35×10^{-9}	1.0×10^{-3}	6.35×10^{-9}
		Waste 1BLA		1.0×10^{-3}	1.0×10^{-3}	1.0×10^{-3}	1.0×10^{-3}	1.0×10^{-3}	1.0×10^{-3}	1.0×10^{-3}	1.0×10^{-3}	1.0×10^{-3}	1.0×10^{-3}
		1–2BTF and 1BLA foundation layer		1.0×10^{-7}	1.0×10^{-7}	1.0×10^{-7}	1.0×10^{-5}	1.0×10^{-3}	1.0×10^{-7}	1.0×10^{-7}	1.0×10^{-7}	1.0×10^{-3}	1.0×10^{-7}
	Silo	Top layer (90 % sand 10 % bentonite)		1.0×10^{-9}	1.0×10^{-9}	1.0×10^{-9}	1.0×10^{-9}	1.0×10^{-9}	1.0×10^{-9}	1.0×10^{-9}	1.0×10^{-9}	1.0×10^{-3}	1.0×10^{-9}
		Bottom layer (90 % sand 10 % bentonite)		1.0×10^{-9}	1.0×10^{-9}	1.0×10^{-9}	1.0×10^{-9}	1.0×10^{-9}	1.0×10^{-9}	1.0×10^{-9}	1.0×10^{-9}	1.0×10^{-3}	1.0×10^{-9}
		Waste Silo		1.0×10^{-6}	1.0×10^{-6}	1.0×10^{-6}	1.0×10^{-6}	1.0×10^{-6}	1.0×10^{-6}	1.0×10^{-6}	1.0×10^{-6}	1.0×10^{-3}	1.0×10^{-6}
		Concrete lid w/gas evac channels	Kx = Ky	1.0×10^{-9}	1.0×10^{-9}	1.0×10^{-7}	1.0×10^{-5}	1.0×10^{-3}	1.0×10^{-9}	1.0×10^{-9}	1.0×10^{-9}	1.0×10^{-3}	1.0×10^{-9}
			Kz	3.01×10^{-7}	3.01×10^{-7}	4.0×10^{-7}	1.03×10^{-5}	1.0×10^{-3}	3.01×10^{-7}	3.01×10^{-7}	3.01×10^{-7}	1.0×10^{-3}	3.01×10^{-7}
		Bentonite walls					$F = 1.54\times10^{-12}\cdot z(m)+2.11\times10^{-10}$					1.0×10^{-3}	F
		Central ring of Silo bentonite walls					$F = 1.54\times10^{-12}\cdot z(m)+2.11\times10^{-10}$					1.0×10^{-3}	1.0×10^{-3}
Plugs		Structural plug		1.0×10^{-6}	1.0×10^{-6}	1.0×10^{-6}	1.0×10^{-6}	1.0×10^{-6}	1.0×10^{-5}	1.0×10^{-4}	1.0×10^{-3}	1.0×10^{-3}	1.0×10^{-6}
		Sealed hydraulic sections of bentonite		1.0×10^{-12}	1.0×10^{-12}	1.0×10^{-12}	1.0×10^{-12}	1.0×10^{-12}	1.0×10^{-9}	1.0×10^{-6}	1.0×10^{-3}	1.0×10^{-3}	1.0×10^{-12}
SFR3	Vaults	Construction concrete 2BMA		1.0×10^{-9}	1.0×10^{-11}	1.0×10^{-7}	1.0×10^{-5}	1.0×10^{-3}	1.0×10^{-9}	1.0×10^{-9}	1.0×10^{-9}	1.0×10^{-3}	-
		Backfill		1.0×10^{-3}	1.0×10^{-3}	1.0×10^{-3}	1.0×10^{-3}	1.0×10^{-3}	1.0×10^{-3}	1.0×10^{-3}	1.0×10^{-3}	1.0×10^{-3}	-
		Gas evacuation channels		5.0×10^{-9}	5.0×10^{-9}	1.0×10^{-6}	1.0×10^{-5}	1.0×10^{-3}	5.0×10^{-9}	5.0×10^{-9}	5.0×10^{-9}	1.0×10^{-3}	-
		BRT, grouted waste		1.0×10^{-8}	1.0×10^{-8}	1.0×10^{-6}	1.0×10^{-4}	1.0×10^{-3}	1.0×10^{-8}	1.0×10^{-8}	1.0×10^{-8}	1.0×10^{-3}	-
		2BMA waste		1.0×10^{-6}	1.0×10^{-8}	1.0×10^{-4}	1.0×10^{-3}	1.0×10^{-3}	1.0×10^{-6}	1.0×10^{-6}	1.0×10^{-6}	1.0×10^{-3}	-
		BRT and 2–5BLA foundation layer		1.0×10^{-7}	1.0×10^{-7}	1.0×10^{-7}	1.0×10^{-5}	1.0×10^{-3}	1.0×10^{-7}	1.0×10^{-7}	1.0×10^{-7}	1.0×10^{-3}	-
		2BMA foundation layer of macadam		1.0×10^{-3}	1.0×10^{-3}	1.0×10^{-3}	1.0×10^{-3}	1.0×10^{-3}	1.0×10^{-3}	1.0×10^{-3}	1.0×10^{-3}	1.0×10^{-3}	-

Appendix B

Flow tables

SFR 1

Table B-1. Total flow (m^3/year) through the vaults and waste compartments for the Base case studied at different shoreline positions.

		2000 AD	2500 AD	3500 AD	5000 AD
Vaults	1BMA	0.0435	2.67	55.9	58.3
	1BLA	0.122	5.82	122	133
	1BTF	0.0288	2.84	21.7	24.5
	2BTF	0.0429	3.24	40.5	45
	Silo	0.00459	0.178	0.933	1.3
Waste	1BMA	0.00691	0.102	2.94	3.57
	1BLA	0.118	5.39	120	131
	1BTF	0.00943	0.328	3.52	3.98
	2BTF	0.00921	0.213	4.58	5.1
	Silo	0.00446	0.168	0.88	1.29

Table B-2. Total flow (m^3/year) through the vaults and waste compartments for the Base case and the three concrete degradation cases, studied at 2000 AD.

		Base case	Moderate	Severe	Complete
Vaults	1BMA	0.0435	0.0428	0.0462	0.046
	1BLA	0.122	0.127	0.131	0.131
	1BTF	0.0288	0.0329	0.0329	0.0314
	2BTF	0.0429	0.053	0.0549	0.0546
	Silo	0.00459	0.00561	0.00571	0.00572
Waste	1BMA	0.00691	0.00756	0.0234	0.0361
	1BLA	0.118	0.122	0.126	0.126
	1BTF	0.00943	0.0213	0.0217	0.0225
	2BTF	0.00921	0.0303	0.0334	0.0458
	Silo	0.00446	0.00552	0.00565	0.00565

Table B-3. Total flow (m^3/year) through the vaults and waste compartments for the Base case and the three concrete degradation cases, studied at 2500 AD.

		Base case	Moderate	Severe	Complete
Vaults	1BMA	2.67	2.69	2.74	2.74
	1BLA	5.82	6.3	6.44	6.45
	1BTF	2.84	3.04	2.97	2.36
	2BTF	3.24	3.36	3.38	3.37
	Silo	0.178	0.204	0.206	0.207
Waste	1BMA	0.102	0.119	0.946	2.09
	1BLA	5.39	5.88	6.02	6.02
	1BTF	0.328	0.867	0.924	1.43
	2BTF	0.213	1.02	0.982	1.99
	Silo	0.168	0.196	0.198	0.2

Table B-4. Total flow (m^3/year) through the vaults and waste compartments for the Base case and the three concrete degradation cases, studied at 3500 AD.

		Base case	Moderate	Severe	Complete
Vaults	1BMA	55.9	54.9	58.4	58.5
	1BLA	122	140	147	147
	1BTF	21.7	24.1	23.8	20.7
	2BTF	40.5	49.7	51.1	50.9
	Silo	0.933	1.16	1.17	1.18
Waste	1BMA	2.94	3.34	22.7	38.3
	1BLA	120	138	145	145
	1BTF	3.52	6.91	7.57	12.3
	2BTF	4.58	18.9	23.6	39.2
	Silo	0.88	1.15	1.17	1.52

Table B-5. Total flow (m^3/year) through the vaults and waste compartments for the Base case and the three concrete degradation cases, studied at 5000 AD.

		Base case	Moderate	Severe	Complete
Vaults	1BMA	58.3	57.1	61.2	61.3
	1BLA	133	152	159	160
	1BTF	24.5	27.3	27	23.5
	2BTF	45	55	56.6	56.3
	Silo	1.3	1.72	1.75	1.75
Waste	1BMA	3.57	3.78	24.9	41.4
	1BLA	131	150	157	158
	1BTF	3.98	7.9	8.61	13.8
	2BTF	5.1	20.7	26	43.5
	Silo	1.29	1.71	1.76	1.53

Table B-6. Total flow (m^3/year) through the vaults and waste compartments for the Base case and the three plug degradation cases, studied at 5000 AD.

		Base case	Moderate	Severe	Complete
Vaults	1BMA	58.3	58.7	69.4	101
	1BLA	133	135	147	586
	1BTF	24.5	25.8	48.5	667
	2BTF	45	46.5	78.3	497
	Silo	1.3	1.26	1.74	2.1
Waste	1BMA	3.57	3.57	4.49	6.27
	1BLA	131	132	145	564
	1BTF	3.98	3.9	2.18	1.88
	2BTF	5.1	5.03	3.98	2.25
	Silo	1.29	1.25	1.71	2.06

Table B-7. Total flow (m^3/year) through the vaults and waste compartments for the Base case and the no barriers case, studied at 5000 AD.

		Base case	No barriers
Vaults	1BMA	58.3	103
	1BLA	133	465
	1BTF	24.5	672
	2BTF	45	678
	Silo	1.3	1410
Waste	1BMA	3.57	59.2
	1BLA	131	448
	1BTF	3.98	345
	2BTF	5.1	282
	Silo	1.29	1390

Table B-8. Total flow (m^3/year) through the vaults and waste compartments for the Base case, the high flow realization and the low flow realization, studied at 2000 AD.

		Low Flow Case	Base case	High Flow Case
Vaults	1BMA	0.174	0.0435	0.0961
	1BLA	0.117	0.122	0.105
	1BTF	0.081	0.0288	0.0353
	2BTF	0.0716	0.0429	0.0433
	Silo	0.00959	0.00459	0.00496
Waste	1BMA	0.0276	0.00691	0.00522
	1BLA	0.109	0.118	0.102
	1BTF	0.0299	0.00943	0.00835
	2BTF	0.0233	0.00921	0.00666
	Silo	0.00942	0.00446	0.00484

Table B-9. Total flow (m^3/year) through the vaults and waste compartments for the Base case, the high flow realization and the low flow realization, studied at 5000 AD.

		Low Flow Case	Base case	High Flow Case
Vaults	1BMA	54.2	58.3	167
	1BLA	30.9	133	173
	1BTF	26.3	24.5	26.4
	2BTF	20.2	45	49
	Silo	1.32	1.3	1.55
Waste	1BMA	3.41	3.57	1.29
	1BLA	30.6	131	168
	1BTF	4.88	3.98	3.86
	2BTF	4.17	5.1	3.11
	Silo	1.28	1.29	1.55

Table B-10. Total flow (m^3/year) through the vaults and waste compartments for the Base case and the alternative initial state, studied at 2000 AD.

		Base case	AIS
Vaults	1BMA	0.0435	0.042
	1BLA	0.122	0.123
	1BTF	0.0288	0.0288
	2BTF	0.0429	0.0429
	Silo	0.00459	0.00459
Waste	1BMA	0.00691	0.000808
	1BLA	0.118	0.118
	1BTF	0.00943	0.00943
	2BTF	0.00921	0.00921
	Silo	0.00446	0.00446

Table B-11. Total flow (m^3/year) through the vaults and waste compartments for the Base case and the alternative initial state, studied at 2500 AD.

		Base case	AIS
Vaults	1BMA	2.67	2.64
	1BLA	5.82	5.82
	1BTF	2.84	2.84
	2BTF	3.24	3.24
	Silo	0.178	0.178
Waste	1BMA	0.102	0.0144
	1BLA	5.39	5.39
	1BTF	0.328	0.328
	2BTF	0.213	0.213
	Silo	0.168	0.168

Table B-12. Total flow (m^3/year) through the vaults and waste compartments for the Base case and the alternative initial state, studied at 3500 AD.

		Base case	AIS
Vaults	1BMA	55.9	55
	1BLA	122	122
	1BTF	21.7	21.7
	2BTF	40.5	40.5
	Silo	0.933	0.933
Waste	1BMA	2.94	0.385
	1BLA	120	120
	1BTF	3.52	3.52
	2BTF	4.58	4.58
	Silo	0.88	0.88

Table B-13. Total flow (m^3/year) through the vaults and waste compartments for the Base case and the alternative initial state, studied at 5000 AD.

		Base case	AIS
Vaults	1BMA	58.3	57.8
	1BLA	133	133
	1BTF	24.5	24.5
	2BTF	45	45
	Silo	1.3	1.3
Waste	1BMA	3.57	2.21
	1BLA	131	131
	1BTF	3.98	3.98
	2BTF	5.1	5.1
	Silo	1.29	1.29

SFR 3

Table B-14. Total flow (m^3/year) through the vaults and waste compartments for the Base case studied at the different shoreline positions. Note: The 2BMA waste flows are normalized per waste compartment.

		2000 AD	2500 AD	3500 AD	5000 AD
Vaults	2BLA	0.126	3.44	23.7	24.4
	3BLA	0.108	4.38	30.2	31
	4BLA	0.0994	3.57	24.3	24.9
	5BLA	0.107	1.68	16.6	17.3
	BRT	0.122	3.3	20.8	21.8
	2BMA	0.262	4.78	33.8	32.9
Waste	2BLA	0.126	3.44	23.7	24.4
	3BLA	0.108	4.38	30.2	31
	4BLA	0.0994	3.57	24.3	24.9
	5BLA	0.107	1.68	16.6	17.3
	BRT	0.0147	0.528	3.8	4.02
	2BMA	2.42×10^{-6}	3.6×10^{-5}	0.000292	0.000282

Table B-15. Total flow (m^3/year) through the vaults and waste compartments for the Base case and the three concrete degradation cases, studied at 2000 AD. Note: The 2BMA waste flows are normalized per waste compartment.

		Base case	Moderate	Severe	Complete
Vaults	2BLA	0.126	0.135	0.138	0.139
	3BLA	0.108	0.121	0.122	0.122
	4BLA	0.0994	0.106	0.107	0.107
	5BLA	0.107	0.117	0.119	0.119
	BRT	0.122	0.134	0.137	0.137
	2BMA	0.262	0.261	0.261	0.261
Waste	2BLA	0.126	0.135	0.138	0.139
	3BLA	0.108	0.121	0.122	0.122
	4BLA	0.0994	0.106	0.107	0.107
	5BLA	0.107	0.117	0.119	0.119
	BRT	0.0147	0.0372	0.0422	0.0784
	2BMA	2.42×10^{-6}	0.000241	0.0166	0.0883

Table B-16. Total flow (m^3/year) through the vaults and waste compartments for the Base case and the three concrete degradation cases, studied at 2500 AD. Note: The 2BMA waste flows are normalized per waste compartment.

		Base case	Moderate	Severe	Complete
Vaults	2BLA	3.44	4.04	4.14	4.14
	3BLA	4.38	4.87	4.91	4.92
	4BLA	3.57	3.72	3.78	3.79
	5BLA	1.68	1.83	1.84	1.85
	BRT	3.3	3.49	3.52	3.54
	2BMA	4.78	4.76	4.75	4.75
Waste	2BLA	3.44	4.04	4.14	4.14
	3BLA	4.38	4.87	4.91	4.92
	4BLA	3.57	3.72	3.78	3.79
	5BLA	1.68	1.83	1.84	1.85
	BRT	0.528	1.11	1.19	2.28
	2BMA	3.6×10^{-5}	0.00358	0.243	1.24

Table B-17. Total flow (m^3/year) through the vaults and waste compartments for the Base case and the three concrete degradation cases, studied at 3500 AD. Note: The 2BMA waste flows are normalized per waste compartment.

		Base case	Moderate	Severe	Complete
Vaults	2BLA	23.7	27.9	28.7	28.7
	3BLA	30.2	30.8	31	31.1
	4BLA	24.3	25.4	25.8	25.9
	5BLA	16.6	18.1	18.3	18.3
	BRT	20.8	24	24.4	24.4
	2BMA	33.8	33.6	33.6	33.6
Waste	2BLA	23.7	27.9	28.7	28.7
	3BLA	30.2	30.8	31	31.1
	4BLA	24.3	25.4	25.8	25.9
	5BLA	16.6	18.1	18.3	18.3
	BRT	3.8	7.85	8.71	16.9
	2BMA	0.000292	0.029	1.99	10.5

Table B-18. Total flow (m^3/year) through the vaults and waste compartments for the Base case and the three concrete degradation cases, studied at 5000 AD. Note: The 2BMA waste flows are normalized per waste compartment.

		Base case	Moderate	Severe	Complete
Vaults	2BLA	24.4	28.9	29.7	29.7
	3BLA	31	31.5	31.6	31.7
	4BLA	24.9	26.4	26.8	26.8
	5BLA	17.3	18.8	19.1	19.1
	BRT	21.8	25.1	25.5	25.5
	2BMA	32.9	32.7	32.7	32.7
Waste	2BLA	24.4	28.9	29.7	29.7
	3BLA	31	31.5	31.6	31.7
	4BLA	24.9	26.4	26.8	26.8
	5BLA	17.3	18.8	19.1	19.1
	BRT	4.02	8.27	9.16	17.8
	2BMA	0.000282	0.0279	1.91	10.1

Table B-19. Total flow (m^3/year) through the vaults and waste compartments for the Base case and the three plug degradation cases, studied at 5000 AD. Note: The 2BMA waste flows are normalized per waste compartment.

		Base case	Moderate	Severe	Complete
Vaults	2BLA	24.4	24.4	32.7	77
	3BLA	31	31.1	35.8	65.4
	4BLA	24.9	25	32.1	50
	5BLA	17.3	17.4	23	35.3
	BRT	21.8	21.8	26.9	81.7
	2BMA	32.9	32.9	35.3	50.3
Waste	2BLA	24.4	24.4	32.7	77
	3BLA	31	31.1	35.8	65.4
	4BLA	24.9	25	32.1	50
	5BLA	17.3	17.4	23	35.3
	BRT	4.02	4.01	4.31	4.07
	2BMA	0.000282	0.000282	0.000302	0.00043

Table B-20. Total flow (m^3/year) through the vaults and waste compartments for the Base case and the no barriers case, studied at 5000 AD. Note: The 2BMA waste flows are normalized per waste compartment.

		Base case	No barriers
Vaults	2BLA	24.4	77.1
	3BLA	31	65.3
	4BLA	24.9	49.7
	5BLA	17.3	33.2
	BRT	21.8	96.1
	2BMA	32.9	49.7
Waste	2BLA	24.4	77.1
	3BLA	31	65.3
	4BLA	24.9	49.7
	5BLA	17.3	33.2
	BRT	4.02	37.8
	2BMA	0.000282	17.4

Table B-21. Total flow (m^3/year) through the vaults and waste compartments for the Base case, the high flow realization (HFC) and the low flow realization (LFC), studied at 2000 AD. Note: The 2BMA waste flows are normalized per waste compartment.

		Low flow case	Base case	High flow case
Vaults	2BLA	0.128	0.126	0.116
	3BLA	0.12	0.108	0.0896
	4BLA	0.13	0.0994	0.104
	5BLA	0.146	0.107	0.149
	BRT	0.105	0.122	0.178
	2BMA	0.227	0.262	0.673
Waste	2BLA	0.128	0.126	0.116
	3BLA	0.12	0.108	0.0896
	4BLA	0.13	0.0994	0.104
	5BLA	0.146	0.107	0.149
	BRT	0.0268	0.0147	0.0152
	2BMA	9.1×10^{-7}	2.42×10^{-6}	4.34×10^{-6}

Table B-22. Total flow (m^3/year) through the vaults and waste compartments for the Base case, the high flow realization (HFC) and the low flow realization (LFC), studied at 5000 AD. Note: The 2BMA waste flows are normalized per waste compartment.

		Low flow case	Base case	High flow case
Vaults	2BLA	23.5	24.4	23.8
	3BLA	19.2	31	31.9
	4BLA	23.3	24.9	38.2
	5BLA	25.2	17.3	29.2
	BRT	14.4	21.8	26.4
	2BMA	43.7	32.9	129
Waste	2BLA	23.5	24.4	23.8
	3BLA	19.2	31	31.9
	4BLA	23.3	24.9	38.2
	5BLA	25.2	17.3	29.2
	BRT	4.16	4.02	3.48
	2BMA	0.000278	0.000282	0.000592

Table B-23. Total flow (m^3/year) through the vaults and waste compartments for the Base case and the alternative initial state, studied at 2000 AD. Note: The 2BMA waste flows are normalized per waste compartment.

		Base case	AIS
Vaults	2BLA	0.126	0.126
	3BLA	0.108	0.108
	4BLA	0.0994	0.0994
	5BLA	0.107	0.107
	BRT	0.122	0.122
	2BMA	0.262	0.262
Waste	2BLA	0.126	0.126
	3BLA	0.108	0.108
	4BLA	0.0994	0.0994
	5BLA	0.107	0.107
	BRT	0.0147	0.0147
	2BMA	2.42×10^{-6}	2.83×10^{-8}

Table B-24. Total flow (m^3/year) through the vaults and waste compartments for the Base case and the alternative initial state, studied at 2500 AD. Note: The 2BMA waste flows are normalized per waste compartment.

		Base case	AIS
Vaults	2BLA	3.44	3.44
	3BLA	4.38	4.38
	4BLA	3.57	3.57
	5BLA	1.68	1.68
	BRT	3.3	3.3
	2BMA	4.78	4.78
Waste	2BLA	3.44	3.44
	3BLA	4.38	4.38
	4BLA	3.57	3.57
	5BLA	1.68	1.68
	BRT	0.528	0.528
	2BMA	3.6×10^{-5}	4.16×10^{-7}

Table B-25. Total flow (m^3/year) through the vaults and waste compartments for the Base case and the alternative initial state, studied at 3500 AD. Note: The 2BMA waste flows are normalized per waste compartment.

		Base case	AIS
Vaults	2BLA	23.7	23.7
	3BLA	30.2	30.2
	4BLA	24.3	24.3
	5BLA	16.6	16.6
	BRT	20.8	20.8
	2BMA	33.8	33.8
Waste	2BLA	23.7	23.7
	3BLA	30.2	30.2
	4BLA	24.3	24.3
	5BLA	16.6	16.6
	BRT	3.8	3.8
	2BMA	0.000292	3.4×10^{-6}

Table B-26. Total flow (m^3/year) through the vaults and waste compartments for the Base case and the alternative initial state, studied at 5000 AD. Note: The 2BMA waste flows are normalized per waste compartment.

		Base case	AIS
Vaults	2BLA	24.4	24.4
	3BLA	31	31
	4BLA	24.9	24.9
	5BLA	17.3	17.3
	BRT	21.8	21.8
	2BMA	32.9	32.9
Waste	2BLA	24.4	24.4
	3BLA	31	31
	4BLA	24.9	24.9
	5BLA	17.3	17.3
	BRT	4.02	4.02
	2BMA	0.000282	3.27×10^{-6}

Appendix C

Alternative Initial state

SFR 1

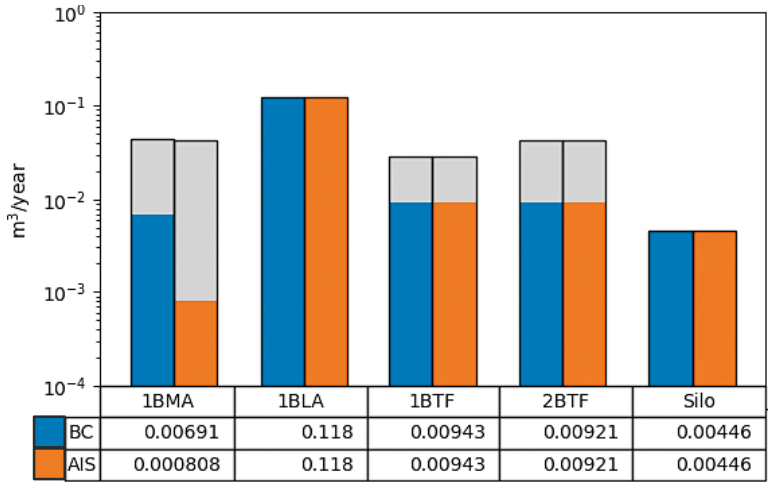

	1BMA	1BLA	1BTF	2BTF	Silo
BC	0.00691	0.118	0.00943	0.00921	0.00446
AIS	0.000808	0.118	0.00943	0.00921	0.00446

Figure C-1. *Total flow (m^3/year) through the waste of the SFR 1 for the Base case and the alternative initial state, studied at 2000 AD. The grey area illustrates the vault flow outside the waste compartment.*

SFR 3

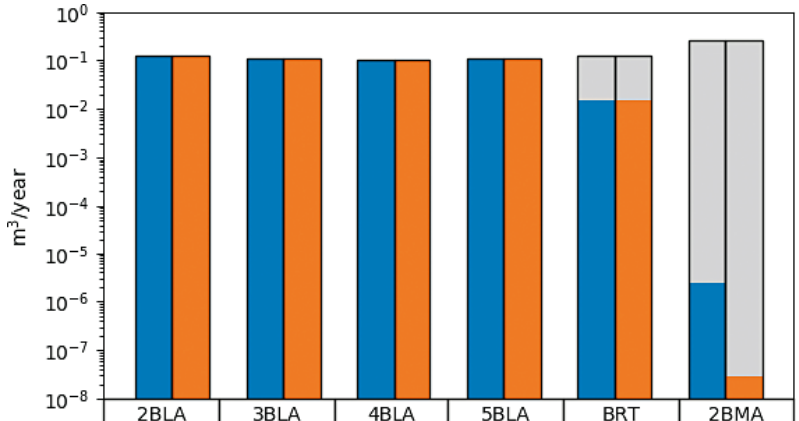

	2BLA	3BLA	4BLA	5BLA	BRT	2BMA
BC	0.126	0.108	0.0994	0.107	0.0147	2.42e-06
AIS	0.126	0.108	0.0994	0.107	0.0147	2.83e-08

Figure C-2. *Total flow (m^3/year) through the waste of the SFR 3 for the Base case and the alternative initial state, studied at 2000 AD. The grey area illustrates the vault flow outside the waste compartment.*

SFR 1

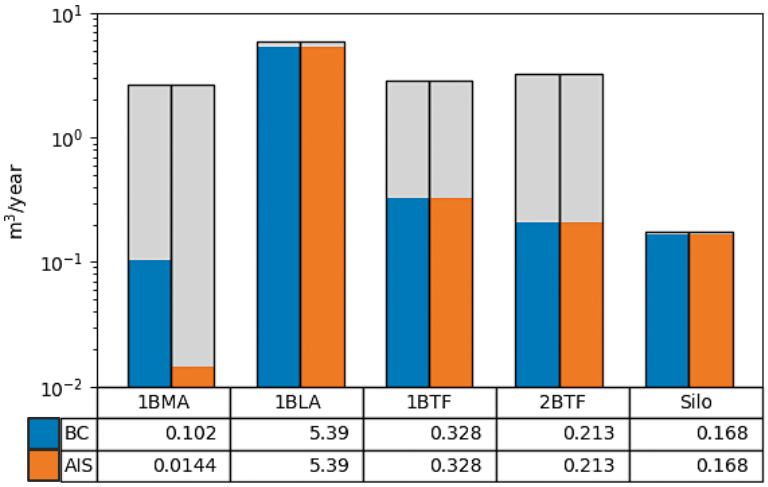

	1BMA	1BLA	1BTF	2BTF	Silo
BC	0.102	5.39	0.328	0.213	0.168
AIS	0.0144	5.39	0.328	0.213	0.168

Figure C-3. *Total flow (m^3/year) through the waste of the SFR 1 for the Base case and the alternative initial state, studied at 2500 AD. The grey area illustrates the vault flow outside the waste compartment.*

SFR 3

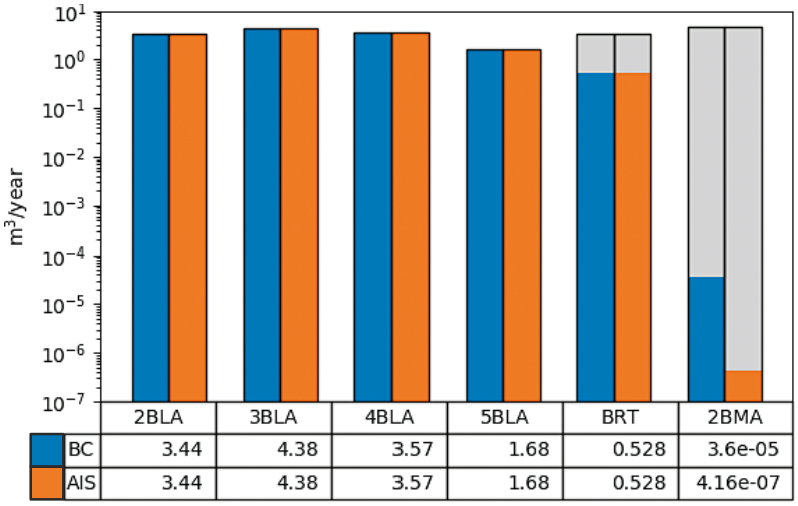

	2BLA	3BLA	4BLA	5BLA	BRT	2BMA
BC	3.44	4.38	3.57	1.68	0.528	3.6e-05
AIS	3.44	4.38	3.57	1.68	0.528	4.16e-07

Figure C-4. *Total flow (m^3/year) through the waste of the SFR 3 for the Base case and the alternative initial state, studied at 2500 AD. The grey area illustrates the vault flow outside the waste compartment.*

SFR 1

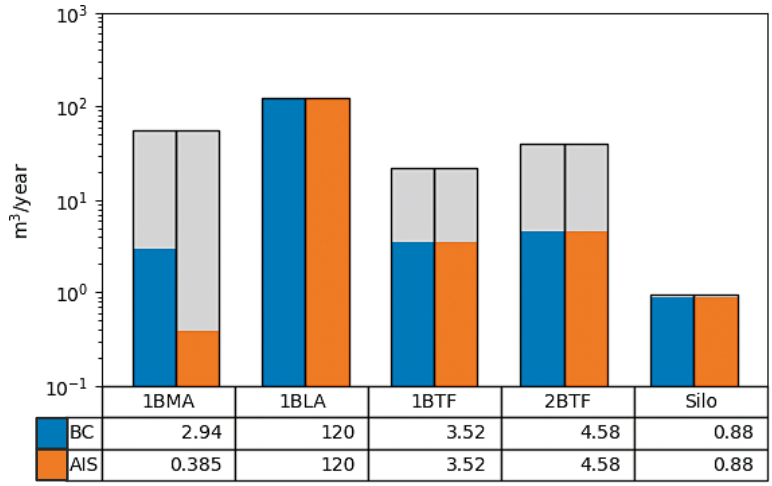

	1BMA	1BLA	1BTF	2BTF	Silo
BC	2.94	120	3.52	4.58	0.88
AIS	0.385	120	3.52	4.58	0.88

Figure C-5. *Total flow (m^3/year) through the waste of the SFR 1 for the Base case and the alternative initial state, studied at 3500 AD. The grey area illustrates the vault flow outside the waste compartment.*

SFR 3

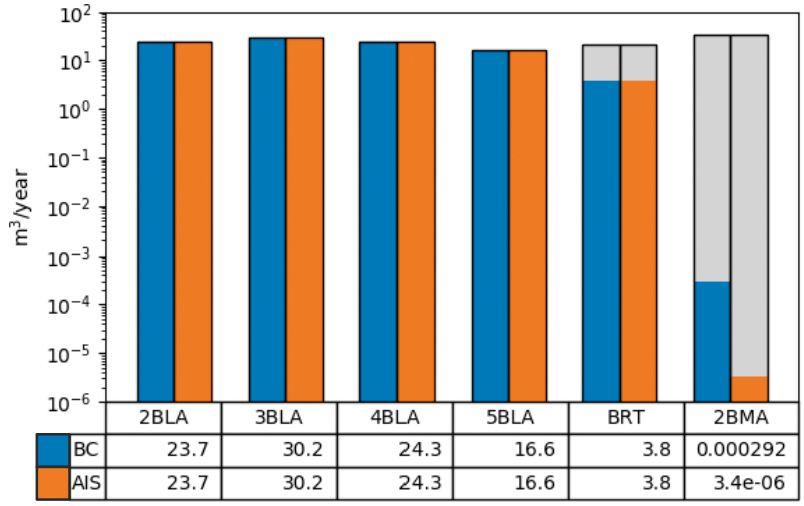

	2BLA	3BLA	4BLA	5BLA	BRT	2BMA
BC	23.7	30.2	24.3	16.6	3.8	0.000292
AIS	23.7	30.2	24.3	16.6	3.8	3.4e-06

Figure C-6. *Total flow (m^3/year) through the waste of the SFR 3 for the Base case and the alternative initial state, studied at 3500 AD. The grey area illustrates the vault flow outside the waste compartment.*

SFR 1

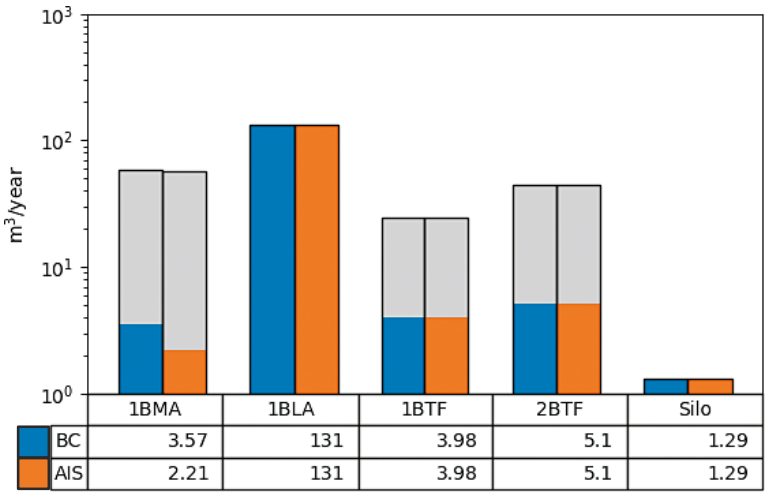

	1BMA	1BLA	1BTF	2BTF	Silo
BC	3.57	131	3.98	5.1	1.29
AIS	2.21	131	3.98	5.1	1.29

Figure C-7. *Total flow (m^3/year) through the waste of the SFR 1 for the Base case and the alternative initial state, studied at 5000 AD. The grey area illustrates the vault flow outside the waste compartment.*

SFR 3

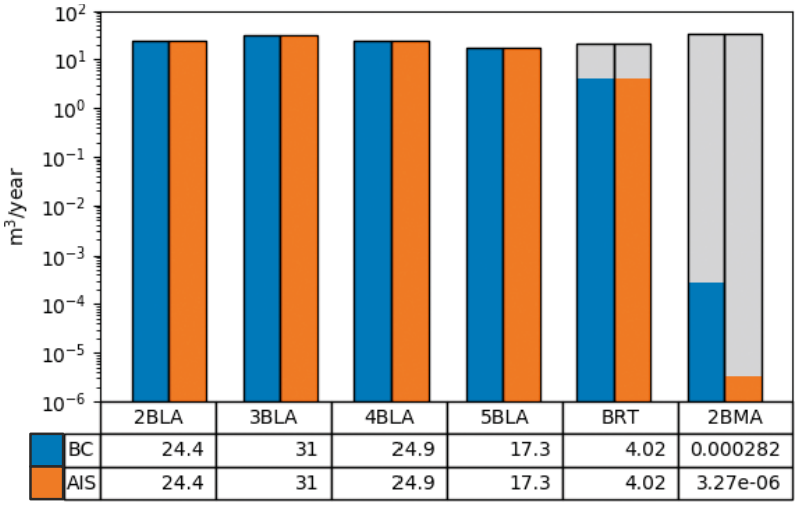

	2BLA	3BLA	4BLA	5BLA	BRT	2BMA
BC	24.4	31	24.9	17.3	4.02	0.000282
AIS	24.4	31	24.9	17.3	4.02	3.27e-06

Figure C-8. *Total flow (m^3/year) through the waste of the SFR 3 for the Base case and the alternative initial state, studied at 5000 AD. The grey area illustrates the vault flow outside the waste compartment.*

Appendix D

Flow in the 1BMA vault for the different degradation states

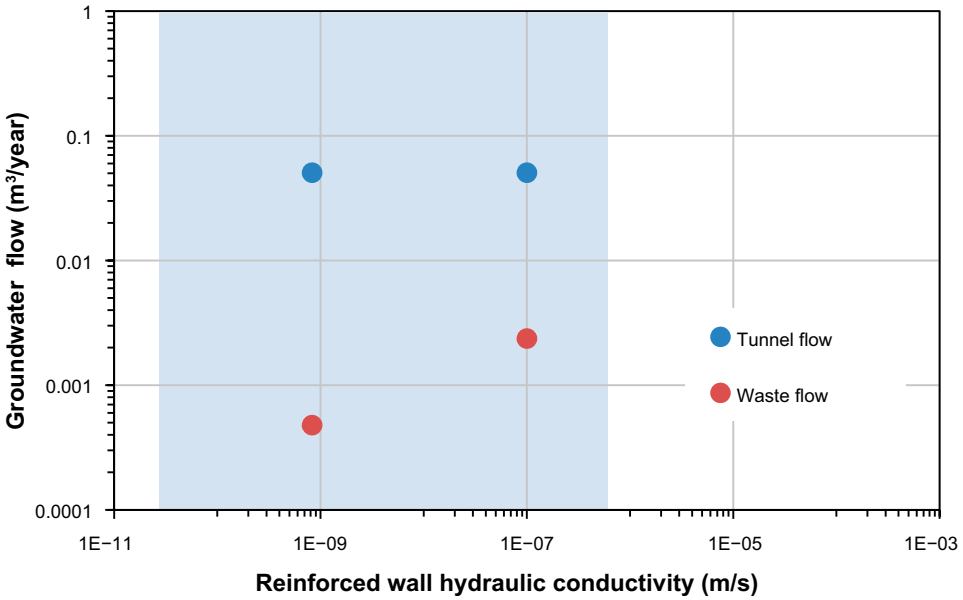

Figure D-1. *Tunnel and waste flow (m^3/year) through the repaired 1BMA as a function of the hydraulic conductivity of the reinforced walls at 2000 AD. The blue area delimitates the range of the rock hydraulic conductivity.*

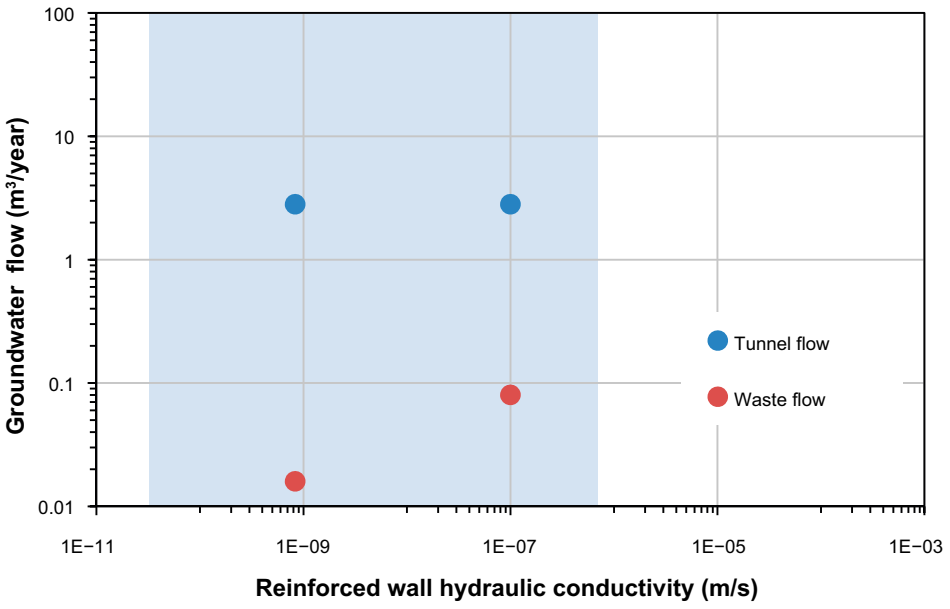

Figure D-2. *Tunnel and waste flow (m^3/year) through the repaired 1BMA as a function of the hydraulic conductivity of the reinforced walls at 2500 AD. The blue area delimitates the range of the rock hydraulic conductivity.*

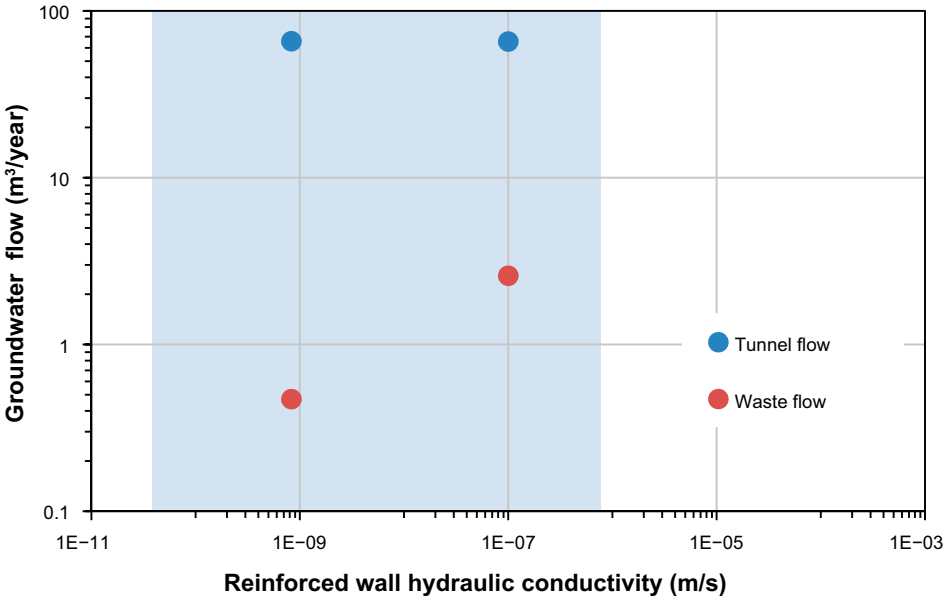

Figure D-3. *Tunnel and waste flow (m^3/year) through the repaired 1BMA as a function of the hydraulic conductivity of the reinforced walls at 3500 AD. The blue area delimitates the range of the rock hydraulic conductivity.*

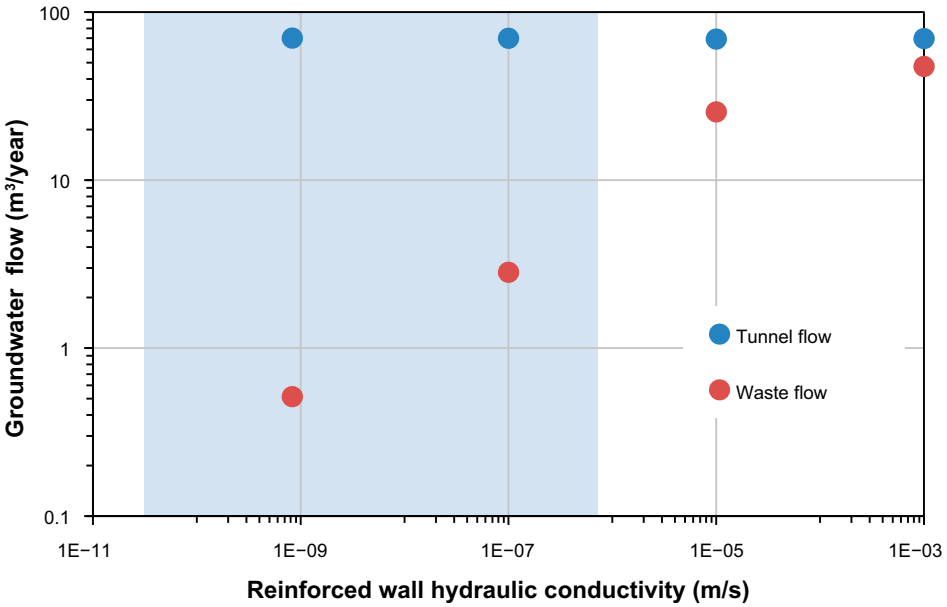

Figure D-4. *Tunnel and waste flow (m^3/year) through the repaired 1BMA as a function of the hydraulic conductivity of the reinforced walls at 5000 AD. The blue area delimitates the range of the rock hydraulic conductivity.*

Appendix E

Cross sectional plots of the 1BMA vault

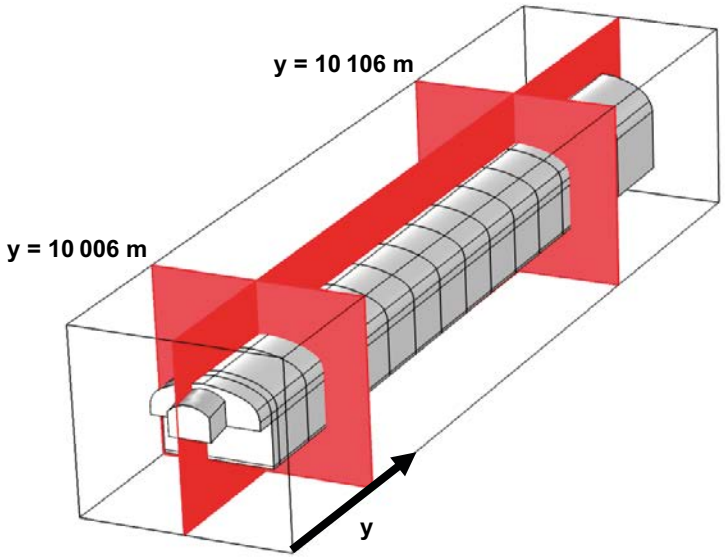

Figure E-1. *Location of the two transverse and one longitudinal cross-sections of the 1BMA vault scale model used for illustrating the changes in the local flow field as the concrete degradation advances.*

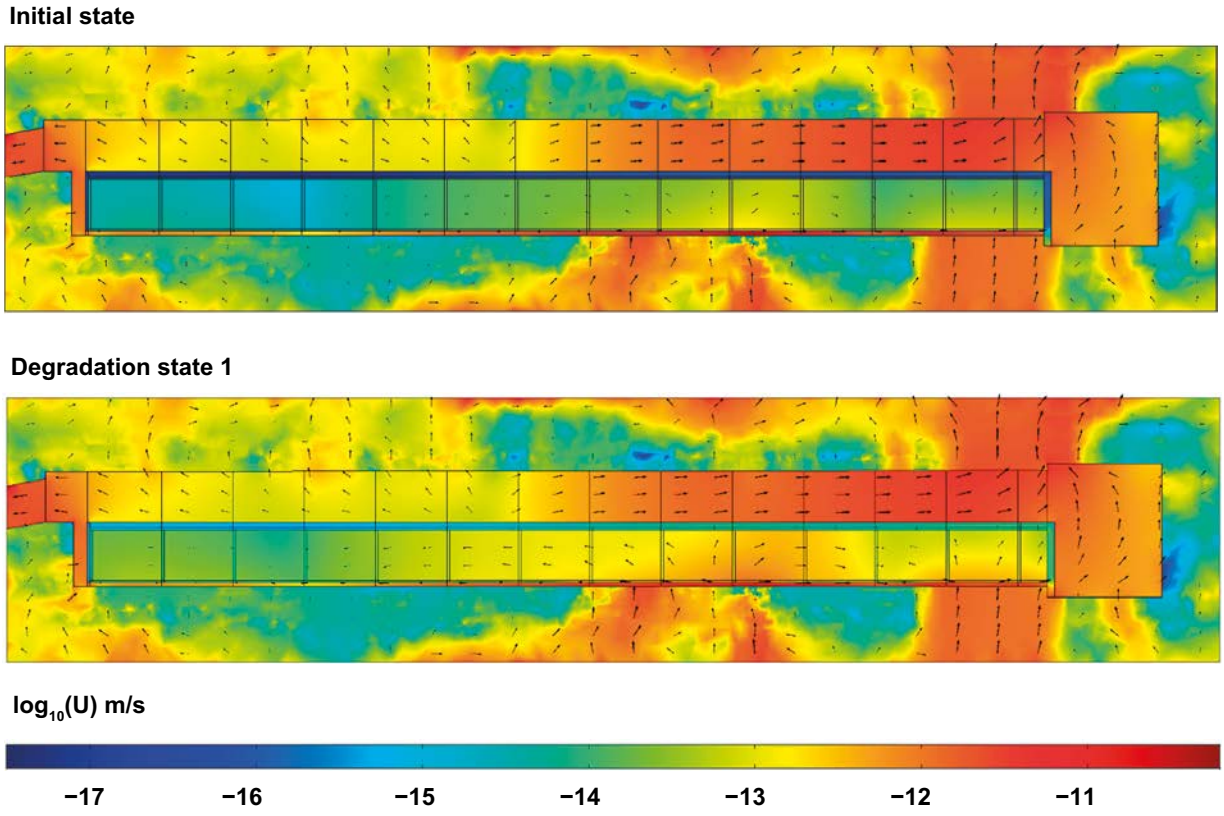

Figure E-2. *Magnitude of the Darcy velocity through the longitudinal section of the encapsulated waste compartments of the 1BMA submodel at 2000 AD.*

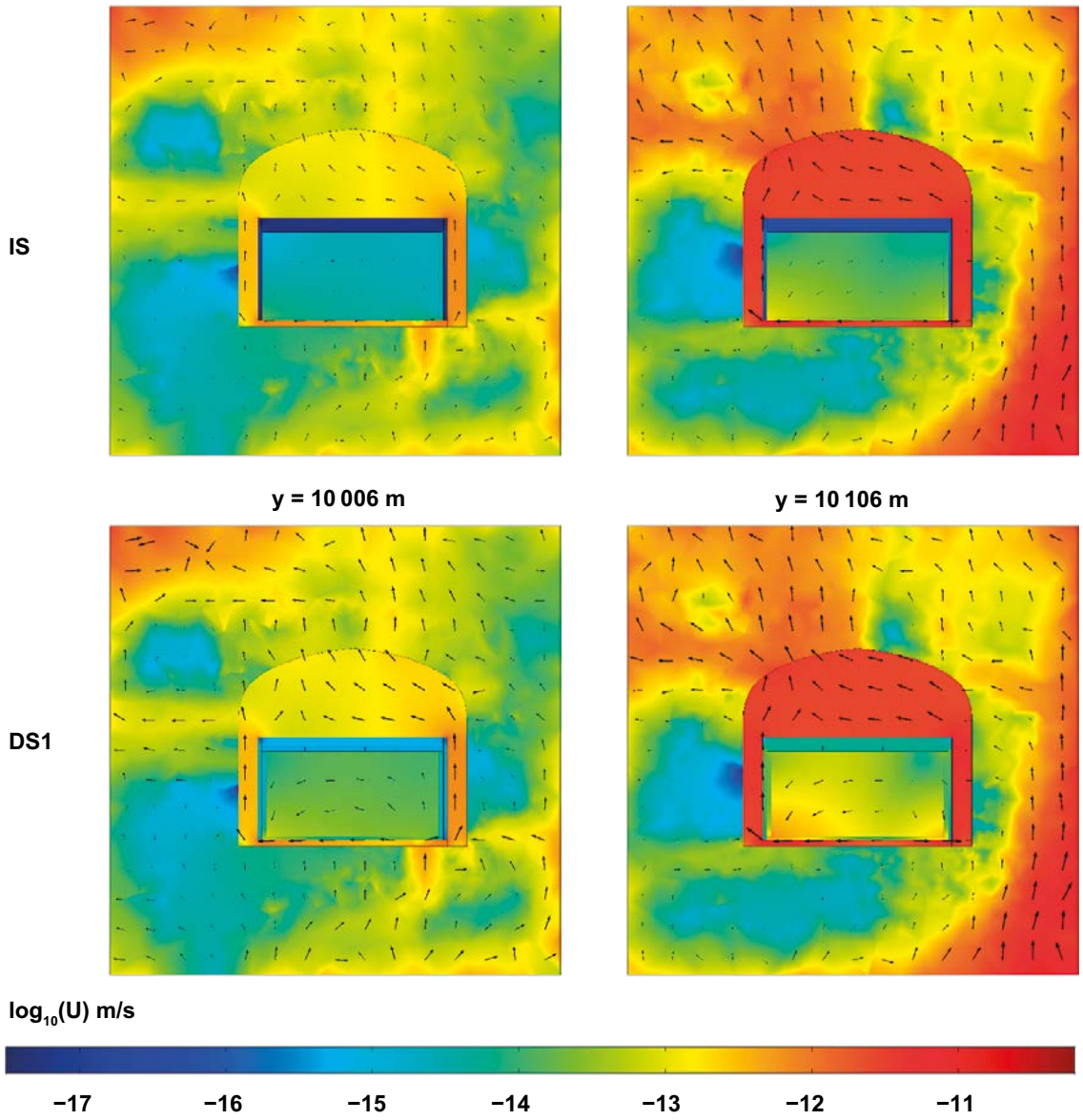

Figure E-3. *Impact of degradation state 1 (DS1) of the walls on the water Darcy fluxes and its magnitude at two cross-sections (xz planes) of the 1BMA submodel at 2000 AD.*

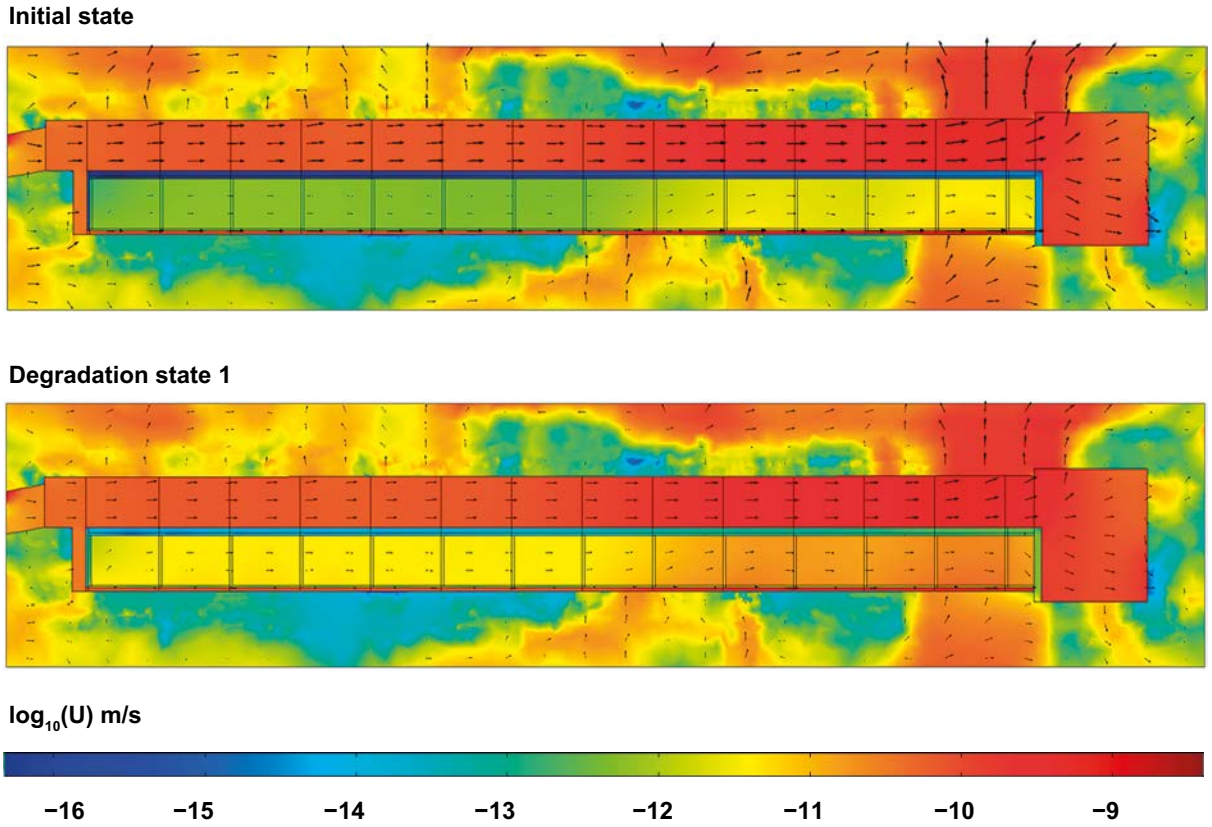

Figure E-4. *Magnitude of the Darcy velocity through the longitudinal section of the encapsulated waste compartments of the 1BMA submodel at 2500 AD.*

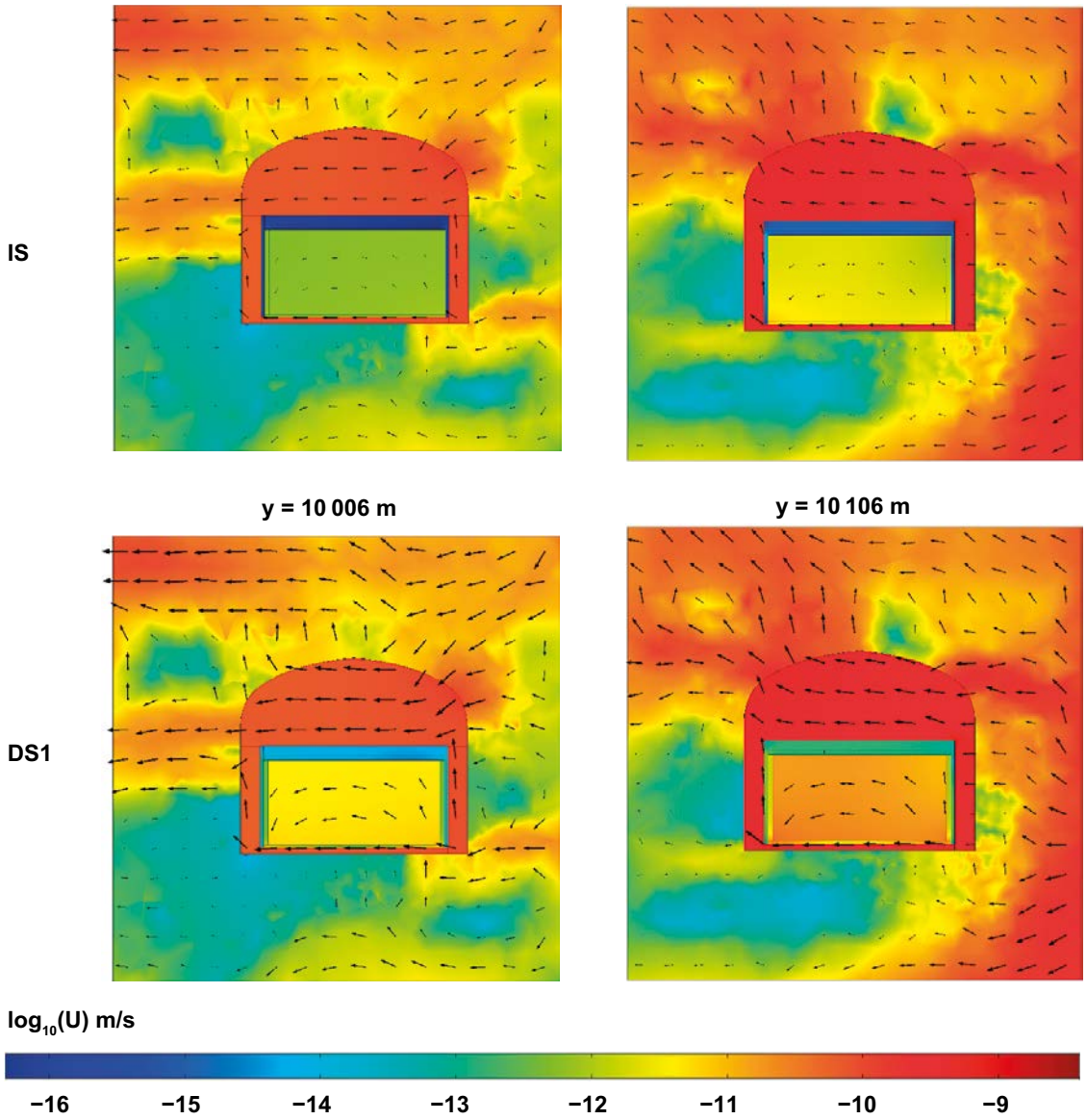

Figure E-5. *Impact of degradation state 1 (DS1) of the walls on the water Darcy fluxes and its magnitude at two cross-sections (xz planes) of the 1BMA submodel at 2500 AD.*

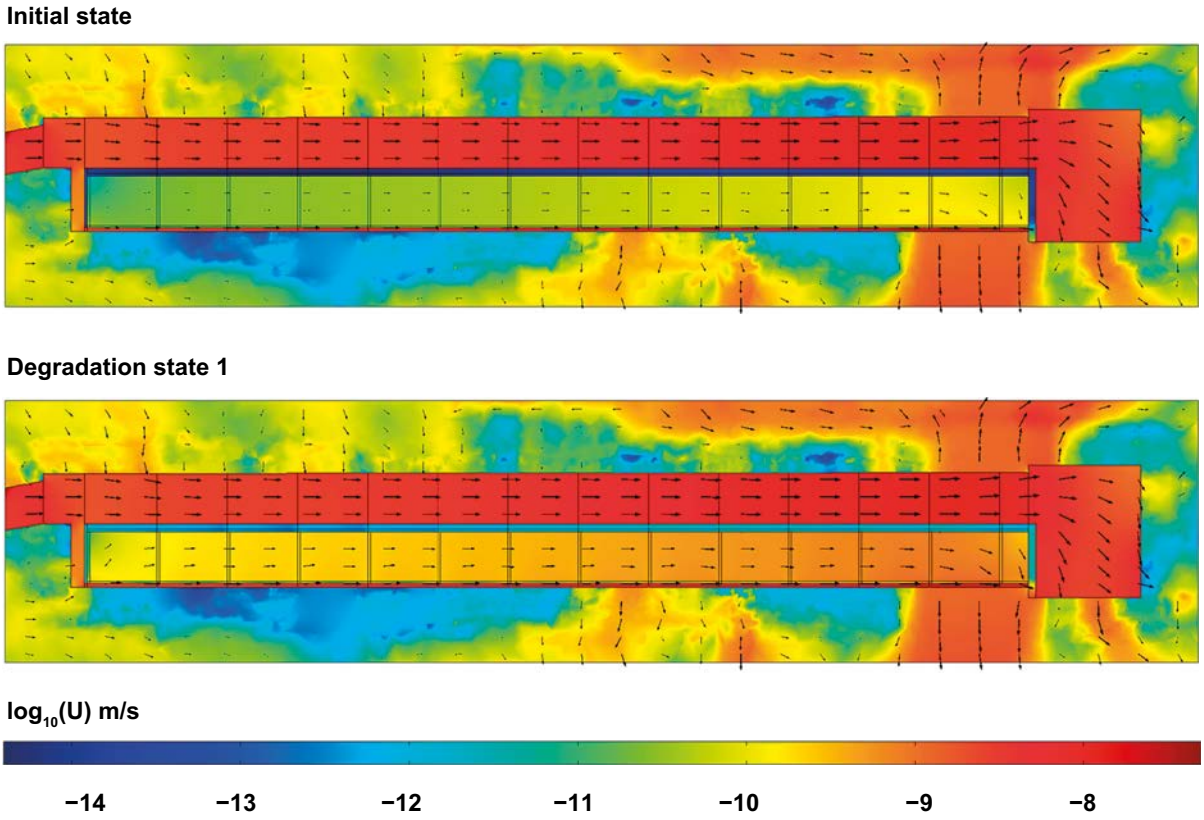

Figure E-6. *Magnitude of the Darcy velocity through the longitudinal section of the encapsulated waste compartments of the 1BMA submodel at 3500 AD.*

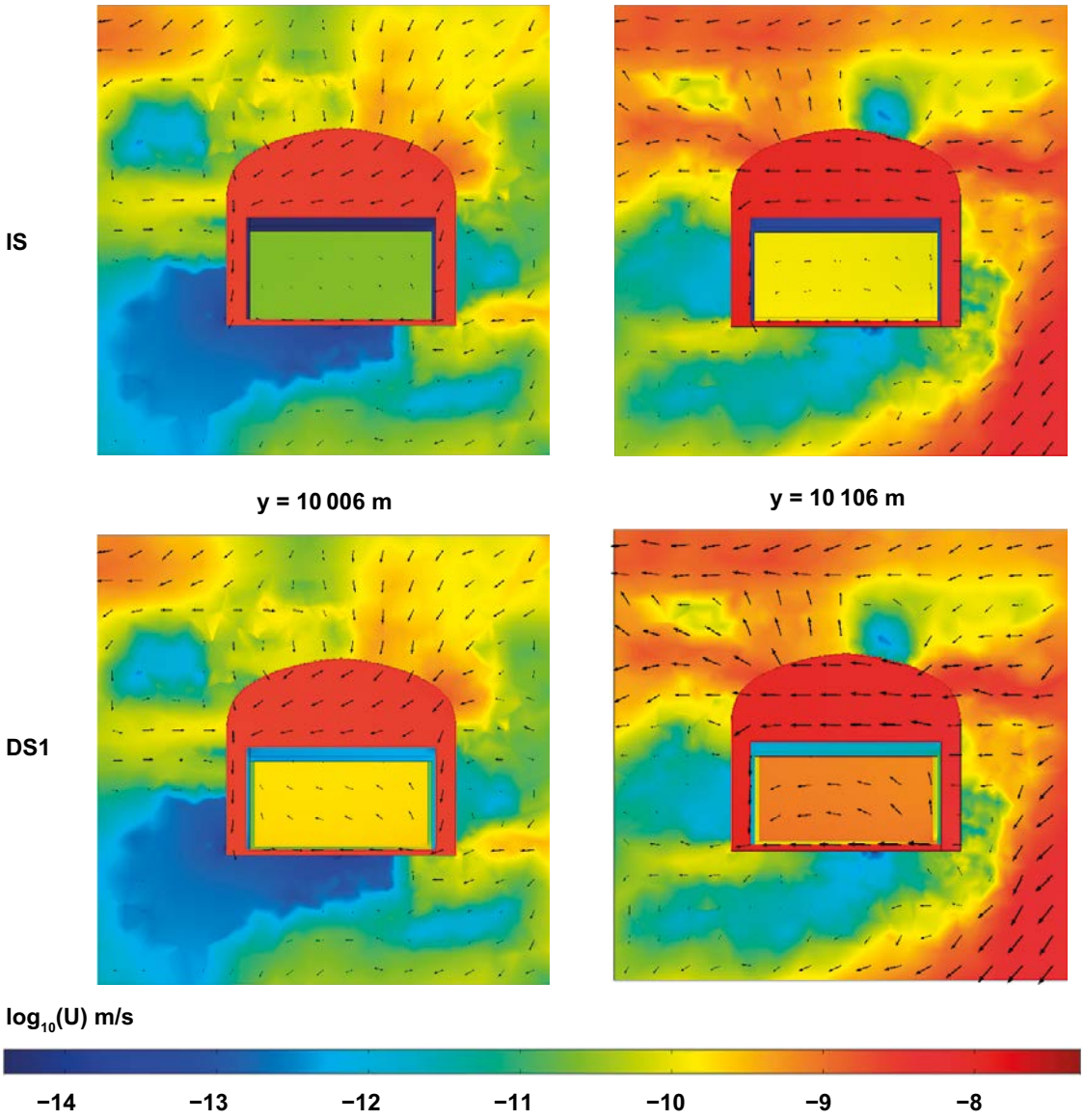

Figure E-7. *Impact of degradation state 1 (DS1) of the walls on the water Darcy fluxes and its magnitude at two cross-sections (xz planes) of the 1BMA submodel at 3500 AD.*

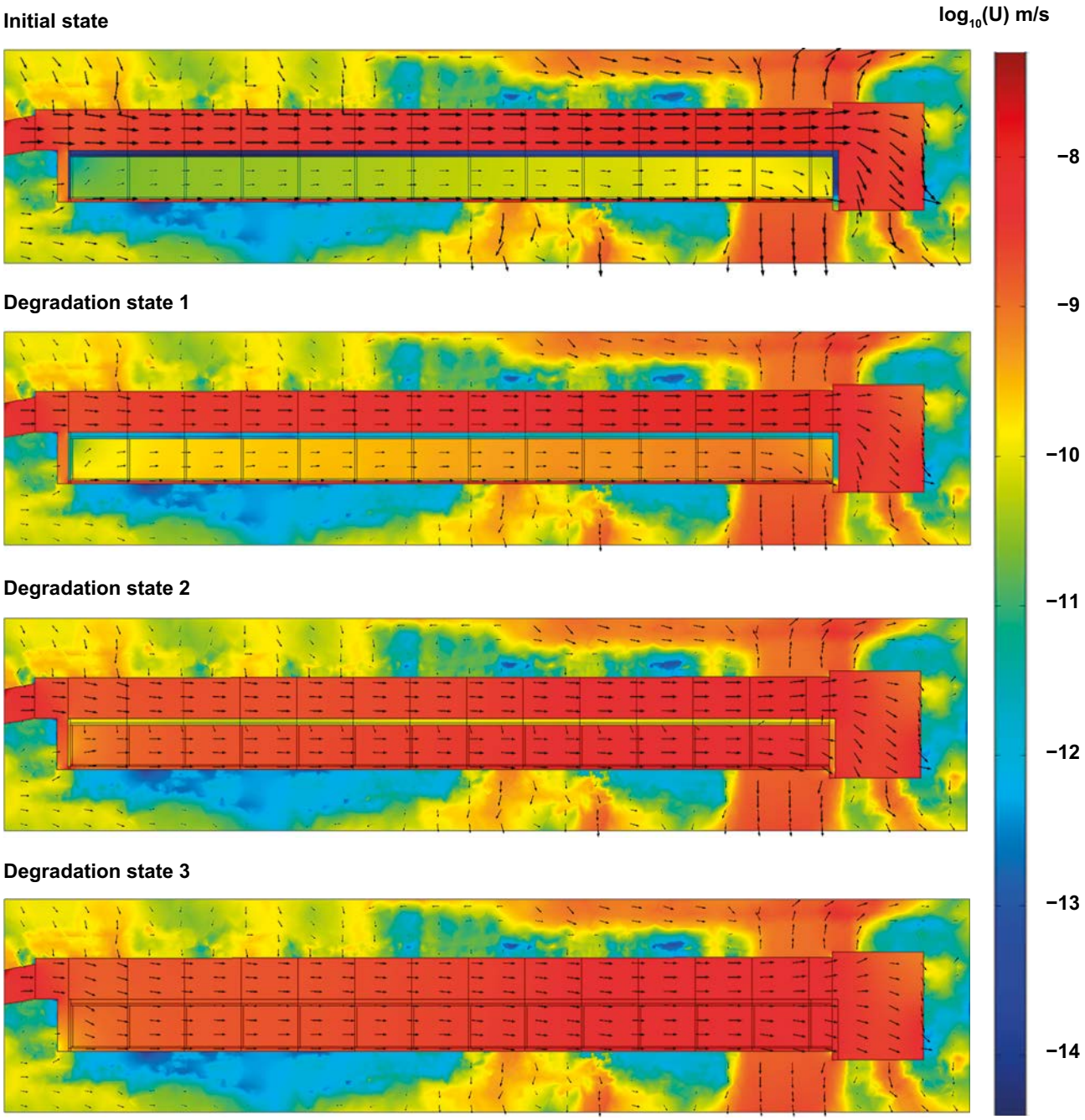

Figure E-8. *Magnitude of the Darcy velocity through the longitudinal section of the encapsulated waste compartments of the 1BMA submodel at 5000 AD.*

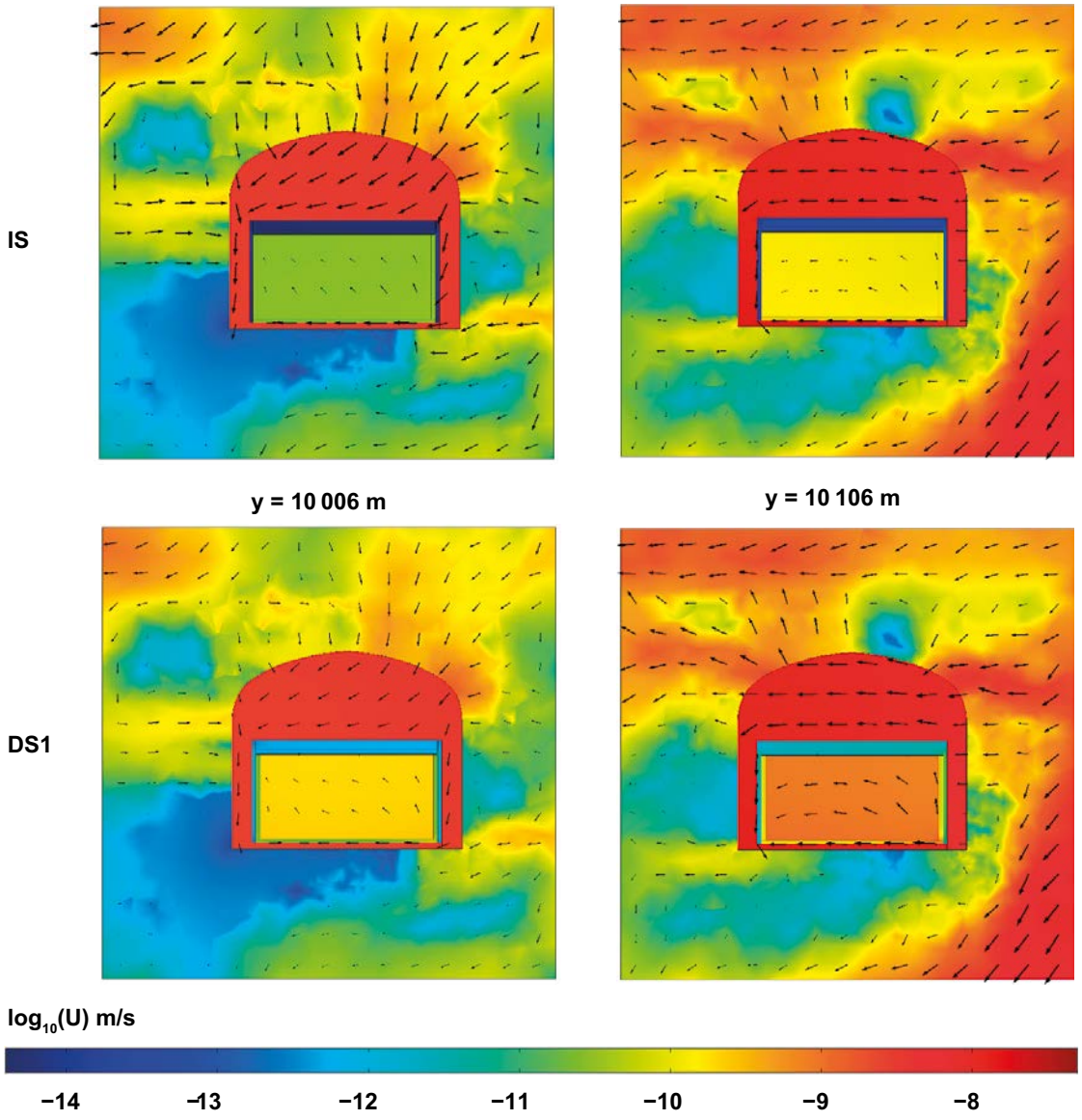

Figure E-9. *Impact of degradation state 1 (DS1) of the walls on the water Darcy fluxes and its magnitude at two cross-sections (xz planes) of the 1BMA submodel at 5000 AD.*

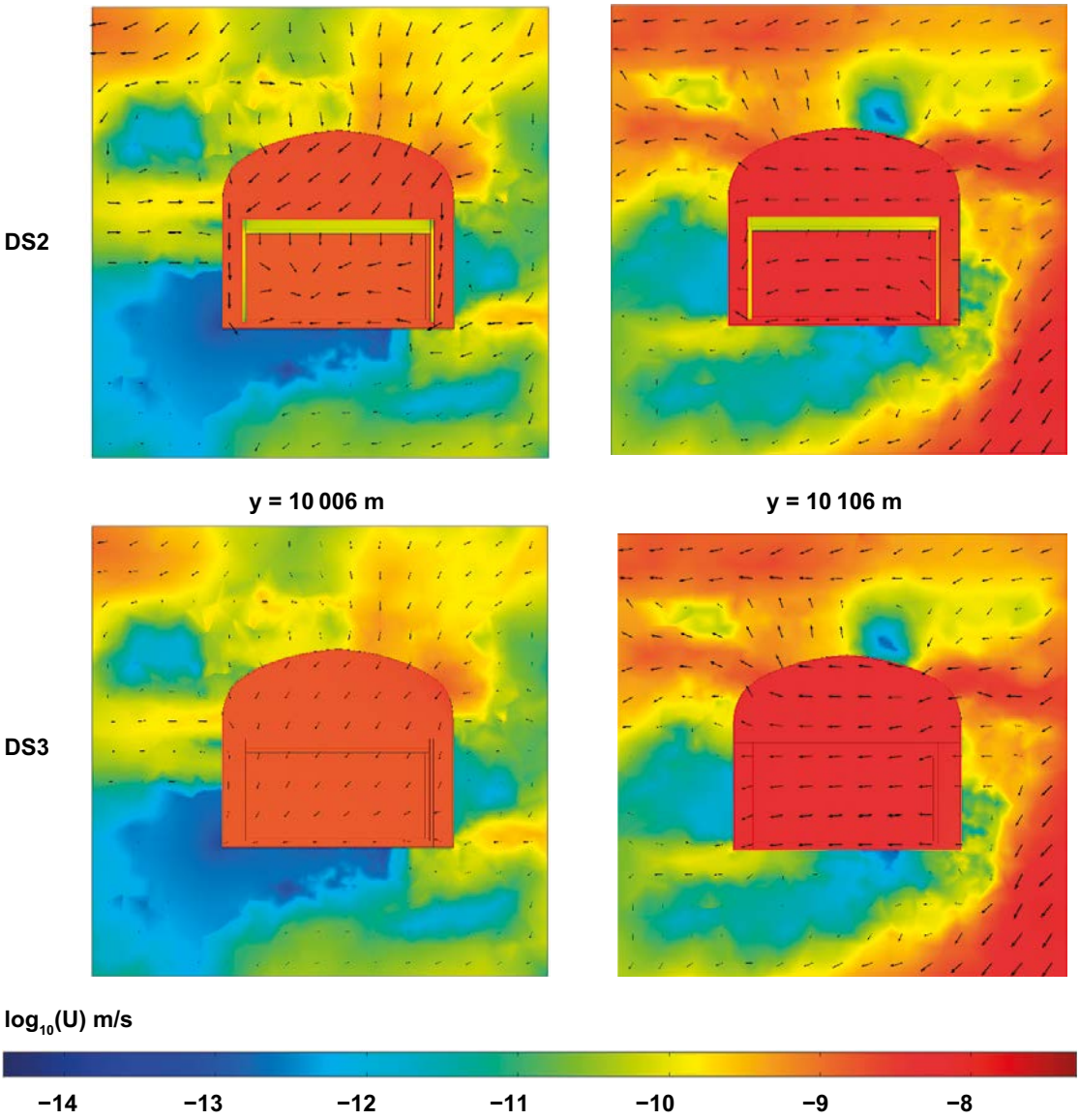

Figure E-10. *Impact of degradation state 2 (DS2) and 3 (DS3) of the walls on the water Darcy fluxes and its magnitude at two cross-sections (xz planes) of the 1BMA submodel at 5000 AD.*

Arkitektkopia AB, Bromma, 2020

SKB is responsible for managing spent nuclear fuel and radioactive waste produced by the Swedish nuclear power plants such that man and the environment are protected in the near and distant future.

skb.se